University of Colorado
Nuclear Physics Laboratory
Department of Physics
and Astrophysics

Technical Progress Report

Contract AT (11-1)-535
November 1, 1971
COO-535-653

DISCLAIMER

TECHNICAL PROGRESS REPORT

CONTRACT AT(11-1)-535

November 1, 1971

COO-535-653

TABLE OF CONTENTS

I. INTRODUCTION

This report summarizes the work carried out at the Nuclear Physics Laboratory of the University of Colorado during the period November 1, 1970, to November 1, 1971, under Contract AT(11-1)-535 between the University of Colorado and the United States Atomic Energy Commission.

During the past year the cyclotron has been in use more (6700 hours) than in any previous annual period. A significant growth in the rate of publication of papers in basic nuclear physics has accompanied the increased cyclotron usage.

Emphasis on studies of the (p,t) and (p,n) reactions is reflected in the 4000 hours of proton beam time reported this year. The second most popular use of the cyclotron was for the study of ^{3}He-induced reactions.

The nuclear theory group has interacted strongly with the experimental group and several of the publications reflect this collaboration. In addition, major advances have occurred this past year in understanding the application of pi-meson beams to the investigation of nuclear structure. This understanding has been valuable in the design of LAMPF experiments which are now being planned.

Major efforts in apparatus development have included the design and construction of a new charged-particle spectrometer and improvement of the neutron time-of-flight facility. It is expected that this apparatus development will strongly enhance our experimental research programs in coming years.

II. EXPERIMENTAL PROGRAM

A. Nuclear Physics

1. Charged Particle Experiments

a. Multi-Nucleon Transfer Reactions

The title of this section emphasizes the specific interests of members of our group in reactions such as (^{3}He,^{7}Be) and (^{3}He,^{6}Li). If, indeed, these reactions occur via a simple, non-exchange transfer process, a great deal of information related to multi-particle, multi-hole structure may be obtained. We have concentrated heavily in the past two years upon: a) setting upper limits to compound-nucleus contributions; b) inferring the internal couplings of the transferred nucleons from selection rules and analog reaction comparisons; c) application of these reactions to specific nuclear structure questions. The results of these investigations are reported in last year's progress report, immediately following in this year's progress report, and in publications referenced in those reports.

Briefly, our investigations of the past two years have shown that:

a) The compound-nucleus yield for low-lying states in multi-nucleon pick-up reactions initiated by ^{3}He projectiles is much smaller than for such reactions involving deuterons or alpha particles[1,2]. At 40 MeV, these compound-nucleus yields are small enough to be neglected even for the ^{40}Ar(^{3}He,^{7}Be)^{36}S reaction where cross sections below 0.1 μb/sterad were observed[3].

b) The multi-particle, multi-hole structure of ^{16}O states inferred by comparison of the intensity of these states as seen in 1, 2, and 3 particle pick-up and stripping experiments is in agreement with recent shell model calculations[1]. This agreement suggests that particle exchange is not important in these reactions.

c) The internal quantum state of the four transferred nucleons in the (^{3}He,^{7}Be) reaction is dominated by a configuration similar to that of the alpha-particle ground state. This point is discussed fully in the next section.

d) Since these results indicate the utility of the (^{3}He,^{7}Be) reaction as a measure of α-widths, we compared the ^{40}Ca(^{3}He,^{7}Be)^{36}Ar and ^{40}Ar(^{3}He,^{7}Be)^{36}S reactions. Possible differences in ^{40}Ar and ^{40}Ca α-clustering have been of recent interest and are discussed fully in a later section of this report.

e) While comparing the ^{19}F(^{3}He,^{7}Li)^{15}O and ^{19}F(^{3}He,^{7}Be)^{15}N reactions we observed Ericson fluctuation at extreme back angles. Comparison of these excitation functions indicated the goodness of isospin at 50 MeV excitation energies in ^{22}Na (also discussed in a later section).

[1] C. Détraz, C. E. Moss, C. D. Zafiratos, and C. S. Zaidins, Nucl. Phys. A167 (1971) 337.
[2] C. Détraz, C. E. Moss, C. S. Zaidins, and C. D. Zafiratos, Phys. Rev. Letters 26 (1971) 448.
[3] C. D. Zafiratos, C. Détraz, C. E. Moss, and C. S. Zaidins, Phys. Rev. Letters 27 (1971) 437.

i. The Mechanism of ^{3}He-Induced Four-Nucleon Pick-up Reactions - C. Détraz, R. A. Emigh, C. E. Moss, C. D. Zafiratos, and C. S. Zaidins

There are some experimental indications that the (^{3}He,^{7}Be) reaction results from a one-step pickup process while the four transferred nucleons are in the internal quantum state of an α-particle. We have attempted to examine in more detail the validity of this hypothesis. For this purpose we have studied experimentally: (i) the variation of the (^{3}He,^{7}Be) cross section with the mass of the target nucleus; (ii) the extent to which the selection rules associated with an α-transfer process are enforced in (^{3}He,^{7}Be) transitions; (iii) the probability that the (^{3}He,^{7}Be) reaction results from the transfer of a 2p + 2n fragment in a T=1 state.

The (^{3}He,^{7}Be) and (^{3}He,^{7}Li) reactions which were studied in the course of this investigation are reported in detail elsewhere[1]. The main results of this study can be summarized as follows:

I. Variation of (^{3}He,^{7}Be) ground-state cross sections with the mass of the target nucleus: A sharp decrease of the cross section has been observed between ^{12}C and ^{40}Ca (table IIAI). Although shell model calculations of the α-spectroscopic factors would predict such a decrease, we find that a simple quantum-mechanical effect, the increase of absorption with the radius of the target nucleus, is large enough by itself to explain the variation of the cross section. Consequently the α-spectroscopic factor prediction is not necessary to explain the sharp decrease between ^{12}C and ^{40}Ca that the shell model predicts.

Table IIAI

Approximate values of the differential cross section of the ground state (^{3}He,^{7}Be$_{(0)}$) transitions on several target nuclei around 10° CM with E(^{3}He)= 41 MeV. (Note the smooth decrease of the cross sections for "α-particle" nuclei and the generally smaller cross sections for the non-α nuclei.)

Target nucleus	^{12}C	^{14}N	^{16}O	^{19}F	^{20}Ne	^{22}Ne	^{27}Al	^{28}Si	^{40}Ar	^{40}Ca
dσ/dΩ (CM) (μb/sr)	800	40	120	100	75	35	15	35	20	20

[1] C. Détraz, C. D. Zafiratos, C. E. Moss and C. S. Zaidins, Nucl. Phys. to be published.

II. α-transfer selection rules: If the four-nucleon fragment transferred in (^{3}He,^{7}Be) reaction is in the internal quantum state of an α-particle, the transitions must obey the selection rules $\Delta T=0$ and $\Delta S=0$, regardless of the fact that ^{3}He and ^{7}Be have both non-zero spins and isospins. We have investigated, at E(^{3}He)=41.4 MeV, the ^{14}N(^{3}He,^{7}Be)^{10}B transition leading to the 1.74 MeV, 0^+, T=1 state of ^{10}B (Fig. IIA1).

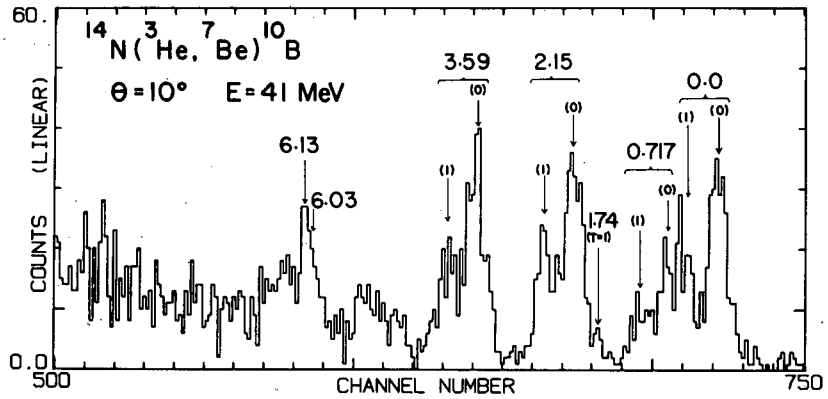

Fig. II A1 Energy spectrum of the ^{7}Be particles emitted at 10° in the ^{14}N(^{3}He,^{7}Be)^{10}B reaction at 41 MeV. Note the weak population of the 0^+, T=1 state at 1.74 MeV in ^{10}B.

This state was observed to be very weakly populated. Its cross section is between 1.5 and 2.5 μb/sr (CM) at forward angles. By comparison with the 0.717 MeV, 1^+, T=0 state which belongs to the same supermultiplet and has therefore the same spatial wave function, and after proper correction for the different spin multiplicities, it is found that, in this case, the $\Delta T=0$ selection rule inhibits the population of the 1.74 MeV, 0^+, T=1 state by a factor of about 5.

The effect of the $\Delta S=0$ selection rule is evident in the very weak population of the 8.88 MeV, 2^- state of ^{16}O in the ^{20}Ne(^{3}He,^{7}Be)^{16}O reaction at 41 MeV (Fig. II A2).

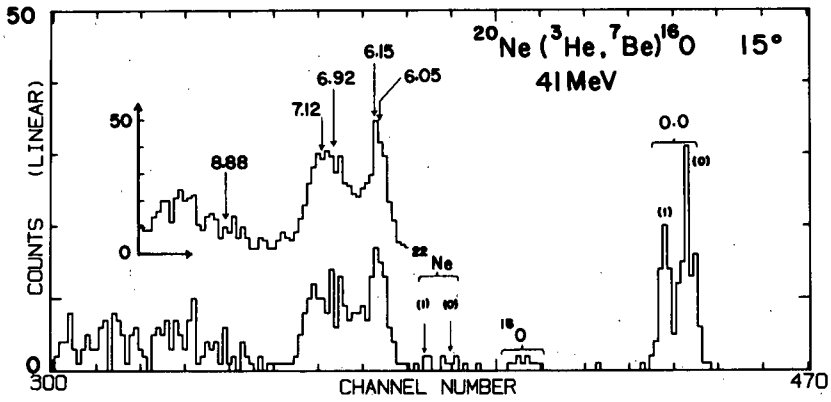

Fig. II A2 Energy spectrum of the ^{7}Be particles emitted at 15° in the ^{20}Ne(^{3}He,^{7}Be)^{16}O reaction at 41 MeV. The peaks labelled ^{16}O and ^{22}Ne result from (^{3}He,^{7}Be) reactions on these contaminants. The insert represents a sum of the ^{7}Be energy spectra at 10°, 15° and 20° properly corrected for the different kinematics. In spite of the improved statistics, no evidence is found for the population of the 8.88 MeV (2^-) state of ^{16}O.

III. T=1 transfer in (^{3}He,^{7}Be) reactions: Although the main features of (^{3}He,^{7}Be) point to the predominance of an α-transfer mechanism, it is interesting to characterize other feasible contributions to the cross section. These include the transfer of 2p + 2n while these four nucleons are in a T=1 state. A sensitive way to identify this mechanism is to look for the analog transition, a ^{4}H-like transfer, such as in the (^{3}He,^{7}Li) reaction. The first results of our (^{3}He,^{7}Li) studies, on ^{19}F and ^{12}C, were presented in last year's progress report. We have extended them to other target nuclei and confirmed the direct character of the reaction mechanism at forward angles of observation.

A comparison between the (^{3}He,^{7}Be) and (^{3}He,^{7}Li) cross sections was made. At forward angles, the ratio R of the (^{3}He,^{7}Li) and (^{3}He,^{7}Be) cross sections in ^{19}F is about 0.2. The pickup of a ^{4}H-fragment, to form ^{15}O in a direct (^{3}He,^{7}Li) reaction, and the pickup of a ^{4}He*(T=1) fragment, to form ^{15}N via the "non-α" transfer part of the (^{3}He,^{7}Be) reaction, constitute two analog processes. The corresponding differential cross sections will be equal to within a phase-space and isospin-coupling correction factor. In the present case this factor is equal to 0.98 and can be considered equal to 1 for all practical purposes. This means that the magnitude of the transition amplitude of the transfer of 2p + 2n while in a T=1 state is $\sqrt{0.2}$ of the (^{3}He,^{7}Be) transition amplitude at very forward angles. The contribution of this T=1 transfer to the (^{3}He,^{7}Be) cross section depends on the relative phases of the transition amplitudes corresponding to the two different 2p + 2n configurations. Interference effects might increase or decrease the figure of 20% which would be obtained by an incoherent summation of the cross sections corresponding to the two different processes, T=0 (α-like) and T=1 transfers. Other direct mechanisms in which the transferred fragment is again not in an α-like state can also contribute, as there exist many ^{4}He states above 20 MeV excitation energy which do not have T=1 but possess a structure similar to that of ^{4}H. This 20% figure must therefore be considered as a lower limit for the "non-α" transfer direct mechanisms.

Only for T_z=1/2 target nuclei are ^{4}H and ^{4}He*(T=1) transfers analog processes. The only other similar case studied is ^{27}Al for which the ratio R of the (^{3}He,^{7}Li) and (^{3}He,^{7}Be) ground state cross sections is again about 0.2. For the other targets studied, the contribution of ^{4}He*(T=1) transfer to the (^{3}He,^{7}Be) cross sections cannot be readily deduced from the values of R. In the cases where the (^{3}He,^{7}Li) ground state transitions could be reliably observed at small angles, the extracted values of R are presented in table II AII.

Table II AII

Ratio R of the (^{3}He,^{7}Li) and (^{3}He,^{7}Be) ground state transitions for several target nuclei at forward angles.

Target nucleus	^{12}C	^{14}N	^{16}O	^{19}F	^{20}Ne	^{27}Al	^{40}Ar
R	.03	.08	.05	.20	.10	.20	.17

IV. ^{4}H- and α- clustering probabilities: The ratios of (^{3}He,^{7}Li) to (^{3}He,^{7}Be) cross sections allow us, in principle at least, to extract relative probabilities for ^{4}H- and α- clustering in the ground state of the target nuclei. More specifically, they should provide us with the ^{4}H- and α- spectroscopic factors for the ground-state transitions. The estimation of D_o, the reaction strength, suffers from many uncertainties in a multi-nucleon transfer where the zero-range approximation is known to be in error. However, with very simplifying assumptions, an estimate of D_o was calculated[1] for both (^{3}He,^{7}Li) and (^{3}He,^{7}Be). D_o was found to be much larger for (^{3}He,^{7}Li) than for (^{3}He,^{7}Be), essentially because the binding energy of ^{4}H in ^{7}Li is much larger than that of ^{4}He in ^{7}Be. As a result, although the (^{3}He,^{7}Li) cross section is only five times smaller than the (^{3}He,^{7}Be) cross section on ^{19}F, it was concluded that the ^{4}H-spectroscopic factor was smaller than the α-spectroscopic factor by almost two orders of magnitude.

It should be noted that, in multi-nucleon transfer reactions, the contributions of complicated excited states of the transferred fragment might not be as negligible as intuitively anticipated. The corresponding spectroscopic factors should be small, but the reaction strength D_o, which increases with the binding energy of the transferred fragment in the nucleus where it is bound, might be able to compensate the spectroscopic unlikeliness.

ii. Isospin Purity at High Excitation Energies as Evidenced by Cross Correlations of Mirror-Channel Fluctuations - C. Détraz, C. E. Moss, C. D. Zafiratos, and C. S. Zaidins

For low-lying energy levels, isospin has been shown to be a good quantum number. With increasing excitation energy, though, the overlap of states with different T increases since the average width Γ of the levels becomes larger than their average separation distance D. The extent to which isospin is a good quantum number is accordingly predicted to deteriorate[1]. However, at still higher excitation energies, Γ becomes so large that it even exceeds the value of the isospin-mixing Coulomb matrix element $\langle H_c \rangle$. In other words, the half-life of the level becomes too short to let the Coulomb forces mix the isospin which should therefore again be a good quantum number[1,2].

Experimental confirmation of good isospin purity of highly excited levels is rather limited. It consists largely of a trend for isospin-nonconserving nuclear reactions (such as $\Delta T=1$ (d,α) reactions) to decrease in cross section with increasing bombarding energy[3]. However, the interpretation of these results in terms of isospin purity of an intermediate compound state is confused by the increasing role of direct mechanisms at higher bombarding energies. We wish to report what we think is experimental evidence of isospin purity for the overlapping levels of ^{22}Na near 53-MeV excitation energy.

In a study of the four-nucleon transfer reactions $^{19}F(^{3}He,^{7}Li)^{15}O$ and $^{19}F(^{3}He,^{7}Be)^{15}N$ near 40-MeV bombarding energy[4], compound-nucleus effects were found to dominate at backward angles, as evidenced by a strong energy dependence of the cross sections. Figure II A3 shows excitation functions at 165° for four decay

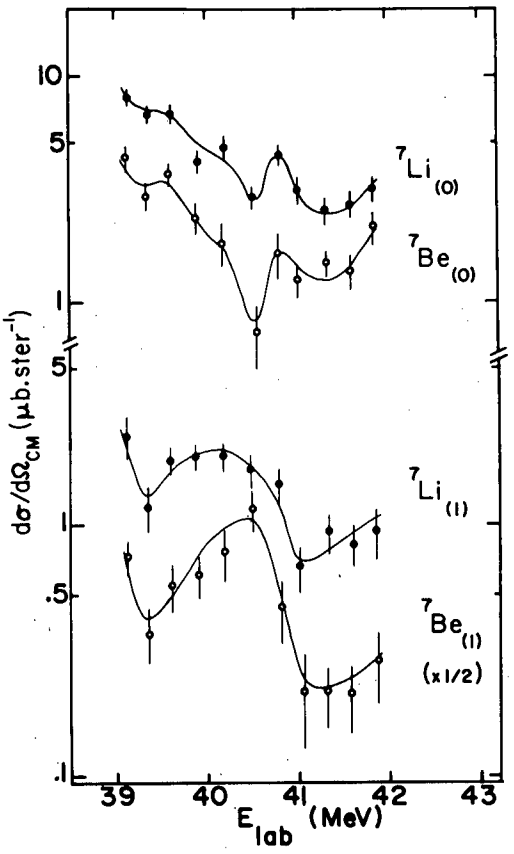

Fig. II A3 Excitation functions at θ_{lab}=165° for the reactions $^{19}F(^{3}He,^{7}Li_{(0)})^{15}O(g.s.)$, $^{19}F(^{3}He,^{7}Li_{(1)})^{15}O(g.s.)$, $^{19}F(^{3}He,^{7}Be_{(0)})^{15}N(g.s.)$, and $^{19}F(^{3}He,^{7}Be_{(1)})^{15}N(g.s.)$ between $E(^{3}He)$=39 and $E(^{3}He)$=42 MeV.

channels. Two involve the ^{15}O ground state (g.s.) with ^{7}Li being in either its ground (0) or first-excited (1) state. The other two involve the mirror nuclear system, ^{15}N and ^{7}Be, either in its ground (0) or first-excited (1) state.

No cross correlation is evident between the $^{7}Li_{(0)}$ and $^{7}Li_{(1)}$, or between the $^{7}Be_{(0)}$ and $^{7}Be_{(1)}$ excitation functions. All of them also strongly differ from the excitation function of the reaction $^{19}F(^{3}He,^{6}Li)^{16}O$ recorded simultaneously[5]. According to Ericson[6], the fact that different decay-channel cross sections fluctuate independently is proof that these oscillations are of statistical origin. Only a very rough estimate of the coherence width Γ could

be extracted from these data because of the short span of incident energies and the strong damping of oscillations at 165° due to the values of the spins[7]. Our estimate for Γ is consistent with the value (~800 keV) which can be extracted from the compilation of Ref. 7 and the value (1.1 MeV) observed for ^{20}Ne at 37.5-MeV excitation energy[8].

Two pairs of excitation functions in Fig. II A3 appear to be correlated. They correspond to the mirror $^{15}O + {}^{7}Li_{(0)}$ and $^{15}N + {}^{7}Be_{(0)}$ decay channels, and to the mirror $^{15}O + {}^{7}Li_{(1)}$ and $^{15}N + {}^{7}Be_{(1)}$ channels. A quantitative analysis of the cross correlations was performed to verify this qualitative indication[9].

Ericson fluctuations result from the coherent sum of the many matrix elements, random in phase and amplitude, which correspond to the overlapping levels constituting the compound state. The fact that in the present work these fluctuations are correlated for mirror decay channels indicates that the mirror nuclear systems equally overlap with the wave functions of these levels. Therefore we conclude that charge symmetry is preserved and that isospin is a good quantum number. Furthermore, as the cross section results from a coherent summation, it is highly sensitive to the details of the wave functions of the overlapping levels, which makes the observed correlation all the more remarkable. The preserved purity of isospin also confirms that the isospin-mixing Coulomb matrix element $\langle H_c \rangle$ is much smaller than $\Gamma \sim 1$ MeV in the range of excitation energies investigated here. At low excitation energies, the values of $\langle H_c \rangle$ typically lie between 1 and 40 keV[10], but larger core-excitation components of the wave functions of highly excited states would increase this value.

The extraction of a quantitative value of isospin purity from mirror-channel correlation coefficients would require a study of reactions with lower spins (to enhance the fluctuations) and higher yields.

---

1 D. H. Wilkinson, Phil. Mag. 1, 379 (1956); A. M. Lane and R. G. Thomas, Rev. Mod. Phys. 30, 257 (1958), in particular the discussion on p. 344.

2 H. Morinaga, Phys. Rev. 97, 444 (1954).

3 C. P. Browne, in Isobaric Spin in Nuclear Physics, edited by J. D. Fox and D. Robson (Academic, New York, 1966), p. 136; J. Jänecke, T. F. Yang, R. M. Polichar, and W. S. Gray, Phys. Rev. 175, 1301 (1968); J. Jobst, S. Messelt, and H. T. Richards, Phys. Rev. 178, 1663 (1969).

4 C. Détraz, C. E. Moss, C. D. Zafiratos, and C. S. Zaidins, Bull. Amer. Phys. Soc. 15, 1597 (1970), and to be published.

5 C. Détraz, C. E. Moss, C. D. Zafiratos, and C. S. Zaidins, Bull. Amer. Phys. Soc 15, 1685 (1970), and to be published.

6 T. Ericson, Phys. Rev. Lett. 5, 430 (1960).

7 T. Ericson, and T. Mayer-Kuckuk, Ann. Rev. of Nucl. Sci. 16, 183 (1966).

8 R. E. Brown, J. S. Blair, D. Bodansky, N. Cue, and C. D. Kavaloski, Phys. Rev. 138, B1394 (1965).

[9] C. Détraz, C. E. Moss, C. D. Zafiratos, and C. S. Zaidins, Phys. Rev. Lett. 26, 448 (1971).
[10] S. D. Bloom, Isobaric Spin in Nuclear Physics, edited by J. D. Fox and D. Robson (Academic, New York, 1966), p. 123; J. C. Hardy, J. E. Esterl, R. G. Sextro, and J. Cerny, UCRL Report No. UCRL-19951, 1970 (unpublished), and Phys. Rev. C (to be published).

iii. Comparison Between the (^{3}He,^{7}Be) α-Pickup Reactions on ^{40}Ca and ^{40}Ar

C. Détraz, R. A. Emigh, C. E. Moss, C. D. Zafiratos, and C. S. Zaidins

Recent studies[1,2] of the backward-angle behavior of elastically scattered alpha-particles have led to the suggestion[3] that the ground state of ^{40}Ca contains a substantially larger degree of alpha clustering than does ^{40}Ar. However, alternative explanations of the elastic scattering data did not invoke alpha-clustering[4,5]. Thus, we are left with an interesting question: are ^{40}Ca and ^{40}Ar substantially different in the degree to which they overlap with a core + alpha model? Since ^{40}Ca is one of the A=4n "alpha-particle" nuclei and furthermore closes the sd shell, while ^{40}Ar contains two more neutrons and two less protons, it seems reasonable that substantial differences with regard to alpha-cluster probabilities could exist between them.

In order to detect possible differences in alpha clustering we studied the (^{3}He,^{7}Be) reaction on targets of ^{40}Ca and ^{40}Ar. A substantial body of evidence already exists for the alpha-pickup character of the (^{3}He,^{7}Be) reaction[6-8]. This evidence shows that compound-nucleus effects are small and that the transferred group of 4 nucleons is predominantly in a $J^\pi=0^+$, T=0 configuration. These quantum numbers alone do not imply that the spatial wave function of the transferred fragment completely overlaps with the wave function of an alpha particle (that is, a ^{4}He nucleus in its ground state). Hence the name alpha-*like* transfer is frequently used. Although it has been established that the four transferred nucleons can be in states other than the ground state of ^{4}He, the contributions of these states are not very important[8].

The situation is quite different in reactions like (^{16}O,^{12}C) or the inverse where, due to j-j coupling in the projectile, nuclear states of quartet structure can be excited though they may have poor overlap with an alpha + core wave function[9]. Such states, for example, can consist of two neutron-proton pairs, each pair coupled to J_{max}, with the two pairs coupled to $J^\pi=0^+$. These states made of (classically) counter-rotating n-p pairs can be strongly excited by (^{16}O,^{12}C) reactions, but the spatial symmetry forced by the L-S coupling of ^{7}Be causes the (^{3}He,^{7}Be) reaction to be dominated by alpha-particle transfer. A comparison of cross sections for the (^{3}He,^{7}Be) reaction is, accordingly, a valid method of comparing alpha-particle spectroscopic factors for the target ground states.

The experimental data presented here were obtained with standard ΔE-E counter telescope methods utilizing 41 MeV ^{3}He projectiles from the University of Colorado 1.3 meter cyclotron. Targets of CaF_2 were used for the $^{40}Ca(^{3}He,^{7}Be)^{36}Ar$ measurements. Target thicknesses were determined both by the energy loss of alpha-particles from ^{241}Am sources and by the Rutherford scattering of 4 MeV alpha-particles. Two gas cells were used for the ^{40}Ar measurements. One cell of larger size was used from $\theta_{lab}=7.5°$ to 25° while the other covered the range from 25° to larger angles. The cross sections obtained at 25° with the two cells agreed to within the statistical errors. Furthermore, the $^{12}C(^{3}He,^{7}Be)^{8}Be$ differential cross sections measured using methane gas in both gas cells agreed with those measured with a solid carbon target. Energy spectra for the two reactions are presented in Fig. II A4. Note that a low-lying 2^{+} level, as well as the

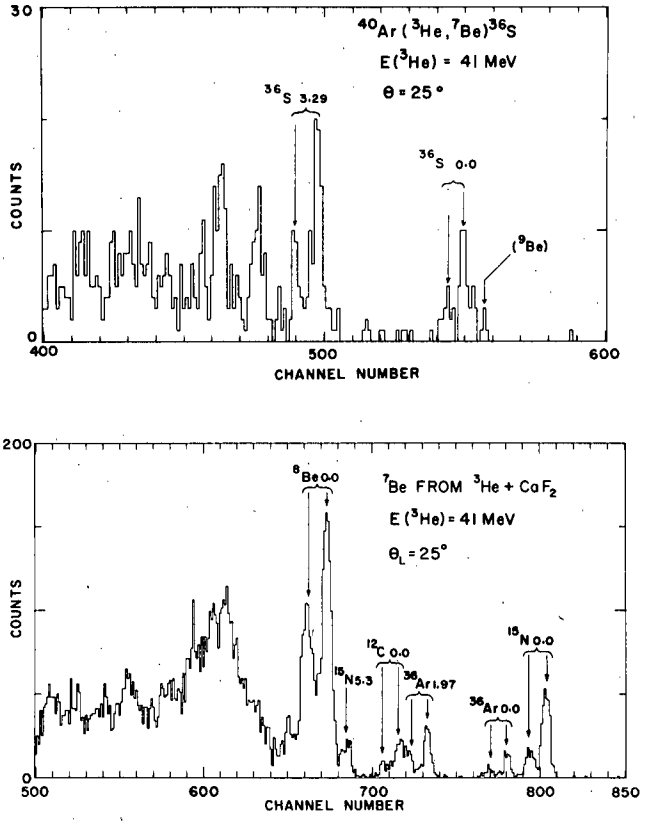

Fig. II A4 Energy spectra of Be ions from 41 MeV ^{3}He bombardment of a CaF_2 + carbon target (bottom) and a gas cell filled with argon gas (top). The ^{7}Be doublets are labeled with the final nucleus and its excitation energy. In the ^{40}Ar spectrum, the peak labeled (^{9}Be) is due to the $^{40}Ar(^{3}He,^{9}Be)^{34}S$ (2.13 MeV) reaction.

ground state, in each residual nucleus is strongly excited. Unfortunately, contaminant problems prevented complete angular distributions from being obtained for these levels in both ^{36}Ar

and ^{36}S. However, no strong difference between ^{36}Ar and ^{36}S was noted in the ratios of 2^+ to ground state strengths. Angular distributions for the $^{40}Ar(^3He,^7Be)^{36}S$ and $^{40}Ca(^3He,^7Be)^{36}Ar$ reactions to the ground states of the residual nuclei are shown in Fig. II A5.

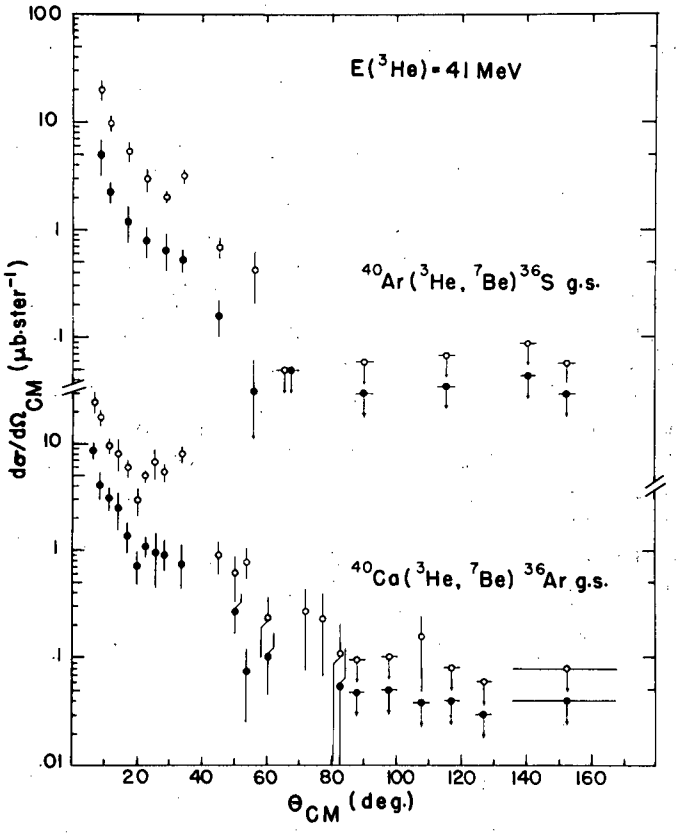

Fig. II A5 Angular distributions for the $^{40}Ar(^3He,^7Be)^{36}S$ (g.s. and $^{40}Ca(^3He,^7Be)^{36}Ar$ (g.s.) reactions. Open circles correspond to the ground state of the ^7Be ejectile; solid circles to its first excited state. The ^7Be excited state data are shifted down by a factor of two for clarity. At backward angles only upper limits were obtained and are indicated by the horizontal bars. Only the statistical errors are shown. The uncertainty in the absolute cross section is estimated to be 30%.

Since the ^7Be ejectile can be observed in either its ground state or first excited state, both angular distributions are shown for each target.

In the appropriate alpha-cluster model of ^7Be the $3/2^-$ ground state and $1/2^-$ first excited state of ^7Be arise from the two possible couplings of the ^3He spin with a 2p relative motion of the ^3He and alpha clusters. Accordingly, an alpha-pickup model of the $(^3He,^7Be)$ reaction would predict no difference in the shape of the angular distributions for these two states aside from small spin-orbit effects. However, the 2J + 1 statistical factor leads to the $3/2^-$ ground state of ^7Be having twice the cross section of the $1/2^-$ level.

The data bear out this prediction. The absence of a backward rise of the angular distributions indicates that the forward angle cross sections are due to a direct process.

In a DWBA model of the (^{3}He,^{7}Be) reaction the probability for finding an alpha-particle coupled to the ground state of the residual nucleus would be contained in an alpha-particle spectroscopic factor defined by:

$d\sigma/d\Omega_j(\text{exp}) = S_{\alpha j}\ d\sigma/d\Omega(\text{DWBA})_j$ where j labels the state of the residual nucleus. DWBA calculations for (^{3}He,^{7}Be) are quite difficult due to the ℓ=1 relative motion in ^{7}Be and the importance of finite-range effects. No great differences are expected for $d\sigma/d\Omega\ (\text{DWBA})_{g.s.}$ between ^{40}Ca and ^{40}Ar since the Q values are very close (-5.45 MeV and -5.22 MeV, respectively) and optical model potentials should be quite similar for the two reactions. Direct comparison of the experimental data will, in this case, give the relative spectroscopic factors. The forward-angle data for the sum of the ^{7}Be ground state and first excited state differential cross sections are shown in Fig. II A6. Though small differences are apparent, the striking feature is the similarity of the cross sections. We conclude, therefore, that the alpha-particle spectroscopic factors for the ground state transition, $S_{\alpha o}$, are quite similar for ^{40}Ar and ^{40}Ca.

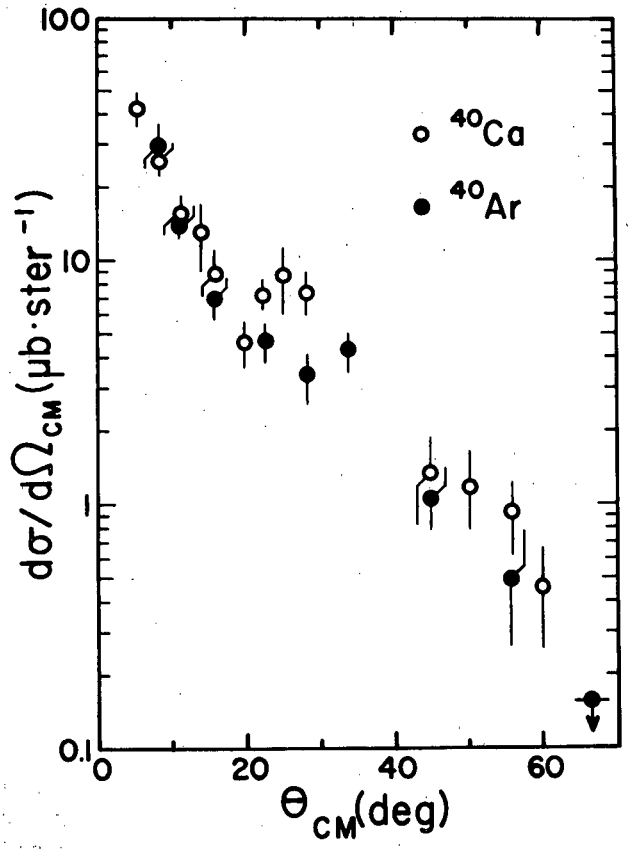

Fig. II A6 The data of Fig. IIA5 with the ^{7}Be(0) and ^{7}Be(1) cross section summed. The Ca and Ar data are here plotted on the same scale for ease of comparison.

The total alpha-particle clustering probability involves a sum over the $S_{\alpha j}$'s, not just $S_{\alpha o}$ for the ground state transition. However, the differences between the structure, and hence $S_{\alpha j}$, of the residual nuclei ^{36}Ar and ^{36}S must be largest for the ground state and become smaller as the excitation energy increases. Hence, the observed similarity of $S_{\alpha o}$ for ^{40}Ca and ^{40}Ar is strong evidence against the hypothesis that these two nuclei have markedly dissimilar alpha clustering.

A report on this work has been published elsewhere[10].

---

1 G. Gaul, H. Lüdecke, R. Santo, H. Schmeing, and R. Stock, Nucl. Phys. A137, 177 (1969).
2 A. Budzanowski, A. Dudek, R. Dymarz, K. Grotowski, L. Jarczyk, H. Niewodniczanski, and A. Strzalkowski, Nucl. Phys. A126, 369 (1969).
3 N. C. Schmeing, Nucl. Phys. A142, 449 (1970).
4 K. A. Eberhard, Phys. Lett. 33B, 343 (1970).
5 W. J. Thompson, Bull. Am. Phys. Soc. 16, 647 (1971).
6 C. Détraz, H. H. Duhm, and H. Hafner, Nucl. Phys. A147, 488 (1970).
7 For evidence of the alpha-transfer character of (^{7}Li,t), the mirror and time-reversed reaction of (^{3}He,^{7}Be), see, e.g. R. Middleton, in Nuclear Reactions Induced by Heavy Ions, edited by R. Bock and W. R. Hering, (North-Holland Publishing Co., Amsterdam, 1970).
8 C. Détraz, C. D. Zafiratos, C. E. Moss, and C. S. Zaidins, to be published.
9 V. Gillet, Proceed. Intern. Conf. onf Properties of Nuclear States (Les Presses de l'Université de Montréal, 1969) p. 483.
10 C. D. Zafiratos, C. Détraz, C. E. Moss, C. S. Zaidins, Phys. Rev. Lett. 27, 437 (1971).

iv. (^{3}He,^{7}Be) Reaction Investigation in the Mass 90 Region - C. Détraz, H. Rudolph, C. D. Zafiratos, C. S. Zaidins

A preliminary study of the (^{3}He,^{7}Be) reaction on ^{92}Zr and ^{93}Nb targets has been made at E(^{3}He)=41 MeV. Data were obtained at laboratory angles of 10°, 15° and 25°. These preliminary measurements show some interesting features.

The cross sections measured are small (a few μb/sr), yet strong selectivity of the final states which are populated indicates that compound-nucleus contributions are very small in this mass region (as they were for lighter nuclei). In particular, the ^{93}Nb(^{3}He,^{7}Be)^{89}Y reaction populates the $9/2^{+}$ first excited state of ^{89}Y with a cross section comparable to that of the ^{92}Zr(^{3}He,^{7}Be)^{88}Sr ground state transition. Yet the $1/2^{-}$ ground state of ^{89}Y is not observed (at least one order of magnitude less than the first excited state, with our present statistics).

This kind of selectivity is expected for a simple pickup reaction. For such a process, the single $g_{9/2}$ proton of ^{93}Nb plays the role of a

spectator while the same paired protons (and neutrons) which were present in ^{92}Zr are picked up, leaving the final nucleus, ^{89}Y, in its first excited state. Although a weak-coupling description of the last proton in both ^{93}Nb and ^{89}Y has been shown (by single-proton stripping studies) to be reasonable, the presence of the extra proton in ^{93}Nb and ^{89}Y may perturb the coupling of the last proton pair. The present (^{3}He,^{7}Be) studies should provide a quantitative measure of this effect.

b. Study of (p,t) Reactions on Intermediate Mass Nuclei

i. Study of the (p,t) Reaction on the Even-A Titanium Isotopes - H. W. Baer, J. J. Kraushaar, C. E. Moss, N. S. P. King, R. E. L. Green, P. D. Kunz, and E. Rost

An extensive analysis has been carried out of the $^{46,48,50}Ti(p,t)$ data taken at 27, 23, and 19 MeV and reported in last year's Progress Report. The angular distribution (5°-110° lab) of approximately thirty transitions at 27 MeV with L=0, 2, 3, and 4 were examined for characteristic features which could be uniquely associated with the L-transfer. Both the empirical systematics and the comparisons with DWBA predictions were found to provide less reliable L-value determinations, other than for L=0, than is often assumed. Our results indicate that data on the second and third maxima of the angular distributions are necessary, though not always sufficient, to uniquely determine the L-value. The major results of the study are shown in Figs. II A7, II A8, and II A9. The optical model potentials used in the various distorted wave calculations are shown in Table II AIII.

A large number of variations in the distorted wave calculations were carried out. We found that the predicted angular distribution shapes are sufficiently sensitive to the input parameters and choice of pickup configurations to make unique L-value determinations difficult. Successful aspects of the DWBA calculations are indicated by the fact that when we employed a recently developed energy dependent mass-3 optical potential, which is described elsewhere in this report, we could reproduce the variations with bombarding energy of the differential cross sections in the $^{50}Ti(p,t)^{48}Ti$ (g.s.) transition. Moreoever, the shapes of numerous L=0,2,3, and 4 transitions at 27 MeV were well described in the range 10° to 115° by using the new mass-3 potential. However, not all data were well described. Representative of this class is the L=2 angular distribution for the 2_1^+ state in ^{44}Ti for which the DWBA calculations gave poor agreement. The data on the 2_1^+ states in $^{46,48}Ti$ were quite well described. We take this as evidence that initial and final state nuclear structure can affect the angular distribution shapes. This point was supported with DWBA calculations which show that the use of the two transfer configurations $(1f_{7/2})^2 \pm 0.5\ (2p_{3/2})^2$ leads to different shapes for

L=0 and 2 transitions. This further emphasizes the fact that it is risky to make L-assignments, as is sometimes done in the literature, by comparing data to DWBA calculations which assume greatly simplified pickup configurations. Even when there is good agreement between the data over a limited angular range and a DWBA calculation with a specific set of assumptions, the L-transfer may not be correctly determined.

The results of this experiment along with the analysis have been prepared for publication. The theory of the distorted wave calculations and detailed theoretical expressions employed in the computer code DWUCK are included in the publication.

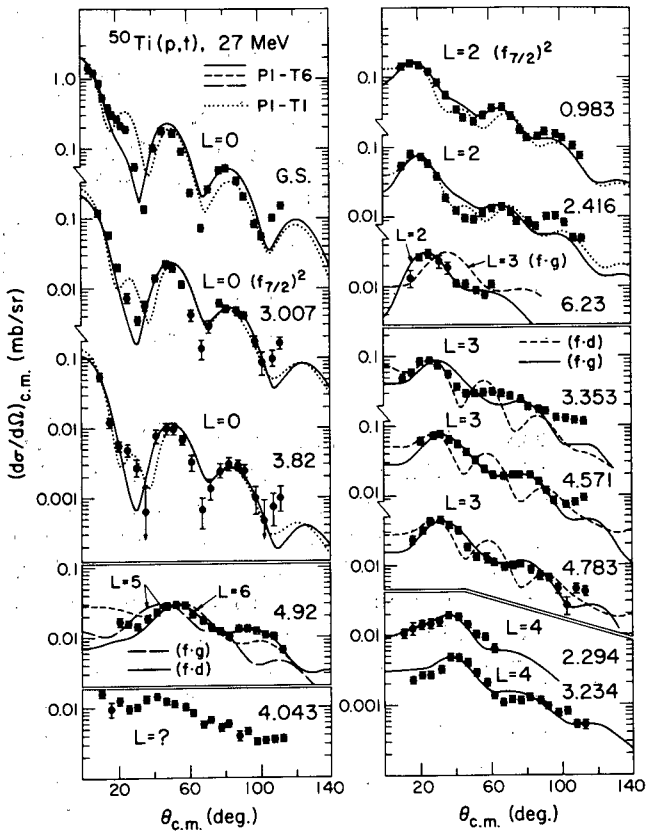

Fig. II A7 Data on the ^{50}Ti(p,t) reaction are shown and compared with DWBA predictions. The calculations displayed with dotted lines employed the optical potential parameter set P1-T1, those with solid lines, long dashes, and short dashes employed parameter set P1-T6. The assumed pick-up configurations were $(1f_{7/2})^2$ for L=0,2,4, and 6 and $(1f_{7/2}1d_{3/2})$ or $(1f_{7/2}1g_{9/2})$ for L=3 and 5. The fits to the L=0,2,4 transitions are quite excellent. The L=3 angular distributions are better fit with an assumed $(1f_{7/2}1g_{9/2})$ pickup than with $(1f_{7/2}1d_{3/2})$ pickup, although the latter is expected to have a larger spectroscopic amplitude. The predictions for the high spin state at 4.92 MeV are sufficiently similar to preclude a unique L assignment.

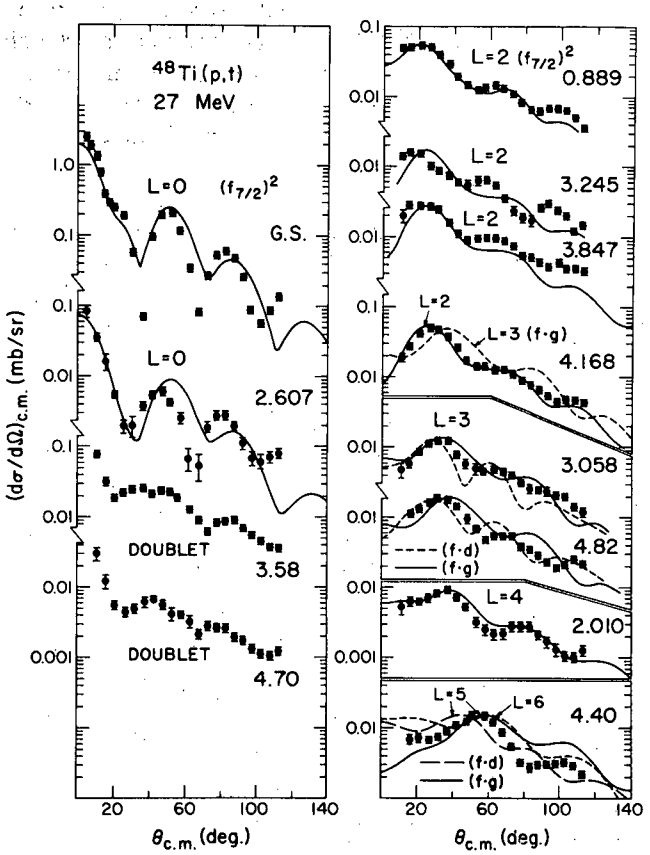

Fig. II A8 Data on the ^{48}Ti(p,t) reaction are shown and compared with DWBA predictions. The optical potential parameter set P1-T6 was employed in all calculations. Assumed pickup configurations are specified in the caption for Fig. II A7. We note that the fits to L=2 transitions are not uniformly good. The predictions for L=3 and L=5 transitions are seen to be quite sensitive to the choice of configurations, differing by nearly 10° in the position of the primary maxima for the two sets of calculations shown. The triton groups leading to states at 3.58 and 4.70 MeV are believed to be doublets. The sharp rise in differential cross sections at forward angles establishes the presence of an L=0 component.

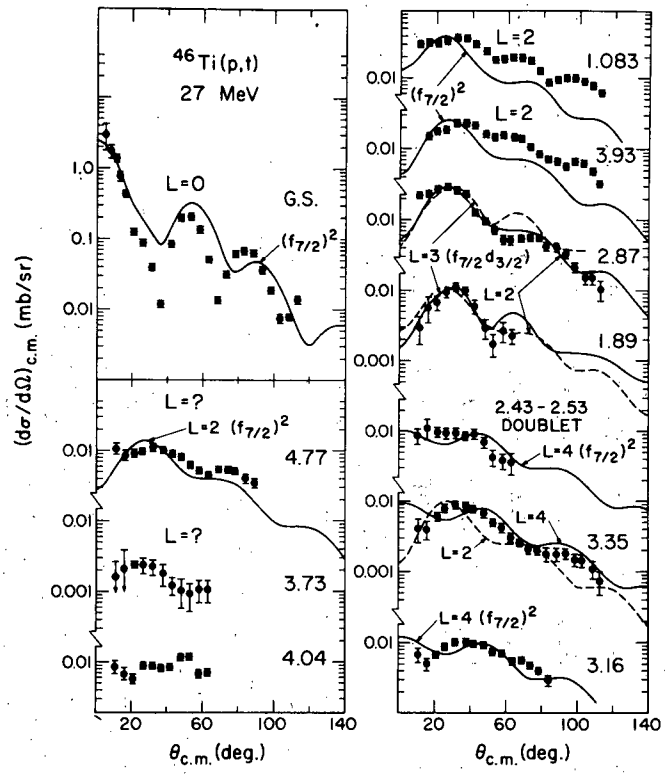

Fig. II A9 Data on the ^{46}Ti(p,t) reaction are shown and compared with DWBA predictions. The optical potential parameter set P1-T6 was employed in all calculations. The assumed pickup configurations are specified in the caption in Fig. II A7. The comparisons between data and calculations indicate that, except for 0^+ states, it is difficult to determine unique J^π values for states in ^{44}Ti on this basis. It is interesting to note that the first peak for the state at 1.083 MeV occurs near 40°, a value characteristic of L=4 transitions in the other nuclei studied. The DWBA description for this state is much poorer than for the other 2_1^+ states. Also of interest is the state at 1.89 MeV. Other studies suggest $J^\pi=0^+$ whereas our data are consistent only with $J^\pi=2^+$ or 3^-.

TABLE II AIII

OPTICAL-MODEL AND BOUND-STATE WELL PARAMETERS USED IN THE DISTORTED-WAVE BORN APPROXIMATION ANALYSIS OF THE ^{50,48,46}Ti(p,t) REACTIONS

Reaction[a]		V (MeV)	r_o (F)	a (F)	W (MeV)	W_D (MeV)	r_o' (F)	a' (F)	V_{so} (MeV)	r_{so} (F)	a_{so} (F)
^{50}Ti+p	P1	55.4	1.12	0.78	3.2	6.4	1.32	0.594	6.2	0.98	0.75
^{48}Ti+p	P1	54.6	1.12	0.78	3.2	6.0	1.32	0.568	6.2	0.98	0.75
^{46}Ti+p	P1	53.7	1.12	0.78	3.2	5.5	1.32	0.540	6.2	0.98	0.75
^{48,46,44}Ti+t	T6	V_t	1.10	0.853	...	W_{tD}	1.308	0.751	...	...	...
^{48,46,44}Ti+t	T1	165.4	1.16	0.752	16.4	...	1.498	0.817	...	...	...
bound state		V_n	1.25	0.65	...	...	...	...	λ=25	1.25	0.65

[a] The optical-model potential U(r) and bound state potential V(r) have the forms

$$U(r) = -V(e^x+1)^{-1} - i(W-4W_D d/dx')(e^{x'}+1)^{-1} + (\hbar/m_\pi c)^2 V_{so}\vec{r}\cdot\vec{\ell}\, r^{-1}d/dr\,(e^{x_{so}}+1)^{-1} + V_C$$

$$V(r) = V_n(e^x+1)^{-1} + (\lambda_n/45.2)V_n r^{-1}\vec{\ell}\cdot\vec{s}(d/dr)(e^x+1)^{-1} + V_C.$$

V_C is the Coulomb potential due to a uniformly charged sphere of radius 1.25 $A^{1/3}$F. The energy dependence of the well depths for triton potential T6 is given by: V_t=138.8 - 0.157 E_t, $4W_{tD}$=149.8 -2.083 E_t + 0.0148 E_t^2 where E_t is the triton laboratory energy. The neutron well depths were adjusted to give each orbit a binding energy $-0.5(S_{2n}+E_x)$, where S_{2n} is the two-neutron separation energy and E_x the excitation energy in the residual nucleus.

ii. The $^{50}Cr(p,t)^{48}Cr$ Reaction - J. R. Shepard, R. A. Ware, J. J. Kraushaar

Significant spectroscopic contributions have arisen from the study of this reaction. Knowledge of both the Q-value for the reaction and the energy level scheme of the residual nucleus, ^{48}Cr, were quite limited. The Q-value quoted in the literature[1] is Q_o=-14.840 ± 0.200 MeV. The value obtained in this study is Q_o=-15.093±0.015 MeV, which differs considerably from the standard value. Energy levels in ^{48}Cr at excitation energies of 0.0, 0.766, 1.862, 3.472, 3.643, 4.162, 4.276, 5.665, and 6.041 MeV were observed. Angular distributions over the range 10°-110° (lab) were measured for the first seven of these states. Comparison of the shapes of these angular distributions with DWBA calculations suggested the following spin and parity assignments: g.s., $J^\pi=0^+$; 0.766, 2^+; 1.862, 2^+ and 4^+ (doublet); 3.472, 2^+; 3.643, 2^+ or 3^-; 4.162, 2^+ or 3^-; 4.276, 0^+. The angular distributions and DWBA calculations are displayed in Fig. II A10. A preliminary assignment of 0^+ for the weak state at 5.665 MeV excitation is based on its low angle enhancement, characteristic of L=0 angular momentum transfers in this mass-energy region.

The nucleus ^{48}Cr occupies a unique place in the $1f_{7/2}$ shell; it is precisely in the middle of the shell, with 4 protons, 4 neutrons, 4 protons holes, and 4 neutron holes. Thus the nucleus could be expected to exhibit many interesting symmetry properties. At present no shell-model calculations of the ^{48}Cr energy levels are available, but this will be remedied soon. Calculations based on a quartet (alpha-cluster) model of ^{48}Cr have been made[2] and suggest a quartet excited state with $J^\pi=0$ at approximately 4.00 MeV. The 0^+ state at 4.276 MeV excitation is a candidate.

---

[1] J. H. E. Mattauch, et al., Nucl. Phys. 67 (1965) 1.
[2] Arima, et al., Phys. Rev. Lett. 25 (1970) 1043.

iii. The $^{52}Cr(p,t)^{50}Cr$ Reaction - H. W. Baer, J. J. Kraushaar, J. R. Shepard, B. W. Ridley

Investigation of the $^{52}Cr(p,t)^{50}Cr$ reaction was highlighted by the discovery of new low-lying 0^+ states. Such states in nuclei of the $1f_{7/2}$ shell and measurements of the relative cross sections for the formation of these states via (p,t) and (t,p) reactions have played an important role in understanding the structure of nuclei in this mass region. This is due, in part, to the fact that the 0^+ states reflect more directly than any other type of state the active configuration vector space. In this section we report such measurements on the (p,t) reaction for four previously unreported 0^+ states in the 3-5 MeV region of the stable nucleus ^{50}Cr. In addition, evidence for new low-lying 3^- and 4^+ states is presented.

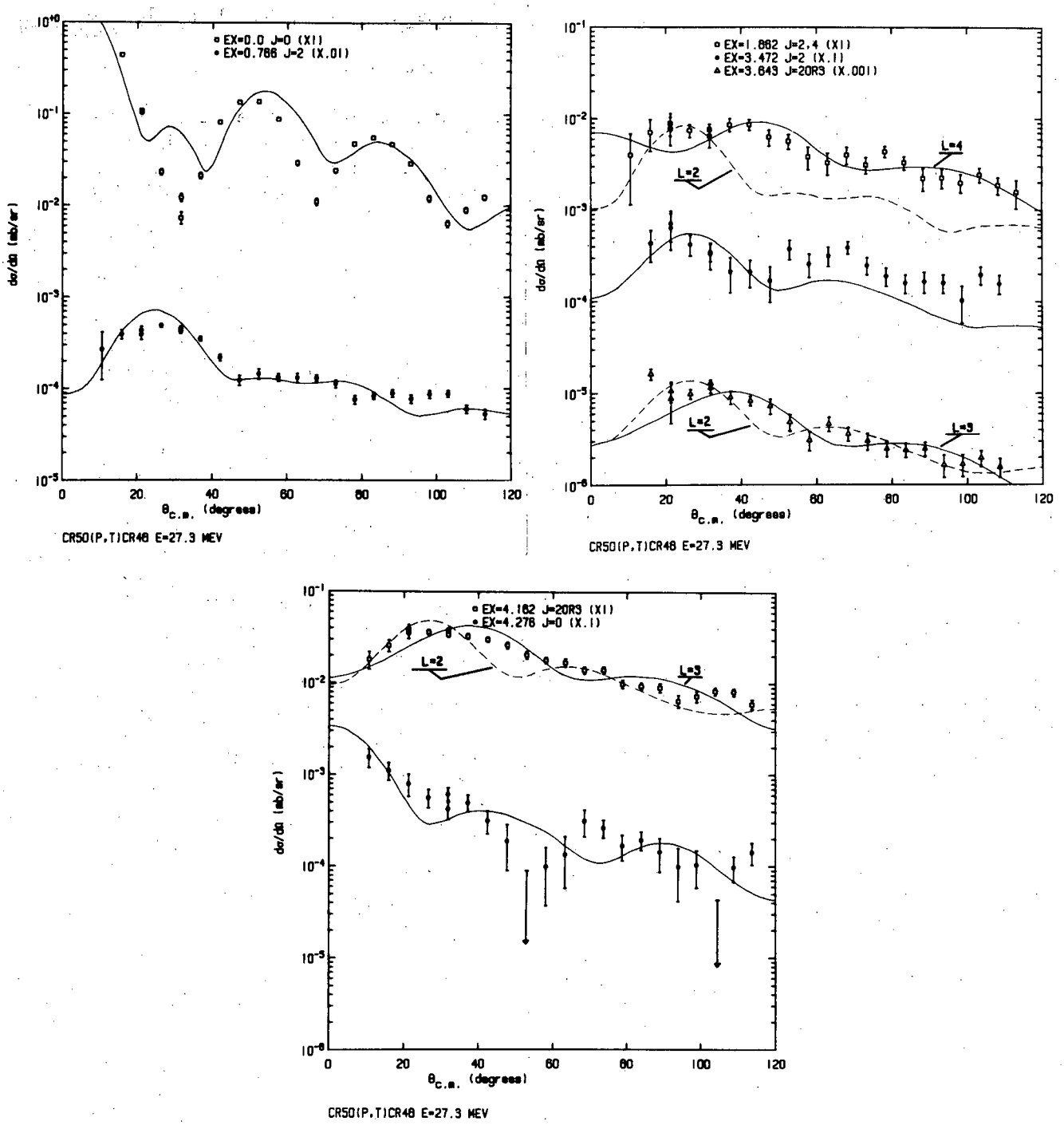

Fig. II A10 Angular distributions for the first seven triton groups in the $^{50}Cr(p,t)^{48}Cr$ reaction at E_p=27.3 MeV. Excitation energies and spin and parity assignments indicated are those measured in this experiment. The indicated DWBA calculations were performed with the following optical model potentials for protons (tritons): V=-53.629 MeV (-165.4 MeV); r=1.12 fm (1.16 fm); a=0.780 fm (0.752 fm); W=-3.306 MeV (-16.4 MeV); W_D=-5.43 MeV (0.0); r'= 1.32 fm (1.498 fm); a'=0.538 fm (0.817 fm); V_{so}=-6.2 MeV (0.0); r_{so}=0.980 fm (0.0); a_{so}=0.750 fm (0.0).

The identification of the 0^+ states is based on the fact that the known[1] L=0 transitions for the (p,t) reaction on nuclei in this mass region at bombarding energies near 27 MeV and at low excitation energies in the residual nuclei all show a sharp rise in the differential cross section between the first minimum and the primary maximum at 0°. This rise is observed, for example, in the L=0 transitions having only a few percent of the ground-state strength in the ^{48,50}Ti(p,t) reactions. In contrast, transitions with $L \geq 2$ have measured differential cross sections which remain nearly constant in this angular range or decrease in approaching 0° (e.g., Fig. II A11). The population of 1^- states has not been reported in this mass region in either the (p,t) or (t,p) reactions. On theoretical grounds, one expects the lowest negative parity states in ^{50}Cr to arise predominantly from the coupling of a $1d_{3/2}$ neutron hole to the $7/2^-$ ground state of ^{51}Cr. This suggests that the lowest 1^- state, which cannot

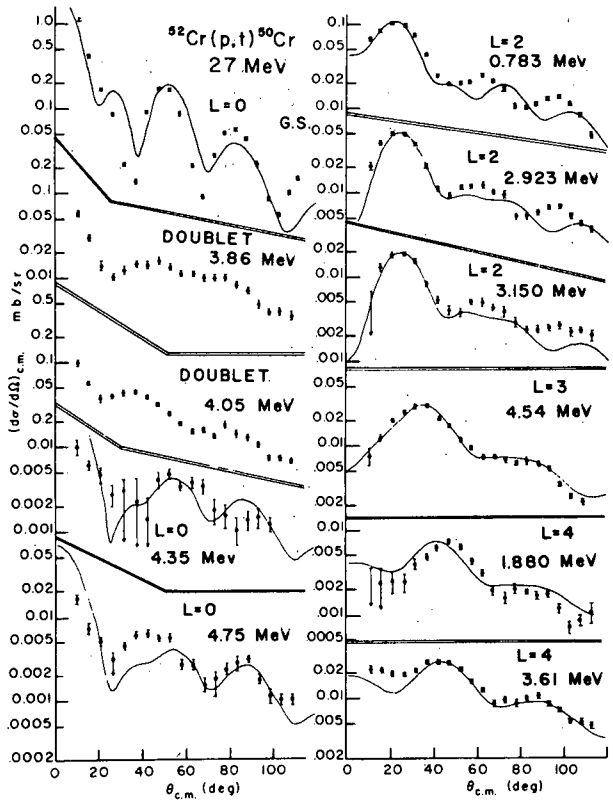

Fig. II A11 Angular distributions of ^{52}Cr(p,t) transitions. The triton groups at 3.86 and 4.05 MeV are believed to be doublets. Solid lines are DWBA calculations corresponding to the pickup of a single neutron pair. The optical potential parameters (in MeV and fm. resp.) are for the proton (triton): V=54.6(165.4), r_o=1.12 (1.16), a=0.78 (0.752), W=3.2 (16.4), W_D=6.0 (0.0), r_o'=1.32 (1.498), a'=0.564 (0.917), V_{so}=6.2 (0), r_{so}=0.98 (0), a_{so}=0.75 (0), in the notation defined in ref. 1. The neutron single-particle wave functions are eigenstates of a Woods-Saxon well (r_o=1.25 fm, a=0.65 fm, λ=25) adjusted to give each neutron one-half the two-neutron separation energy.

contain such a component, lies considerably above the lowest 3^- state. If we assume the latter to be the 4.54 MeV level observed in the present experiment, it is quite probable that the lowest 1^- state lies well above 5 MeV. As a guide to what might be expected for an L=1 angular distribution, we performed DWBA calculations corresponding to $(1f_{5/2}1d_{3/2})$ and $(2p_{3/2}1d_{3/2})$ pickup to states at 3.4-4.5 MeV. All the calculations predict a peak at approximately 15° with a drop in cross section of about 20% at 10° and 20°. The data are incompatible with this prediction. Thus on the basis of the above systematics and theoretical considerations, the measurements displayed in Fig. II All indicate the existence of 0^+ states in ^{50}Cr at 3.86, 4.05, 4.35 and 4.75 MeV. The absence of the oscillatory structure characteristic of L=0 angular distributions for the states at 3.86 and 4.05 MeV is most likely due to contributions from the known nearby states.

A shell model calculation by Pittel[2] which employed $(1f_{7/2})$ matrix elements inferred from recent data on the ^{42}Sc spectrum predicts 0^+ states at 4.6, 6.3, 7.9 and 9.2 MeV. The fact that we observe four 0^+ states below 4.9 MeV thus is evidence that one must extend the vector space in the description of ^{50}Cr.

It is interesting to compare the present observation of four 0^+ states in the 1 MeV band of excitation 3.8-4.8 MeV in ^{50}Cr with the systematics of 0^+ states in neighboring nuclei. In other N=26 nuclei, for example, the following has been found: a total of four 0^+ states in the 3.0-5.0 MeV region of ^{48}Ti, four levels spread over the 2.4-5.7 MeV region of ^{46}Ca and four levels spread over the region 4.1-8.6 MeV of ^{52}Fe. In ^{52}Cr four 0^+ states were observed in the 2.6-5.8 MeV region, whereas only three such states were observed in ^{54}Cr in the same excitation region. From these systematics we see that in ^{50}Cr the four 0^+ states are concentrated into an unusually small excitation region and the explanation of this should be of interest in future theoretical studies.

Spin-parity information is provided on six other states through a comparison of the measured angular distributions with those of known L-values in the present reaction and with DWBA calculations. The following new J^π assignments are given: 2^+ for states at 2.923 and 3.150 MeV; 4^+ for states at 1.880 and 3.61 MeV. The value 3^- is strongly suggested for the state at 4.54 MeV on the basis of the position of the first peak in the angular distribution and the good agreement with the DWBA prediction. No other 3^- state has been reported for ^{50}Cr.

---

[1] H. W. Baer, et al., Phys. Rev. Lett. 25 (1970) 1035; Bull. Am. Phys. Soc. 15 (1970) 528; Univ. of Colorado Technical Progress Report AT(11-1)-535.

[2] S. Pittel, private communication.

iv. Investigation of the $^{26}Mg(p,t)^{24}Mg$ Reaction Near E_p=26 MeV - J. R. Shepard, J. J. Kraushaar, H. W. Baer

The $^{26}Mg(p,t)$ reaction proved to be of particular interest. In this reaction a state of unnatural parity, the 5.22 MeV 3^+ state of ^{24}Mg, was found to be strongly excited although the selection rules evolving from the assumption of a simple single-step DWBA reaction mechanism forbid such an excitation. Furthermore, drastic deviations from DWBA theoretical predictions were observed for the experimental angular distributions of transitions to higher-lying (> 6 MeV) excited states. This effect is shown in Fig. II A12. These facts indicated that processes other than the usual single-step DWBA mechanism were operative. Compound nuclear effects were ruled out by thorough examination of the variation with energy of both the magnitudes and shapes of the angular distributions for transitions to the first eight states in ^{24}Mg, including the 5.22 MeV 3^+ state. As Figs. II A12 and II A13 show, no variation of either type with energy was observed, suggesting negligible compound nuclear contributions. Another possible non-standard DWBA process which could account for the excitation of the 5.22 MeV 3^+ state is a spin-transfer reaction which requires the presence of an S=1 (rather than the usually assumed S=0 configuration) dineutron component in the triton. This type of reaction can be easily treated with the DWBA, and is, of course, a major factor in the $(p,^3He)$ reaction. By employing spin-transfer, the DWBA predicts a cross section consisting of an incoherent sum of L=2 and L=4 orbital-angular-momentum-transfer angular distributions. However, the theoretical calculations show that the strength of the L=2 component should be the greater of the two by at least a factor of 15 to 20. The experimental angular distribution for the transition to the 5.22 MeV 3^+ state can be seen, by referring to Fig. II A12, to have a shape much more like that of the 6.00 MeV 4^+ state than that of any angular distribution involving an L=2 transfer. Thus it seems very unlikely that such a spin transfer mechanism is significant in the excitation of the 3^+ state.

Supporting this conclusion is the relatively large magnitude of the cross section for excitation of this state. Peterson and Rudolph[1] have shown that spin transfer effects in the $^{57}Fe(p,t)^{55}Fe$ reaction account for less than 5% of the $1/2^- \rightarrow 1/2^-$ transition. Interpretation and extrapolation of this number is of course dangerous, but in view of the fact that the cross section for the excitation of the 3^+ state in ^{24}Mg is 30-50% of that for nearby excited states, the spin transfer mechanism seems all the more unlikely.

The conclusion of these invetigations was that multi-step processes not accounted for by simple single-step DWBA calculations were responsible for the excitation of the 5.22 MeV 3^+ state and possibly for the unusual shapes of the angular distributions for the transitions to the higher-lying excited states. This contention is supported by the fact that Ascuitto *et al.*[2] have shown that multi-

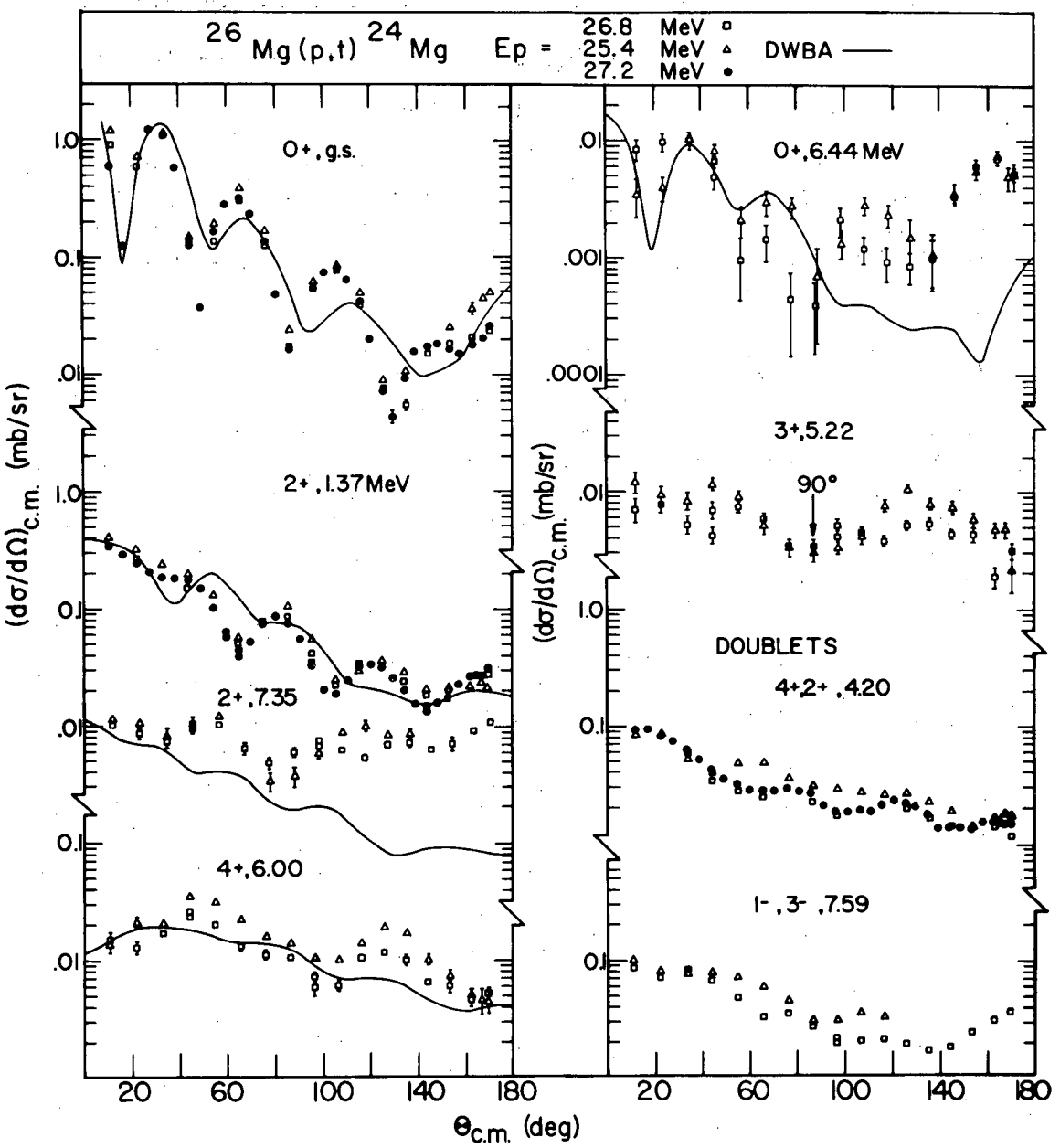

Fig. II A12 Angular distributions at two (in some cases, three) incident proton energies for the first eight triton groups in the $^{26}Mg(p,t)^{24}Mg$ reaction. The solid curves indicate the renormalized results of DWBA calculations made for a proton energy of 26.8 MeV. The DWBA optical model parameters used are proton (triton): V=-50.2 MeV (-164.0 MeV); v=1.121 fm (1.14 fm); a=0.674 fm (0.690 fm); W=-4.28 MeV (-14.7 MeV); W_D=-3.42 MeV (0.0); r'=1.326 fm (1.600 fm); a'=0.546 fm (1.08 fm); V_{so}=-8.56 MeV (0.0); r_{so}=0.899 fm (0.0); a_{so}=0.665 fm (0.0). These, and all subsequent DWBA calculations presented for (p,t) reactions, were performed as indicated in Baer et al., Phys. Lett. 35B (1971) 395.

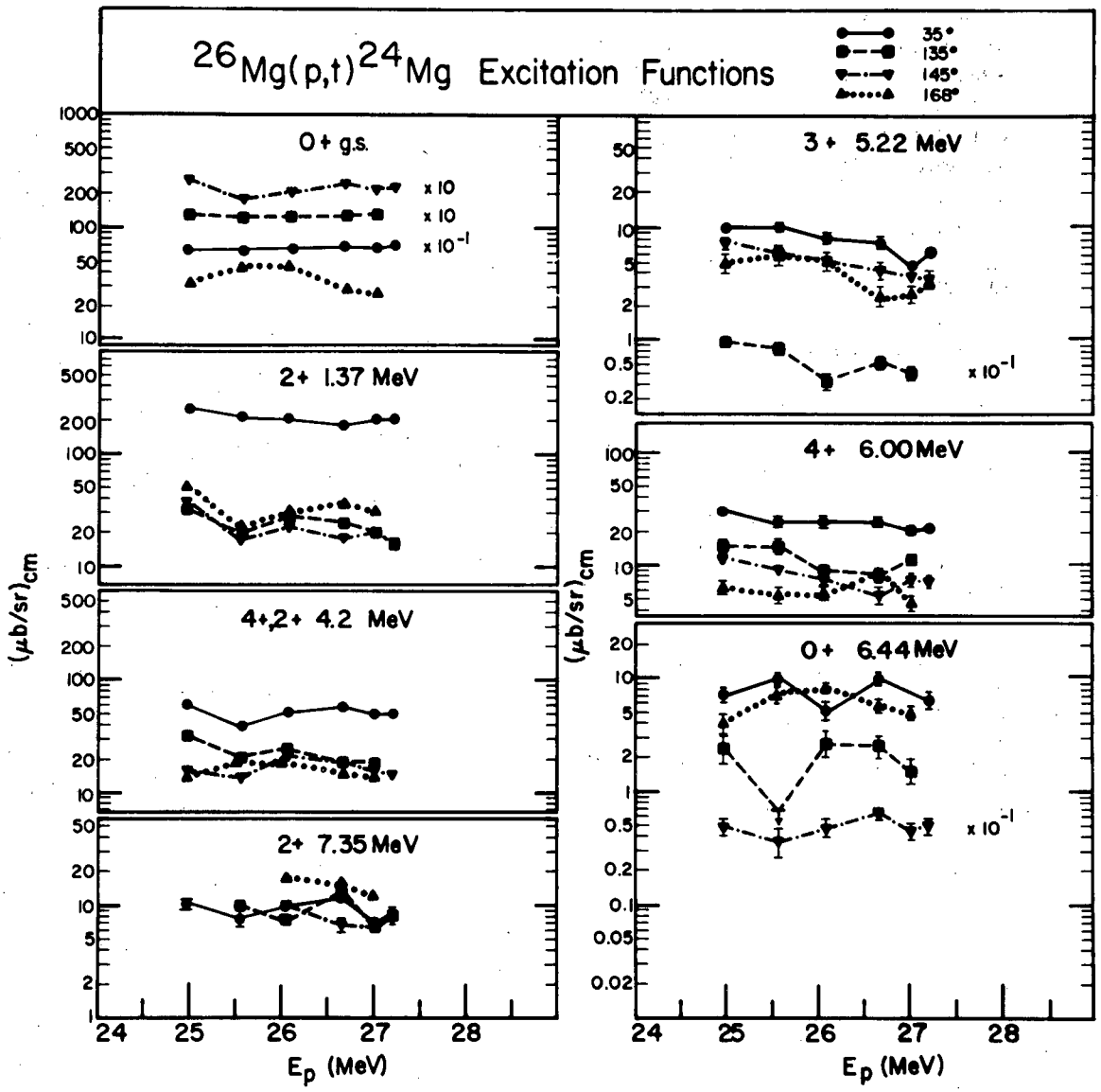

Fig. II A13 Excitation functions for the first seven triton groups in the ^{26}Mg(p,t)^{24}Mg reaction as measured at several angles. The relatively large drop in the $\theta_{c.m.}$=135° cross section for the transition to the 6.44 MeV 0^+ state is probably due to the steep angular dependence of this cross section there, and its consequent kinematic sensitivity.

step processes have a large effect on both the shapes and magnitudes of angular distributions resulting from the (p,t) reaction at 20 MeV on the highly deformed nucleus ^{176}Yb. By using the same approach, Ascuitto et al.[2] have predicted that even for the moderately collective nucleus, ^{62}Ni, multi-step effects can enhance the cross sections by a factor of two or more over standard DWBA predictions. The likelihood of strong multi-step effects in the ^{26}Mg(p,t)^{24}Mg reaction is further supported by an investigation of the ^{24}Mg(d,p)^{25}Mg reaction by Braunschweig et al.[3] in which they found that multi-step effects appear to enhance standard DWBA cross sections by a factor of two. They point out that this result contrasts strongly with work done by Penny[4] considering the (p,d) reaction on spherical vibrational nuclei (such as Ni) where similar enhancements were only on the order of 10%. Thus it would seem that the large degree of collectivity in the Mg nuclei could provide an explanation for the moderately strong transition to the 5.22 MeV 3^+ state.

In the future, as coupled-channels DWBA codes become available, comparison of their predictions with these data will provide a stringent test of their accuracy.

---

1 R. J. Peterson and H. Rudolph (to be published).
2 R. D. Ascuitto et al., Phys. Lett. 34B (1971) 17.
3 D. Braunschweig et al., Phys. Lett. 35B (1971) 273.
4 S. K. Penny, Ph.D. Thesis, Oak Ridge National Laboratory (1965).

v. A Study of the ^{64}Zn(p,t)^{62}Zn Reaction at 27.5 MeV - L. C. Farwell, J. J. Kraushaar, H. W. Baer

The study outlined in last year's Progress Report was completed and the results submitted for publication. A summary of the work is contained below.

The ^{64}Zn target used in the study had an areal density of 1.01 mg/cm^2 and was enriched to 99.9%. Tritons were detected with a ΔE-E counter telescope and conventional electronics. The energy resolution was 80-100 keV FWHM. A typical triton spectrum is shown in Fig. II A14. The energy calibration was determined at θ_L=30° by employing the known levels and Q-values for the ^{50,46}Ti(p,t) reactions. The Q-value of the ^{64}Zn(p,t)^{62}Zn reaction was measured to be -12.493 ± 0.010 MeV. The excitation energies are shown in Fig. II A14 and table II AIV.

Because the (p,t) reaction has cross sections for L=0 transitions that are strongly peaked at forward angles, low angle data were important in searching for the excited 0^+ states. A low angle

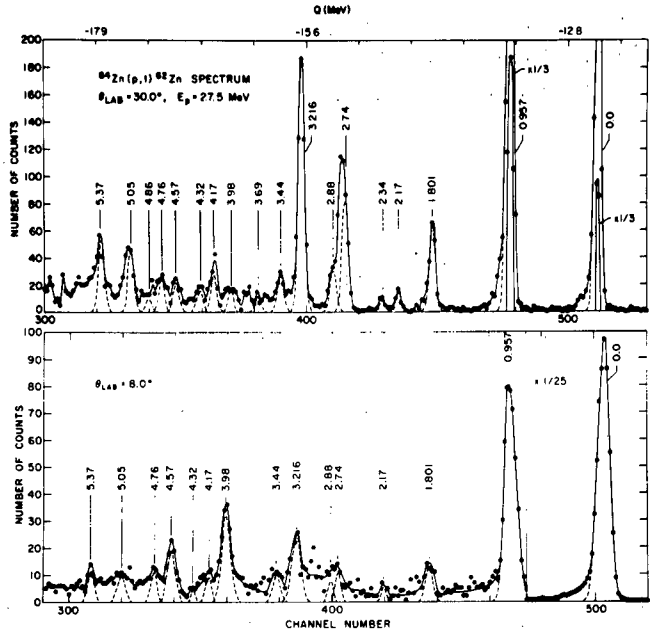

Fig. II A14 Triton spectra of $^{64}Zn(p,t)^{62}Zn$ taken at 30° and 8° (lab). The dotted lines represent the Gaussian curves fit to the peaks and the solid line represents the total fit including the background. Typical energy resolution is 80 keV FWHM. An approximate Q-value scale is shown at the top.

E_x (MeV)	J^π	Configuration	$(2L+1)\frac{\sigma_{EXP}}{\sigma_{DWBA}}$ (x 10^{-3})
0.0	0^+	$(1f_{5/2})^2$	15.0
		$(2p_{3/2})^2$	0.51
0.957± 0.005	2^+	$(1f_{5/2})^2$	8.5
		$(2p_{3/2})^2$	0.40
1.801± 0.007	2^+	$(1f_{5/2})^2$	1.0
2.17 ± 0.01	4^+	$(1f_{5/2})^2$	0.81
		$(1f_{5/2}{}^2p_{3/2})$	0.03
2.34± 0.02			
2.74± 0.02	3^-	$(1g_{9/2}{}^2p_{3/2})$	0.14
2.88± 0.02			
3.216±0.006	4^+	$(1f_{5/2})^2$	16.2
		$(1f_{5/2}{}^2p_{3/2})$	0.99
3.44 ±0.01	2^+	$(1f_{5/2})^2$	1.7
3.69 ±0.02	2^+	$(1f_{5/2})^2$	1.3
3.93 ±0.02	0^+	$(1f_{5/2})^2$	0.30
4.17 ±0.01	4^+	$(1f_{5/2})^2$	5.4
		$(1f_{5/2}{}^2p_{3/2})$	0.20
4.32 ±0.02			
4.57 ±0.01	0^+	$(1f_{5/2})^2$	0.44
4.76 ±0.02	2^+	$(1f_{5/2})^2$	2.0
4.86 ±0.02	2^+	$(1f_{5/2})^2$	2.0
5.05 ±0.02	2^+	$(1f_{5/2})^2$	4.5
5.37 ±0.02	4^+	$(1f_{5/2})^2$	12.6
		$(1f_{5/2}{}^2p_{3/2})$	0.82

Table II AIV Excitation energies and transition strengths determined in the present study are shown here. The transition strengths are sensitive to the configuration assumed in the DWBA calculation, and correspond to the pick-up configuration assumed in the adjacent column. A detailed interpretation of these strengths is not possible since complete wave functions for the initial and final states were not employed.

spectrum taken at 8° is shown in comparison with the 30° spectrum in Fig. II A14. The angular distributions for the 0^+ states are shown in Fig. II A15.

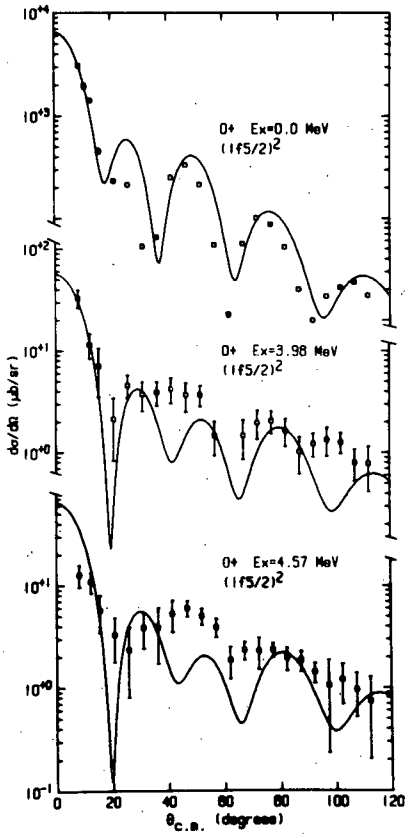

Fig. II A15 Angular distributions for populating 0^+ states in ^{62}Zn. The rise in cross sections at forward angles, characteristic of L=0 transitions, makes it possible to identify new 0^+ states at 3.98 and 4.57 MeV. The DWBA calculation for the ground state transition is seen to describe the data rather well.

Candidates for L=2,3, and 4 transfer assignments are shown in Figs. II A16, II A17, and II A18, respectively. States for which spin-parity assignments could not be uniquely determined are presented in Fig. II A19. Based on systematics, the L values for these states shown in Fig. II A19 have been limited to 1, 2, or 3. Furthermore, the states at 3.69 and 4.86 MeV have been limited to L=2 or 3 due to the similarity of their angular distributions to those 2^+ and 3^- states shown. An L=2 DWBA calculation is shown for these two states for reference only.

Systematics of the angular distributions from the ^{46,48,50}Ti (p,t) studies carried out at this laboratory were applied to the angular distributions from this study to aid in determining the L assignments for the levels observed in ^{62}In. The results of the spin-parity determinations are summarized in the level diagram shown in Fig. II A20. Also shown are the level diagrams of three other even-A Zn isotopes. Our search for the 0^+ member of the 2-phonon triplet near 2 MeV excitation, suggested from the other zinc isotopes, revealed no 0^+ state below 3.9 MeV excitation.

DWBA calculations were performed with optical model potentials P1-T1 which were described in last year's Progress Report. Different

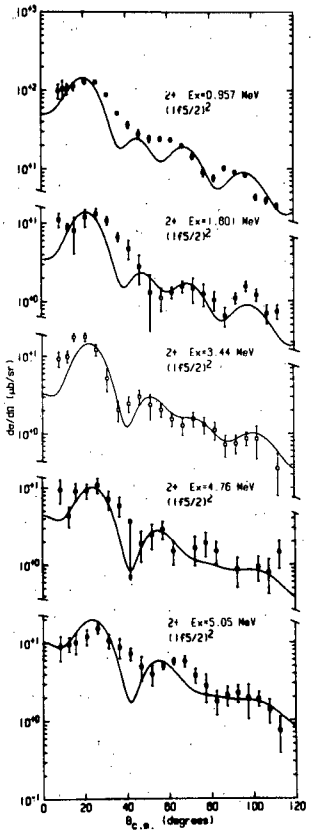

Fig. II A16 The data on five states are compared to calculations for L=2 transitions. The detailed similarity of the data on the states at 1.801 and 3.44 MeV with the 0.957 MeV state establishes 2^+ for these states. The 2^+ assignments for the other three states are considered tentative. An L transfer of 3 can not be ruled out for the states at 4.76 and 5.05 MeV, and they were given tentative assignments of 2^+ and 3^-. The best fit of the DWBA theory for a L=2 transition can be seen to be for the state at 3.44 MeV.

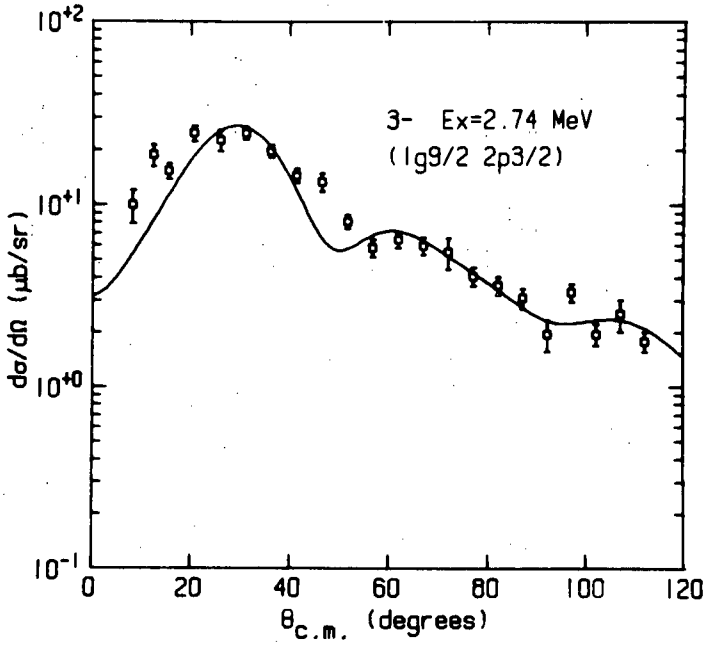

Fig. II A17 Data on the 2.74 MeV state are compared with the DWBA calculations for an L=3 transition. A tentative 3^- is suggested for this state on the basis of the empirical systematics and the reasonably good description provided by the DWBA calculation. The assumed $(1g_{9/2}^2 2p_{3/2})$ transfer configuration used here is somewhat arbitrary.

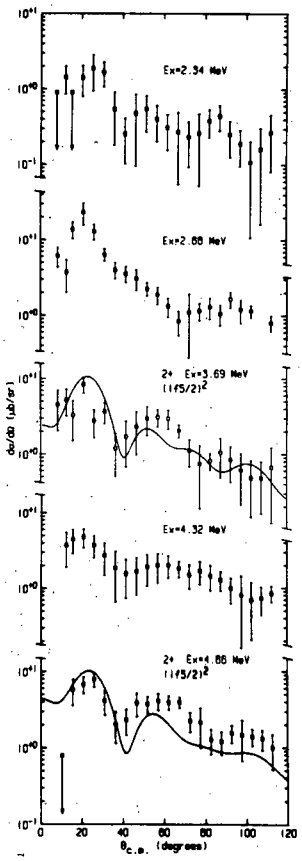

Fig. II A18 Data on possible L=4 transitions are compared with calculations. On the basis of empirical systematics a definite 4^+ is assigned to the first three states. A tentative 4^+ is suggested for the state at 5.37 MeV.

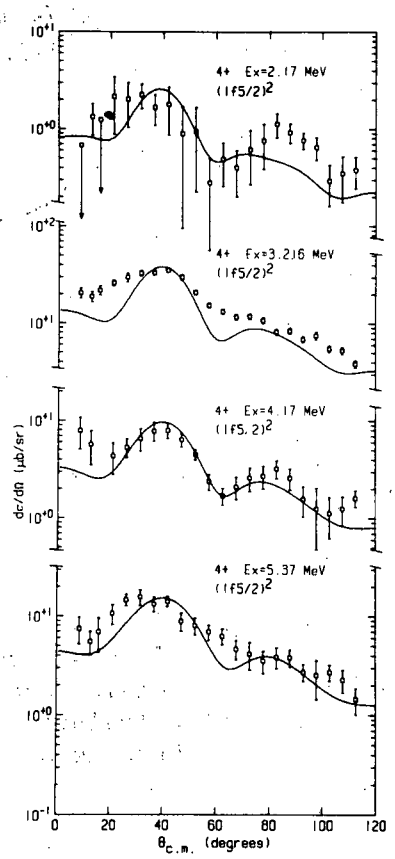

Fig. II A19 The data on these states do not permit a unique L-value determination. Based on systematics, however, L=0 and $L \geq 4$ may be ruled out on the basis of the position of the first maximum. Furthermore, the states at 3.69 and 4.86 have been limited to L=2 or 3 on the basis of their similarity to the L=2 or 3 states previously shown. The L=2 DWBA calculations shown for these states are for reference only.

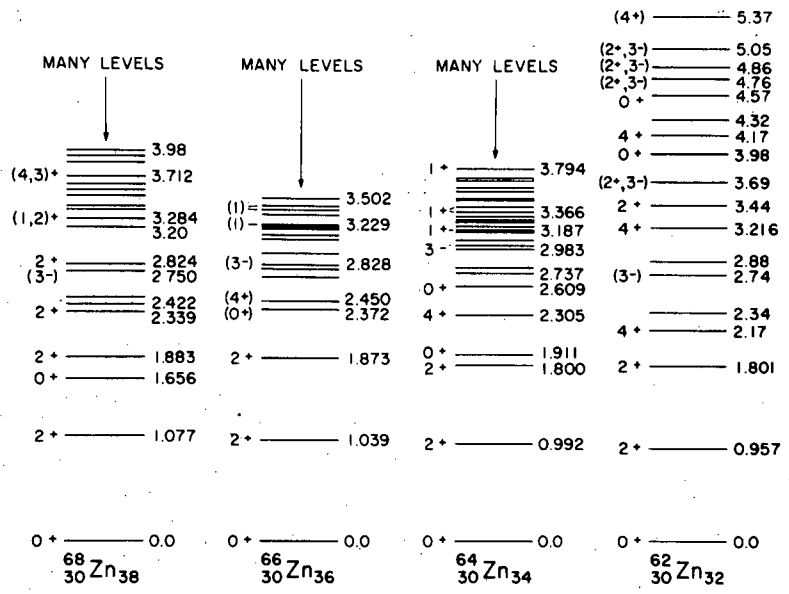

Fig. II A20 A summary of our results on ^{62}Zn is compared with the level diagrams of three other even-mass zinc nuclei. Our search for a 0^+ state near 2 MeV in ^{62}Zn revealed no such state below the 0^+ state at 3.98 MeV. This appears to rule out the existence of a 2-phonon triplet in ^{62}Zn, which is suggested by the level schemes of ^{64,66}Zn.

triton potentials were tried but offered no improvement over the parameter set used. Different pick-up configurations were also tried. The only major difference in the configuration calculations was the relative magnitude of the predicted curves. Transition strengths were extracted for some of the states and various configurations, and they are listed in table II AIV.

vi. The ^{90}Zr(p,t)^{88}Zr Reaction - J. R. Shepard, H. W. Baer, J. J. Kraushaar

Angular distributions for the 0^+ g.s., 1.057 MeV 2^+, 1.517 MeV 0^+, and 1.800 MeV 2^+, 4^+ (doublet) transitions in the ^{90}Zr(p,t)^{88}Zr reaction at E_p= 27 MeV have been measured over an angular range of 10°-110° (lab). These angular distributions and accompanying DWBA calculations are shown in Fig. II A21.

It is important to note that the DWBA calculations more closely reproduce the experimental angular distributions for this reaction than for any of the other (p,t) reactions investigated in this

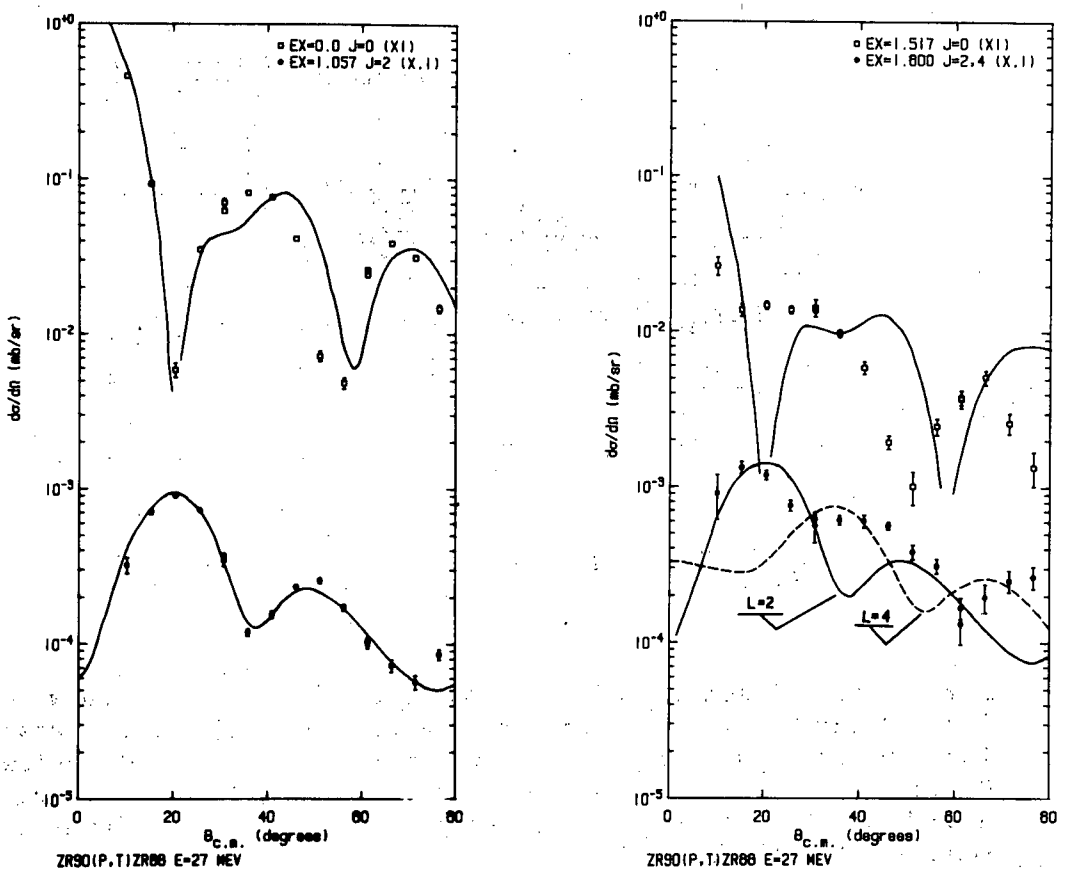

Fig. II A21 Angular distributions for the first four triton groups in the $^{90}Zr(p,t)^{88}Zr$ reaction at E_p=27 MeV. Excitation energies and spin-parity assignments indicated are taken from the literature and are well known. The DWBA calculations shown were performed with the following optical model parameters for protons (tritons): V=-56.4 MeV (-166.6 MeV); r=1.12 fm (1.16 fm); a=0.780 fm (0.752 fm); W=-3.24 MeV (-22.9 MeV); W_D=-6.4 MeV (0.0 MeV); r'=1.32 fm (1.498 fm); a'=0.590 fm (0.817 fm); V_{so}=-6.2 MeV (0.0 MeV); r_{so}=0.980 fm (0.0 fm); a_{so}=0.750 fm (0.0 fm).

series of experiments. With the exception of the 1.517 MeV 0^+ state, the DWBA fits to experiment are excellent. The significance of this fact is only now beginning to be studied, but it is hoped that comparison of this reaction with those involving the lighter targets will shed light on the reasons for failure of the DWBA to describe satisfactorily the reactions in lower mass regions.

c. An Investigation of the Excited States of ^{50}Mn and of Energy Dependent Effects in the ^{50}Cr(^{3}He,t)^{50}Mn Reaction - W. L. Fadner, J. J. Kraushaar, and L. C. Farwell

Differential cross sections were measured for the ^{50}Cr(^{3}He,t)^{50}Mn reaction at 21.4, 29.7, and 37.5 MeV with an energy resolution of about 85 keV. Angular distributions were obtained for eight levels in ^{50}Mn ranging from the 0^+ ground state to 2.00 MeV excitation. The data were compared to both macroscopic and microscopic distorted-wave calculations with the use of a tensor force when appropriate. Several J, π assignments were made within two possibilities: $5^+,6^+$ (E_x-0.23); $2^+,1^+$ (0.66); $1^+,2^+$ (0.81); 7^+ (1.03); and 3^+, 4^+ (1.15). Tentative assignments were 4^+, 3^+ (1.81) and 6^+, 5^+ (1.92). The resulting level scheme was compared to the levels of ^{46}V and to shell-model calculations.

Fig. II A22 is a summary of information available on the level structure of ^{46}V, of ^{50}Cr and of ^{50}Mn. It is expected that isobaric analogs of the 0^+, 2^+ and 4^+ states at E_x= 0.0, 0.783 and 1.879 MeV in ^{50}Cr will be seen in the ^{50}Mn level scheme. In the present experimental work the only good candidates for the 2^+ IES are the states at 0.66 and 0.81 MeV excitation, appreciably lower than predicted, and closer to the 2^+ level of the parent ^{50}Cr nucleus. It

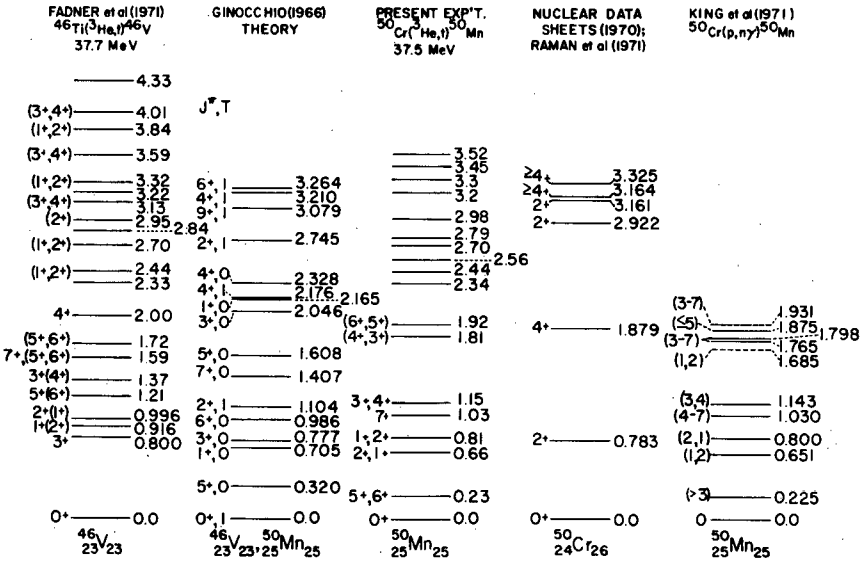

Fig. II A22 A summary of information available relevant to the level structure of ^{50}Mn.

is reasonable to expect that the 4^+ IES in ^{50}Mn will occur near the excitation energy of 1.879 MeV for the 4^+ state in ^{50}Cr. Thus, the state in ^{50}Mn at 1.81 MeV is a candidate for the 4^+ IES. No 6^+ state in ^{50}Cr has yet been reported, although presumably it would lie somewhere near 3.0 MeV excitation.

Experimental angular distributions for the states in ^{50}Mn just mentioned, along with theoretical curves, are shown in Figs. II A23, II A24, and II A-25. The dashed curves were calculated by using the collective model (macroscopic) description.

The macroscopic description of the transition to the IGS (dashed lines, Fig. II A23) is reasonably good at 21.4 and 37.5 MeV incident energy, but poor at 29.7 MeV. It is possible that a slightly different value of the ratio V_{1V}/W_{1S} would improve the description at 29.7 MeV without degrading those at 21.4 and 37.5 MeV, but such optimization was not considered essential for the present investigation. The values of the asymmetry strengths required to fit the IGS data are shown in Fig. II A26. A striking decrease as a function of energy can be seen, indicating that the present DWBA calculations are not satisfactorily predicting the strengths of the differential cross section as a function of energy. This general result appears to be independent of the parameter set used.

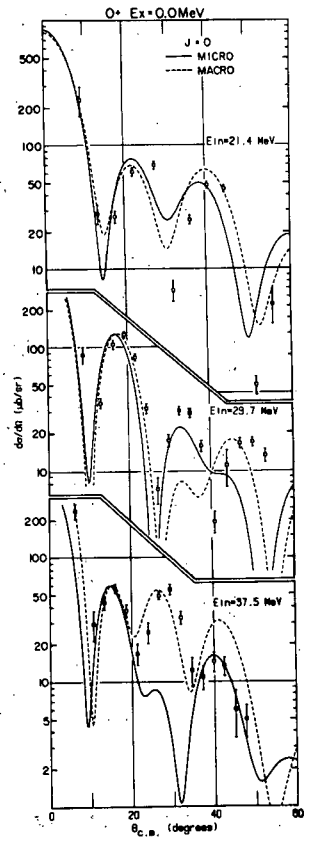

Fig. II A23 Experimental angular distributions and theoretical curves for the ^{50}Cr(^{3}He,t)^{50}Mn transition to the 0^+ isobaric analog ground state.

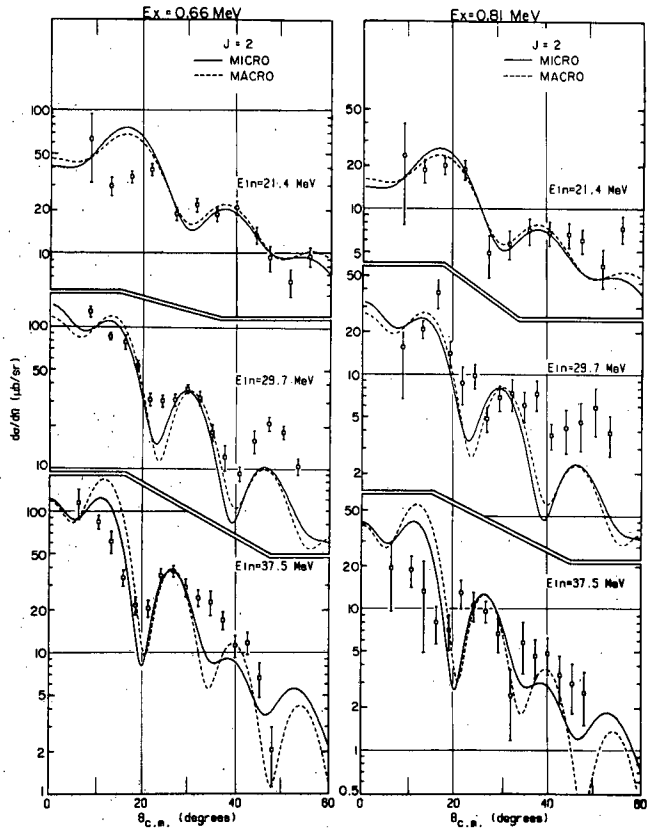

Fig. II A24 Experimental angular distributions and theoretical curves for the $^{50}Cr(^{3}He,t)^{50}Mn$ transitions to two excited states which are candidates for a 2^+ assignment.

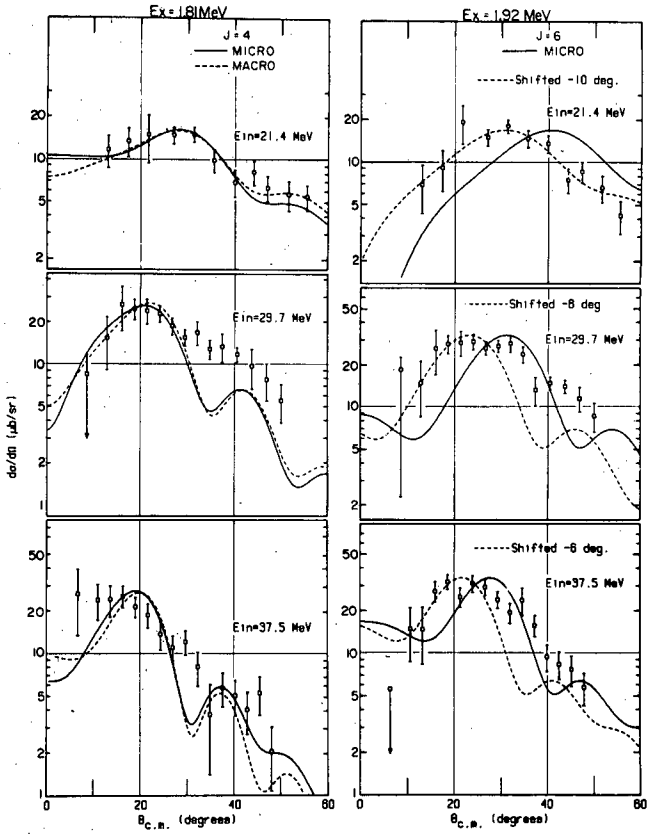

Fig. II A25 Experimental angular distributions and theoretical curves for $^{50}Cr(^{3}He,t)^{50}Mn$ transitions to two excited states which are candidates for 4^+ and 6^+ assignments. The theoretical J=6 curves have been shifted as labeled in order to help examine the angular disagreement between theory and experiment.

In Fig. II A24 the dashed lines represent macroscopic DWBA calculations for an L transfer of 2. Descriptions of the data are fair for both the 0.66 and 0.81 MeV states. Calculations for angular momentum transfers other than 2 provided significantly poorer descriptions of the data for these two states. Although minor differences are expected in the predicted angular distributions for a 1^+ versus a 2^+ final state, especially at lower angles, this ambiguity could not be satisfactorily removed on the basis of comparing the curves to the data. The extracted values of the deformation parameter β_2 for the three parameter sets are shown in Fig. II A26. It can be seen that β_2 values increase slowly with energy. They are essentially independent of the parameter set used. Assuming the 0.66 MeV state to be the 2^+ IES, the average of β_2 for the three optical parameter sets and three energies is 0.59 ± 0.11. Assuming the 0.81 MeV state to be the 2^+ IES, the average β_2 is $0.31 \pm .05$. On this basis, the preferred assignment would be 2^+ and 1^+ for the 0.66 and 0.81 MeV states respectively. Consistency in the microscopic strengths also supports this preference, as will be shown later.

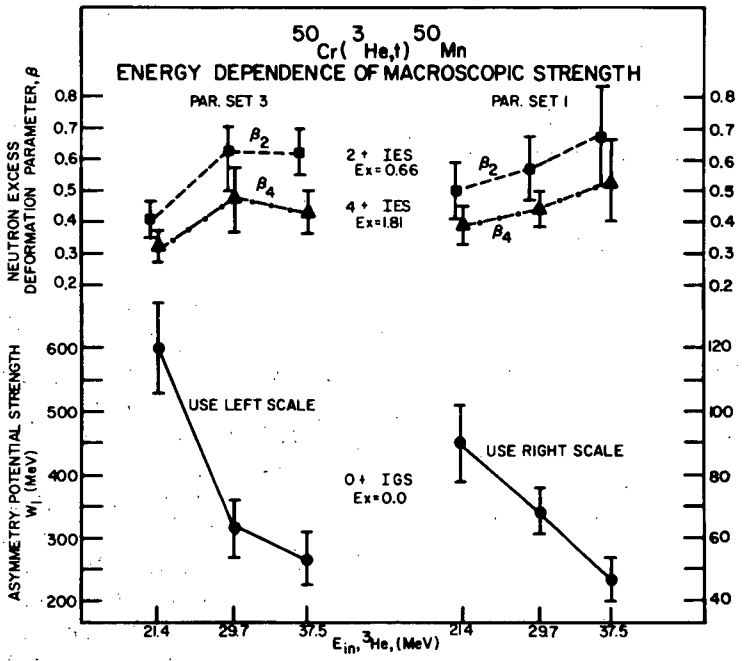

Fig. II A26 Energy dependence of extracted macroscopic strengths for $^{50}Cr(^3He,t)^{50}Mn$ transitions to the 0^+ isobaric analog ground state and to 2^+ and 4^+ isobaric analog excited states.

As shown in Fig. II A25, the description of the data for the 1.81 MeV state was good for an incident energy of 21.4 MeV and acceptable for the other energies, assuming a 4^+ IES. A second possibility for the 4^+ IES is the 1.15 MeV state, since it displays an angular distribution characteristic of an L transfer of 4. However, this state is much lower in excitation energy than the 4^+

state at 1.879 MeV in the parent ^{50}Cr nucleus, so this assignment is considered to be rather unlikely. Extracted values of β_4 for these possible 4^+ IES are shown in Fig. II A26. As in the case of the β_2 parameter, there is a mild energy dependence to the β_4 values, and a negligible dependence upon the parameter set used.

The even J states just discussed were also compared to theoretical angular distributions by using a microscopic model and the results are shown in Figs. II A23, II A24, and II A25.

Angular distributions calculated by using a tensor interaction based on a one-pion exchange potential (OPEP) are compared to data for the states with excitation energies of 0.23, 0.81, 1.03 and 1.15 MeV in Figs. II A27 and II A28.

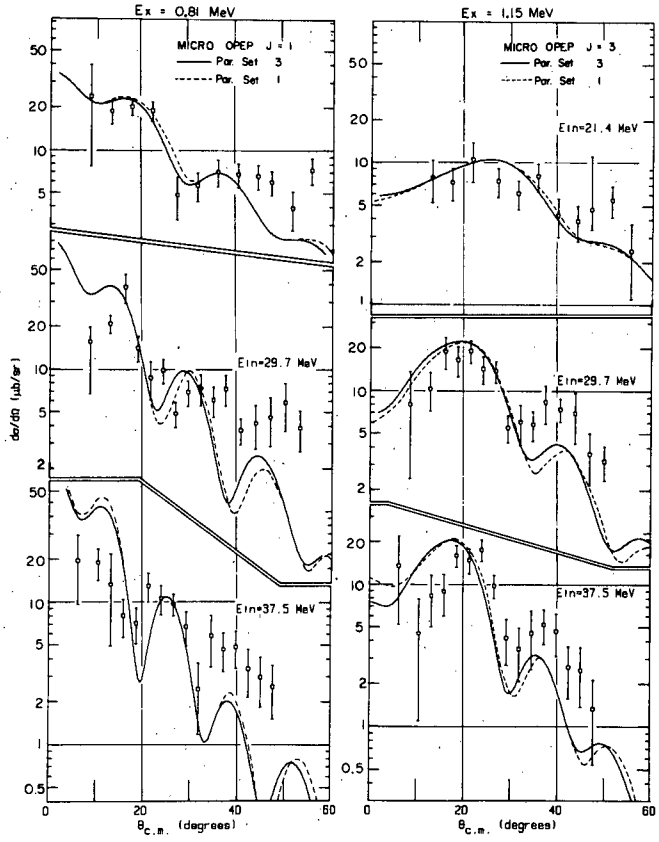

Fig. II A27 Experimental angular distributions and theoretical curves for ^{50}Cr(^{3}He,t)^{50}Mn transitions to excited states which are candidates for 1^+ and 3^+ assignments.

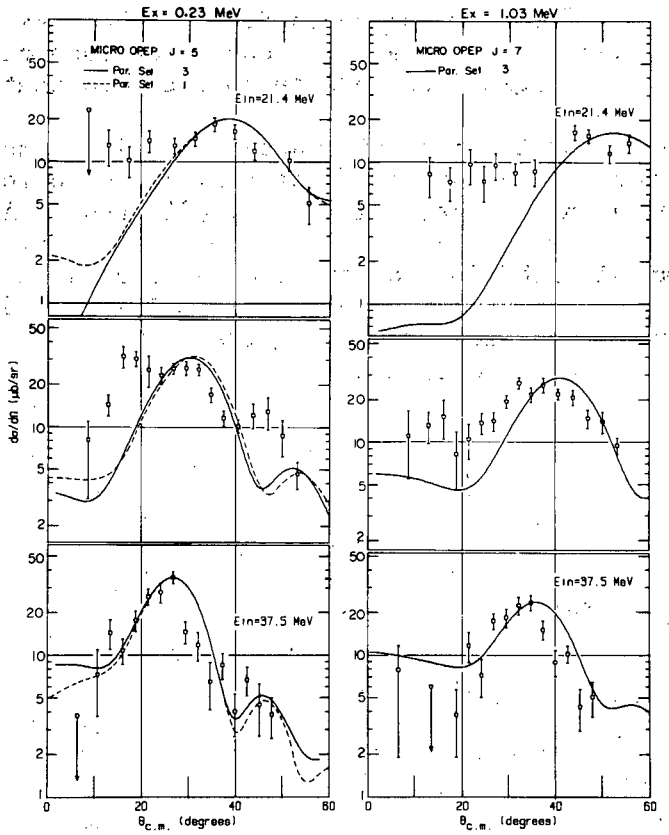

Fig. II A28 Experimental angular distributions and theoretical curves for $^{50}Cr(^{3}He,t)^{50}Mn$ transitions to excited states which are candidates for 5^+ and 7^+ assignments.

The theoretical 1^+ and 3^+ angular distributions are compared to the data for the states at 0.81 and 1.15 MeV respectively in Fig. II A27. The theoretical descriptions are acceptable at 21.4 MeV and fair at the other energies. The 1^+ and 3^+ theoretical angular distributions are similar in shape to those calculated for angular momentum transfers of 2 and 4 respectively, using only a central potential (solid lines in Figs. II A24 and II A25).

d. Energy Dependence in the $^{54}Fe(^{3}He,t)^{54}Co$ Reaction -

W. L. Fadner, H. Rudolph, J. J. Kraushaar

An investigation is underway to determine the extent of the energy dependence in the shapes and magnitudes of angular distributions from the $^{54}Fe(^{3}He,t)^{54}Co$ reaction. Data taken at incident energies of 21.4, 24.0[1], 30.2[2] and 37.5 MeV are being compared to results obtained for the $^{50}Cr(^{3}He,t)^{50}Mn$ reaction and to DWBA calculations. The ground state and several excited states are

being studied. As in the other energy dependence studies of the (^{3}He,t) reaction, the interaction strengths required to normalize the DWBA curves to the data have been found to decrease with increasing energy. Although the energy dependent effects seen for the ^{54}Fe(^{3}He,t)^{54}Co reaction are similar to those for the ^{50}Cr(^{3}He,t)^{50}Mn reaction (included elsewhere in this report), the effects are significantly smaller for the ^{54}Fe target.

---

[1] Data from H. Rudolph and R. L. McGrath, to be published. Also H. Rudolph, thesis (State University of New York at Stony Brook (1970).

[2] Data from G. Bruge, A. Bussiere, H. Faraggi, P. Kossanyi-Demay, J. M. Loiseaux, P. Roussel, and L. Valentin, Nucl. Phys. A129 (1969) 417.

e. Energy Dependence in (^{3}He,t) Transitions to Isobaric Analog Ground States - W. L. Fadner, J. J. Kraushaar, S. I. Hayakawa

Transitions to the isobaric analog ground states of ^{50}Cr, ^{54}Fe, ^{62}Ni and ^{90}Zr have been studied with the (^{3}He,t) reaction in the energy range of 21.4 to 37.5 MeV. Some of the data have been reported previously[1-4]. The bulk of the data were recently taken with the University of Colorado cyclotron. Experimental angular distributions show striking energy dependent variations, as indicated in Fig. II A29. Each nucleus examined showed an individual characteristic energy dependence in the shape of the angular distributions. Two different models were used to investigate these features: a simplified shell model (microscopic) and a generalized optical model (macroscopic). Distorted wave calculations were made by using the computer code DWUCK with several optical model parameter sets, including the three shown in table II AV.

Table II AV

Optical Model Parameter Sets. Set 1 has been used in several previous studies. Sets 2 and 3 are new energy dependent sets described elsewhere in this progress report. E refers to the projectile energy in MeV. Notation here is in accordance with Ref. 1 except that R and I subscripts refer to real and imaginary terms, respectively.

	V_{OV} (MeV)	r_R (F)	a_R (F)	W_{OV} (MeV)	W_{OS} (MeV)	r_I (F)	a_I (F)
Set 1	170.60	1.14	0.712	18.50	---	1.600	0.829
Set 2	182.87-0.02E	1.10	0.763	---	160.03 $-1.944E_2$ $+.0135E^2$	1.222	0.807
Set 3	137.98-.148E	1.10	0.853	---	150.65 $-2.019E_2$ $+.0142E^2$	1.308	0.751

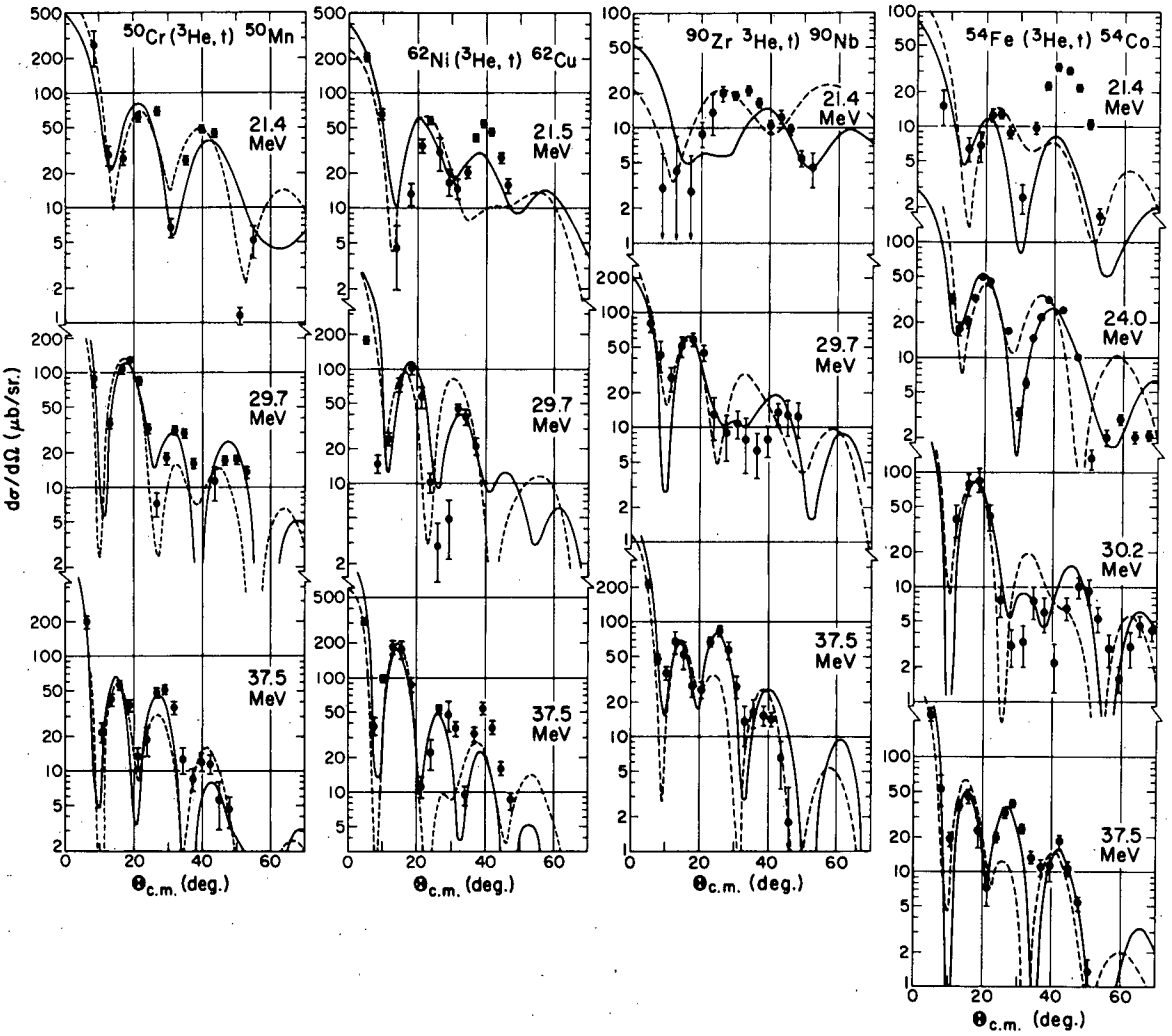

Fig. II A29 Differential cross sections for (^{3}He,t) transitions to isobaric analog ground states of several nuclei. The solid curves represent DWBA calculations which use parameter set 1, table II AV, and a generalized optical model with interaction terms selected for each nucleus to fit the data reasonably well. The dashed curves represent DWBA calculations which use parameter set 2 and a simplified shell model, with a Yukawa interaction of 1.0 F range.

In general the experimental angular distributions were poorly described by the microscopic model. The dashed lines in Fig. II A29 illustrate an example of such calculations. Differences in results occurred for different parameter sets, but no set seemed to be significantly better than others in describing the entire range of nuclei and energies.

The macroscopic model gave a somewhat better description, as shown by the solid lines of Fig. II A29. However, adequate descriptions with the macroscopic model required different ad hoc interaction potential prescriptions for each nucleus and each optical model family. Since the interaction potential has been shown to be related to the neutron excess, one might expect different prescriptions for each nucleus, but no consistent method of predicting these prescriptions in advance has yet been developed.

The interaction strengths required to fit the data are summarized in Fig. II A30. The error bars are in some cases large due to the aforementioned inadequacies of the theory in describing the data. For both the macroscopic and microscopic models, a general tendency towards decreasing strength with increasing energy is evident. These energy dependent effects are essentially independent of the parameter set used, although the extracted strengths may differ by an overall constant.

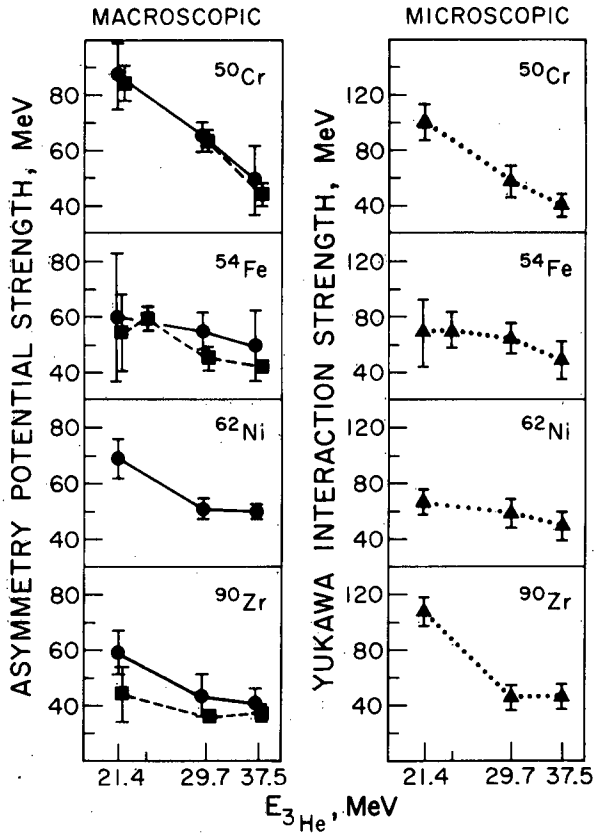

Fig. II A30 Interaction strengths as a function of incident energy. The circular data points and solid lines represent interaction potential strengths for the generalized optical (macroscopic) model with parameter set 1 and $V_{1V}=W_{1S}$. (See Ref. 1 for definitions of these terms.) The square data points and dashed lines are for the same conditions except that V_{1V}/W_{1S}=3.0, 5.0, 1.0, and 9.2 respectively for the targets ^{50}Cr, ^{54}Fe, ^{62}Ni, and ^{90}Zr. The triangular data points and dotted lines represent the Yukawa interaction strength (with range 1.0 F) for a simplified shell (microscopic) model, with energy dependent parameter set 2. The same general results were found with other parameter sets.

It had been reported in a previous paper[1] that extracted interaction (macroscopic model) potential strengths, W_1, obtained in different studies differed significantly. Studies[1,5,6] at an incident energy of 37.5 MeV gave a value of W_1 of 4-60 MeV, while others[2,7,8] at 25 and 30 MeV gave values of W_1 ranging from 80 to 140 MeV. Furthermore, a value of about 95 MeV was obtained for W_1 from an elastic scattering analysis[9] of ^{3}He and triton particles at 20 MeV. The energy dependent effects seen in Fig. II A30 account for much of the discrepancy in W_1 values obtained. The remaining difference is undoubtedly due to the use of different optical model parameter sets and uncertainties in obtaining the W_1 values. Consistency in the extracted strengths can only be expected for similar parameter sets and for data taken at the same energy.

Although DWBA formulations are still of use in (^{3}He,t) studies, the poor description of the energy dependence, in shape and in strength, is evidence of basic inadequacies in the theories as they are presently used.

---

1 W. L. Fadner, R. E. L. Green, S. I. Hayakawa, J. J. Kraushaar, and R. R. Johnson, Nucl. Phys. A163 (1971) 203.

2 G. Bruge, A. Bussiere, H. Faraggi, P. Kossanyi-Demay, J. M. Loiseaux, P. Roussel, and L. Valentin, Nucl. Phys. A129 (1969) 417.

3 H. Rudolph and R. L. McGrath, to be published, also H. Rudolph, thesis (1970).

4 S. I. Hayakawa, R. R. Johnson and J. L. Schoonover, Bull. Am. Phys. Soc. 15 (1970) 804.

5 P. D. Kunz, E. Rost, G. D. Jones, R. R. Johnson, and S. I. Hayakawa, Phys. Rev. 185 (1969) 1528.

6 W. L. Fadner, L. C. Farwell, R. E. L. Green, S. I. Hayakawa, and J. J. Kraushaar, Nucl. Phys. A162 (1971) 239.

7 R. M. Drisko, P. G. Roos, and R. H. Bassel, Proceedings of the International Conference on Nuclear Structure, Tokyo, Japan, 1967, Supplement to J. Phys. Soc. Japan 24 (1968) 347.

8 J. J. Wesolowski, E. H. Schwarcz, P. G. Roos, and C. A. Ludemann, Phys. Rev. 169 (1968) 878.

9 P. P. Urone, L. W. Put, H. H. Chang, and B. W. Ridley, Nucl. Phys. A163 (1971) 225.

f. ^{2}H + ^{3}He Elastic Scattering and the ^{2}H(^{3}He,^{4}He)^{1}H Reaction - T. R. King and W. R. Smythe

The studies of ^{2}H + ^{3}He elastic scattering and the ^{2}H(^{3}He,^{4}He)^{1}H reaction have been concluded.

Excitation functions for ^{2}H + ^{3}He elastic scattering, measured at laboratory scattering angles of 17°, 40°, and 55° are shown in Fig. II A31. All the measured cross sections show a smooth variation with energy, and there is no indication of resonant behavior. The

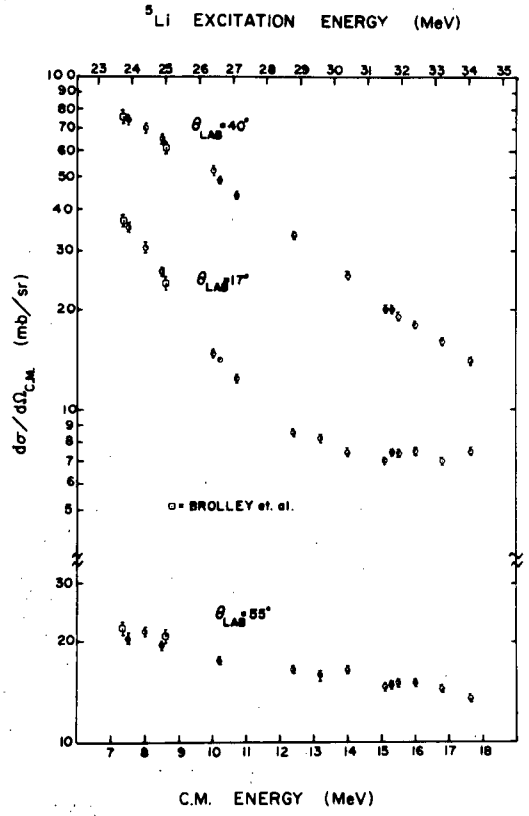

Fig. II A31 Excitation functions for ^{2}H + ^{3}He elastic scattering at laboratory angles of 17°, 40°, and 55°. These angles correspond to the minima and the central maximum of the angular distributions. The cross sections were measured by detecting recoil ^{2}H; probable error in absolute cross sections is 3% or less in all cases. Points obtained from the data of Brolley et al.[2] by linear interpolation are denoted by squares.

probable error in the absolute cross sections is 3% or less for these data.

Excitation functions for the reaction ^{2}H(^{3}He,^{4}He)^{1}H, measured at laboratory angles of 60°, 100°, 125°, and 165° are shown in Fig. II A32. Again, there is no departure from a smooth energy variation. The probable error in the absolute cross sections is 3% or less. The data below 8.5 MeV c.m. energy were taken with a beam-energy degrader. The beryllium foil beam energy degrader proved to be a rapid and convenient way to vary the bombarding energy without retuning the cyclotron.

It is concluded that no states exist in ^{5}Li in the region from 23.4 to 34 MeV having significant reduced widths for two-body decay. Such states have widths less than 0.8 MeV in this region of excitation. In particular, there was no indication of a broad (1.5 MeV) state at about 25 MeV in excitation, as was seen in ^{7}Li(p,t)^{5}Li by McGrath et al.[1]

Angular distributions for elastic scattering and the ^{2}H(^{3}He,^{4}He)^{1}H reaction were measured at 18.7, 20, 21.26, 25.5, 35, and 44.1 MeV. The elastic scattering angular distributions measured at 25.5, 35, and 44.1 MeV bombarding energy are shown in Fig. II A33. The reaction angular distributions, measured at the same energies, are shown in Fig. II A34. In general there is a smooth change in both shape and amplitude with energy, for both elastic scattering

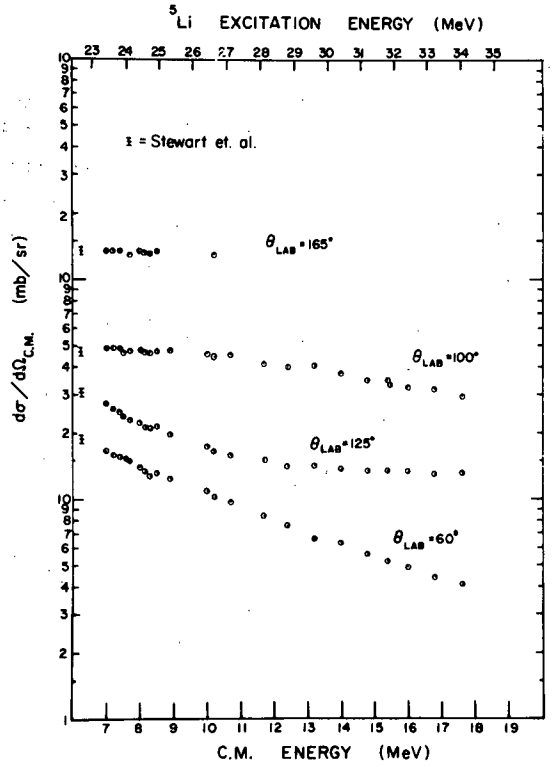

Fig. II A32 Excitation functions for ^{2}H(^{3}He, ^{4}He)^{1}H at laboratory angles of 165°, 125°, 100°, and 60°. The cross sections were measured by detecting protons; the angles correspond to c.m. angles of about 10°, 38°, 60°, and 102°. The probable error in absolute cross section is 3% or better for all the data points. Points obtained from the data of Stewart et al.[3] by linear interpolation are denoted by crosses.

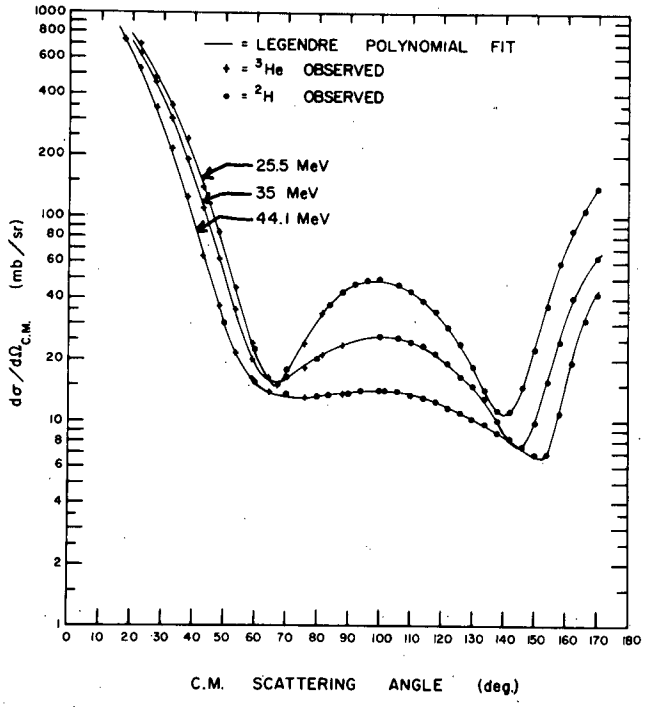

Fig. II A33 Angular distributions for ^{2}H + ^{3}He elastic scattering at ^{3}He bombarding energies of 25.5, 35, and 44.1 MeV. Probable error of the absolute cross sections is 2.5%. It is interesting to note the behavior of the central maximum: it becomes less pronounced as the energy is increased, and has almost disappeared at 44.1 MeV. The solid curve is the result of fitting the data with a Legendre polynomial series of the form $d\sigma/d\Omega = \sum_L a_L P_L$ (cos θ); terms up to L=12 were used.

and the $^{2}H(^{3}He,^{4}He)^{1}H$ reaction. Probable error in the absolute cross sections is about 2.5% for both the elastic scattering and reaction data.

A more complete description of this work is being prepared for publication.

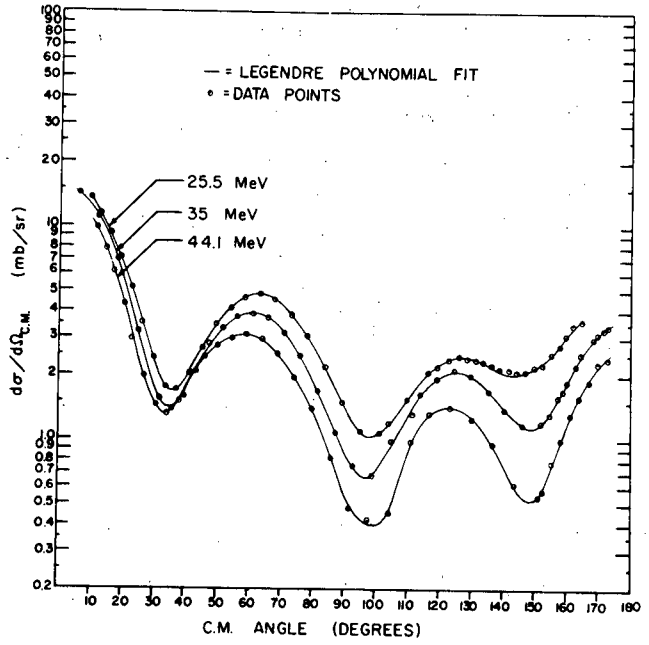

Fig. II A34 Angular distributions for the reaction $^{2}H(^{3}He,^{4}He)^{1}H$ at bombarding energies of 25.5, 35, and 44.1 MeV. Probable error of the absolute differential cross sections is 2.5%. The solid curve is the result of fitting the angular distributions with a Legendre polynomial series (as for the elastic data); terms up to L=8 were used.

---

1 R. L. McGrath, J. Cerny, and S. W. Cosper, Phys. Rev. 165 (1967) 1126.

2 J. E. Brolley, Jr., T. M. Putnam, L. Rosen, and L. Stewart, Phys. Rev. 117 (1959) 1307.

3 L. Stewart, J. E. Brolley, Jr., and L. Rosen, Phys. Rev. 119 (1960) 1649.

g. The $^{26}Mg(^{4}He,^{6}He)^{24}Mg$ Reaction

R. J. Peterson, B. W. Ridley, H. H. Chang, and H. W. Baer

This study of a two-neutron pickup reaction was begun in order to provide data complementary to (p,t) data. Although the angular distributions for ^{6}He leaving ^{24}Mg in several excited states did appear to be direct, in that they display regular oscillatory

shapes, we found the yield to be highly sensitive to incident beam energy. An excitation function at a lab angle of 40° is shown in Fig. II A35. This evidence of a non-direct process precludes any useful two-neutron pickup spectroscopy. This work has been published as a Comment[1].

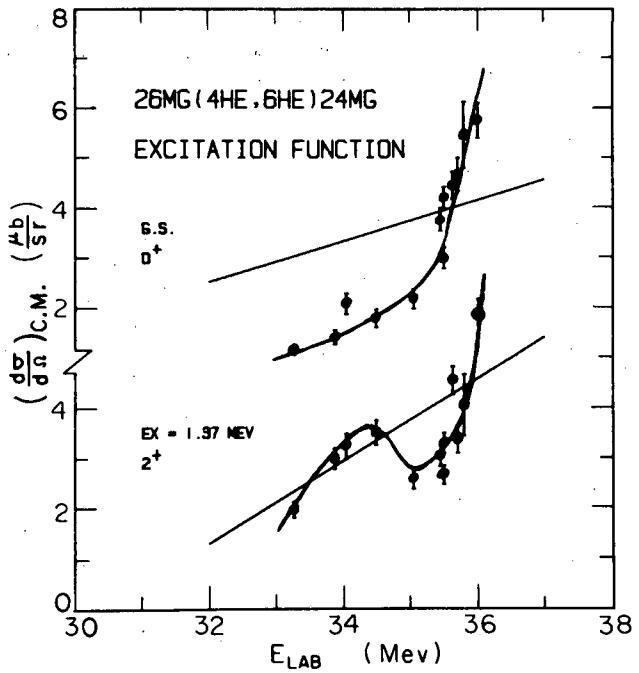

Fig. II A35 The differential cross sections for the $^{26}Mg(^{4}He,^{6}He)^{24}Mg$ reactions to the ground state (0^+) and 1.37 MeV state (2^+) are shown as functions of the incident energy.

---

[1] R. J. Peterson, et al. Phys. Rev. 4C (1971) 278.

h. Study of the Excited States of ^{57}Ni via the $^{58}Ni(p,d)$ and $^{58}Ni(^{3}He,\alpha)$ Reaction - F. M. Edwards, J. J. Kraushaar, B. W. Ridley

Angular distributions for the excited states of ^{57}Ni were obtained from 10° to ~110° with energies E_p=27.5 MeV[1] and $E_{^3He}$=37.7 MeV. An E + ΔE detector telescope in conjunction with standard mass identification techniques was used to obtain the data; the (p,d) and ($^3He,\alpha$) spectra had energy resolution of 75 keV and 130 keV FWHM respectively. The spectra are shown in Fig. II A36. Excited states at 2.45 and 3.01 MeV, which were first seen in ($\alpha,n\gamma$) experiments[2] and later reported in ($^3He,\alpha$) experiments[3], were also seen in our

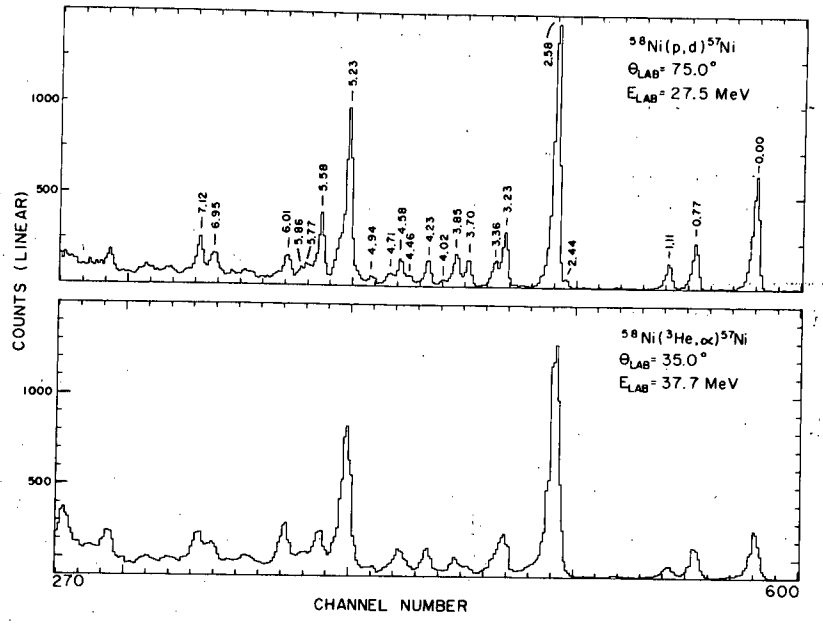

Fig. II A36 Examples of (p,d) and (^{3}He,α) spectra.

(p,d) spectra, but were not resolved in the (^{3}He,α) spectra. The presence of an excited state at 3.36 MeV, first reported in a (^{3}He,$\alpha\gamma$) experiment[4], is confirmed by the (p,d) spectra. One may also see from the (^{3}He,α) spectra that, although the 3.23 and 3.36 MeV states are not resolved, the width of the peak clearly indicates two components. Finally, several new states were observed in the (p,d) spectra. The 4.02, 4.46, 4.71, 5.77 and 5.86 MeV states were previously unreported, although Gould et al.[4] reported the 4.58 MeV level as an unresolved group, and Fou and Zurmühle[5] reported a level at 5.85 MeV, which must be the 5.77 and 5.86 MeV states.

The theoretical comparisons for the (p,d) reaction are nearly completed. DWBA calculations were carried out with the computer code DWUCK. The proton and deuteron optical model parameters were obtained from the "average" formulas of Becchetti and Greenlees[6], and Newman et al.[7] respectively. They are listed in table II AVI. Finite range and non-local effects were included in the calculations with finite range parameter R=0.695 and non-locality parameters $\beta_p=\beta_n=0.85$, $\beta_d=0.54$.

The results of the fits are shown in the figures. It is worth noting that the $\ell_n=3$ (Figs. II A38, II A39) and $\ell_n=0$ (Fig. II A40) assignments for the 3.36 and 5.58 MeV states, and the $\ell_n=1$ (Fig. II A37) assignment for the 4.46 and 4.94 MeV states, are previously unreported. From the (^{3}He,$\alpha\gamma$) reaction, Gould et al.[4] assigned the 6.01 MeV level as having $d_{3/2}$ configuration. The present work

Table II AVI

Optical model parameters

Particle	V_R	r_R	a_R	W_V	W_{SF}	r_I	a_I	V_{so}	r_{so}	a_{so}
Proton	48.93	1.17	0.750	3.35	5.33	1.32	0.534	6.2	1.10	0.750
Deuteron	96.8	1.08	0.814	0	12.84	1.30	0.782	7.0	1.08	0.814

$U(r) = V(r) + iW(r)$

$V(r) = -V_R f(r,R_R,a_R) + V_{so}\vec{\sigma} \cdot \vec{\ell}\ (\hbar/m_\pi c)^2 (1/r)d/dr[f(r,R_{so},a_{so})]$

$W(r) = -W_V f(r,R_I,a_I) + W_{SF} 4a_I (d/dr)[f(r,R_I,a_I)]$

where $f(r,R,a) = [1 + \exp(r-R)/a]^{-1}$

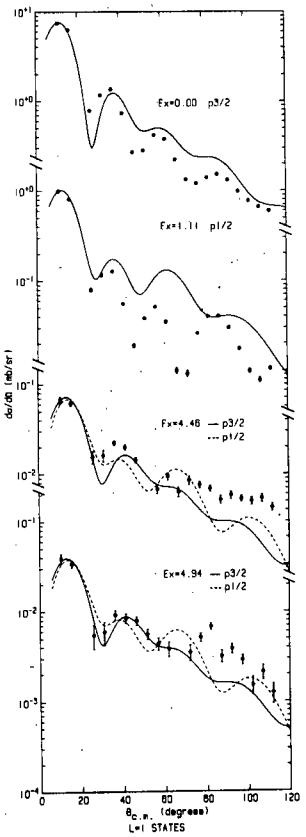

Fig. II A37 ℓ=1 transitions. The spin assignments for the E_x=0.00 and 1.11 MeV states (3/2 and 1/2 respectively) are well known from many previous experiments. The ℓ and J assignments for the E_x=4.46 and 4.94 MeV states are previously unreported; a definite J assignment cannot be made for these states from angular dependence.

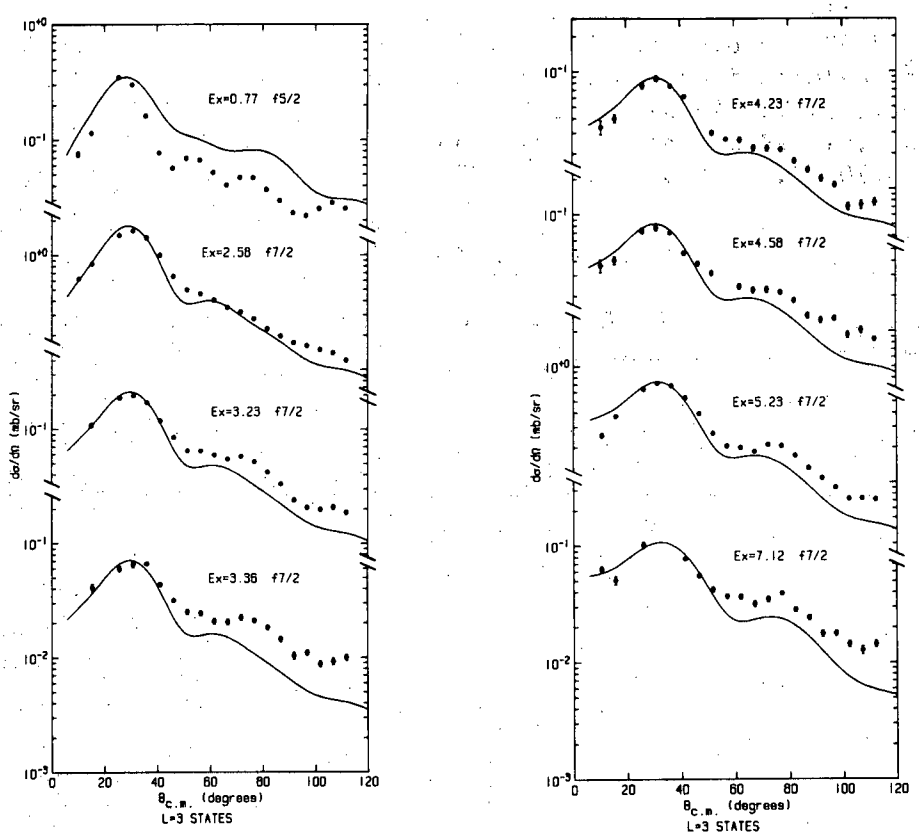

Figs. II A38 and II A39 ℓ=3 transitions. The ℓ values for the E_x=3.36 and 7.12 MeV states are previously unreported.

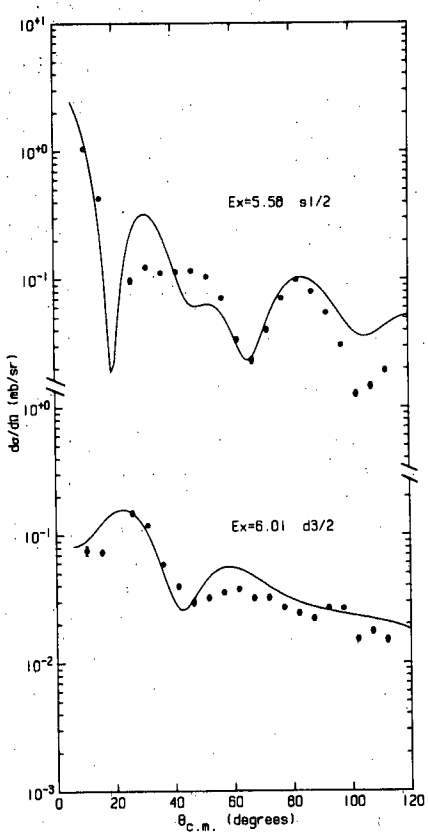

Fig. II A40 ℓ=0 and ℓ=2 transitions. No ℓ=0 states have been previously reported. The ℓ=2 assignments for the E_x=6.01 MeV state supports the work of Gould *et al.*[4]

confirms this assignment. The J-dependence of the angular distributions is readily seen by comparing the $2p_{3/2}(E_x=0.00)$ and $2p_{1/2}(E_x=1.11)$ (see Fig. II A37) or the $1f_{5/2}(E_x=0.77)$ and $1f_{7/2}(E_x=2.58)$ levels (see Fig. II A38). The current results of the (p,d) calculations, including spectroscopic factors, are shown in table II AVII. Angular distributions were not obtained for the 2.45 and 3.01 MeV states, and assignments have not yet been made for the 3.70, 3.85, 4.02, 4.71, 5.77, 5.86 and 6.95 MeV states.

Table II AVII

Excitation energies, ℓ_n, J, and spectroscopic factors obtained from the $^{58}Ni(p,d)^{57}Ni$ reaction.

E_x	ℓ_n	J	S
0.00	1	3/2	0.67
0.77	3	5/2	0.45
1.11	1	1/2	0.12
2.45			
2.58	3	7/2	2.38
3.01			
3.23	3	7/2	0.31
3.36	3	7/2	0.11
3.70			
3.85			
4.02			
4.23	3	7/2	0.16
4.46	1	(1/2,3/2)	0.023
4.58	3	7/2	0.16
4.71			
4.94	1	(1/2,3/2)	0.012
5.23	3	7/2	1.57
5.58	0	1/2	0.74
5.77			
5.86			
6.01	2	3/2	0.58
6.95			
7.12	3	7/2	0.35

DWBA analysis of the $(^3He,\alpha)$ data is now in progress and should be completed in the near future. Gamma decay via the reaction $^{54}Fe(\alpha,n\gamma)^{57}Ni$ is also currently being studied in collaboration with Dr. N. S. P. King of the University of California at Davis, and Dr. E. F. Gibson of Sacramento State College.

[1] Data taken concurrently with ^{58}Ni(p,t) studies by J. R. Shepard.
[2] M.C. Bertin and R. G. Hirko, Particles and Nuclei - to be published.
[3] R. W. Zurmühle, D. P. Balamuth and James E. Holden, Phys. Rev. 2 (1970) 1577.
[4] C. R. Gould, D. P. Balamuth, P. F. Hinrichsen, and R. W. Zurmühle, Phys. Rev. 188 (1969) 1792.
[5] Cheng-Ming Fou and Robert W. Zurmühle, Phys. Rev. 140 (1965) 1283.
[6] F. D. Becchetti, Jr., and G. W. Greenlees, Phys. Rev. 182 (1969) 1190.
[7] E. Newman, L. C. Becker, and B. M. Preedom, Nucl. Phys. A100 (1967) 225.

i. Two-Nucleon Pickup from ^{57}Fe and ^{89}Y - R. J. Peterson and H. Rudolph

We have studied the (p,t) and (p,^{3}He) reactions at 27 MeV and the (d,α) reaction at 16 MeV on the spin 1/2 targets ^{57}Fe and ^{89}Y. The low target spin limits the number of orbital angular momentum transfers, L, which may occur in populating each final state. Fig. II A41 shows a triton spectrum from the ^{57}Fe(p,t)^{55}Fe reaction, and in Fig. II A42 is shown an alpha particle spectrum from the ^{89}Y(d,α)^{87}Sr reaction. Angular distributions for many states have

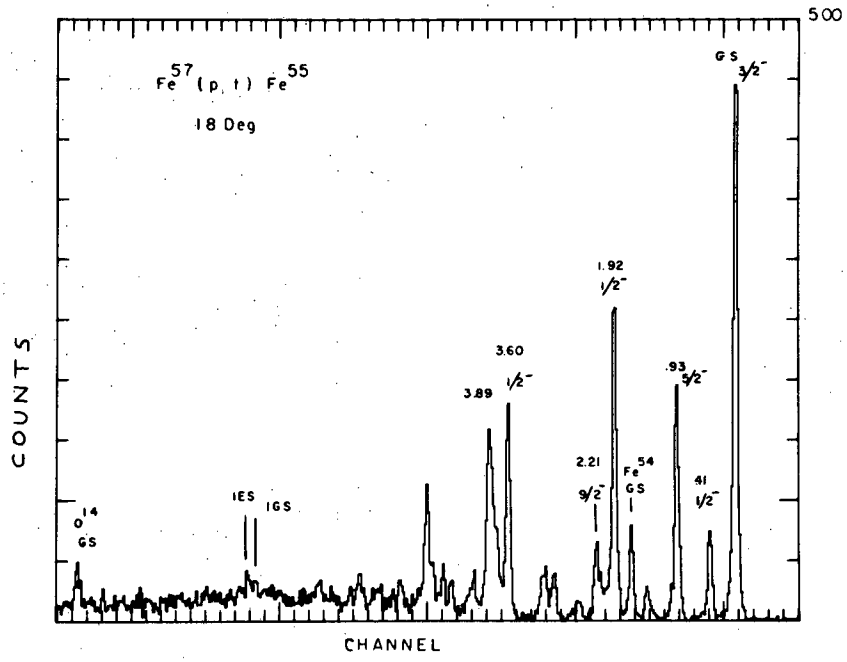

Fig. II A41 Triton energy spectrum from the reaction ^{57}Fe(p,t)^{55}Fe at E_p=27.3 MeV.

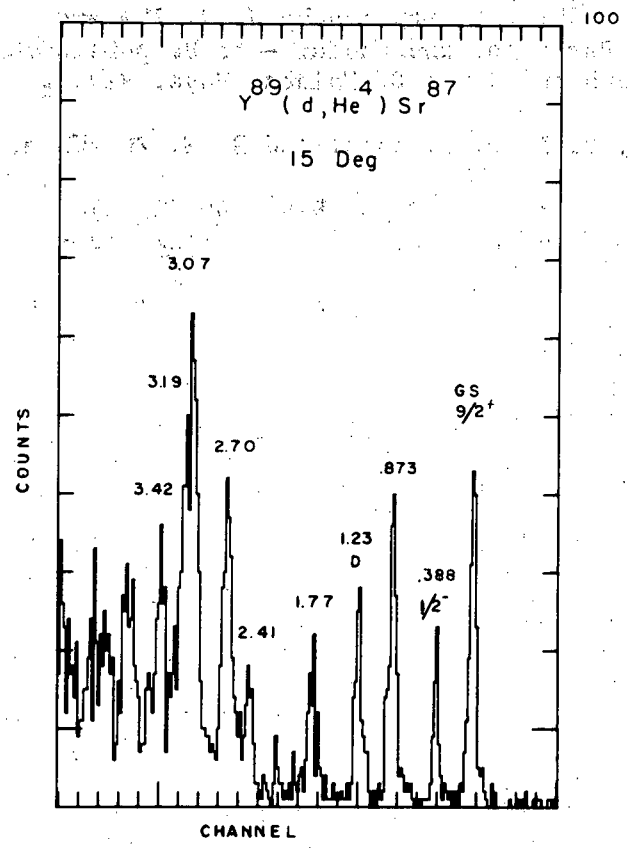

Fig. II A42 Alpha energy spectrum from the reaction $^{89}Y(d,\alpha)^{87}Sr$ at E_d=16.5 MeV.

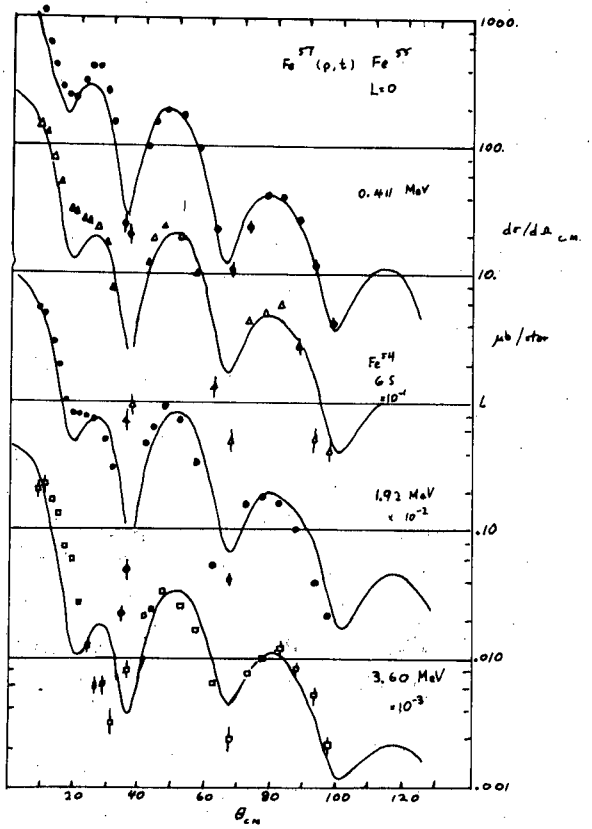

Fig. II A43 Several prominent L=0 transitions in the $^{57}Fe(p,t)^{55}Fe$ reaction.

been obtained, and DWBA fits are complete for most of the data. The data and fits for the prominent L=0 transitions in the $^{57}Fe(p,t)^{55}Fe$ reaction are shown in Fig. II A43. The optical model parameter set used in the calculations are the P1-T1 set of Baer et al.[1]

The magnitudes of the observed cross sections are being interpreted in terms of the relevant shell model configurations. Three specific spectroscopic nuggets are worthy of note. In the $^{57}Fe(p,^3He)^{55}Mn$ reaction we find that the angular distribution of a ^3He group corresponding to an excitation of 1.29 MeV is strongly forward peaked (Fig. II A44. A known $11/2^-$ state at this energy

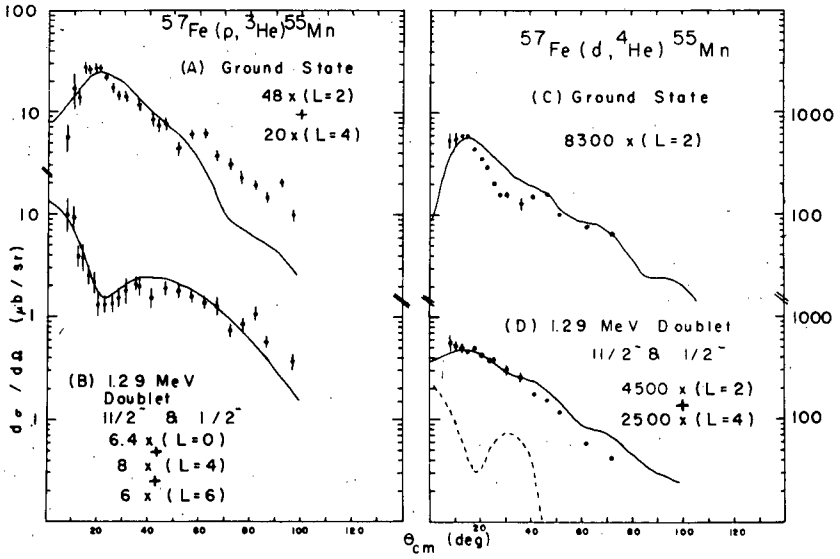

Fig. II A44 The data for the $^{57}Fe(p,^3He)$ and $^{57}Fe(d,^4He)$ reactions to the ground state and 1.29 MeV doublet in ^{55}Mn are compared to the relevant DWBA predictions. The weighting of the DWBA predictions required for each fit is shown in the figure.

could not be populated by the L=0 transfer indicated by the data. The absence of an L=0 transfer in the (d,α) data constrains the new state to have spin $1/2^-$. A $1/2^-$ to $3/2^-$ transition would exhibit an L=0 pattern in both the $(p,^3He)$ and (d,α) reaction (with LSJ=011). The data imply that only LSJ=000 is present, and the spin of the state must be $1/2^-$. The excitation of this level by two-nucleon pickup, and by no other reaction, indicates a complex nature for the unexpected $1/2^-$ state. Calculations including a larger basis of multiparticle-multihole states than previously considered have succeeded in describing the properties of this state (see Theory Section of this report)[2].

It has been observed[3] that inelastic proton scattering from the $1/2^-$ ground state of ^{89}Y to the $9/2^+$ state at 0.906 MeV is dominated by an M4 core polarization term (LSJ=314). The (d,α) pickup reaction from ^{89}Y to the $9/2^+$ ground state of ^{87}Sr is found to proceed both by L=5 (LSJ=515,514) and L=3 (LSJ=314) (see Fig. II A45). The L=3 pickup cannot occur if one assumes a simple nature for the initial and final states[4], and must involve a spin flip process analogous to the M4 core polarization found in inelastic scattering. This correlation between scattering transitions and two-nucleon transfer transitions is an extension of what has been previously noted for S=0 transitions[5].

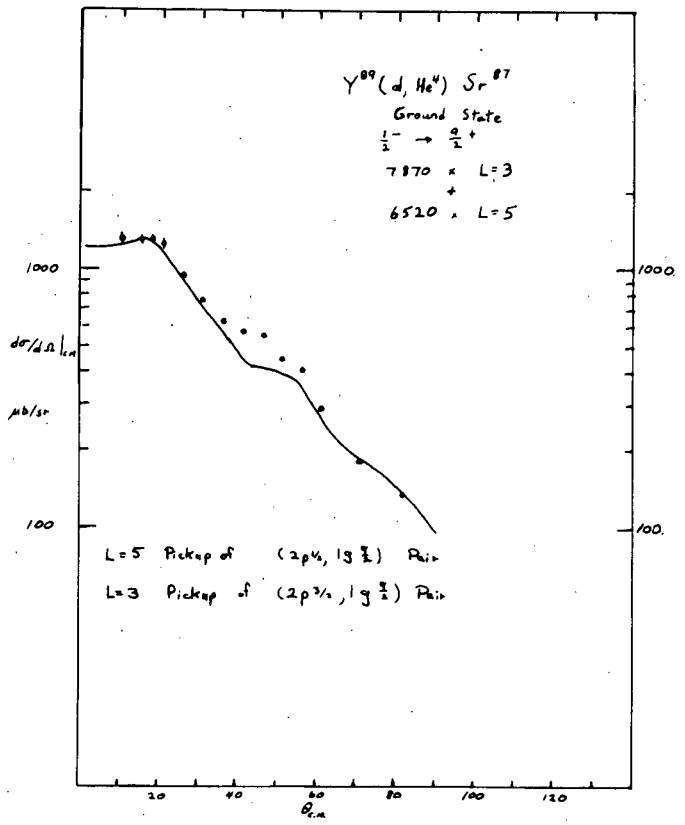

Fig. II A45 The data for the $^{89}Y(d,\alpha)$ reaction to the ^{87}Sr $9/2^+$ ground state are compared to the DWBA prediction.

We find an upper limit of 2 μb/sr for the (p,t) cross section to the $9/2^+$ state of ^{87}Y at 0.381 MeV. This result is consistent with very pure shell model configurations in the initial and final states[4].

---

1 H. W. Baer et al., Phys. Rev. Letters 25 (1970) 1035.
2 R. J. Peterson, S. Pittel, and H. Rudolph, submitted to Phys. Letters.
3 M. L. Whiten, A. Scott, and G. R. Satchler, to be published.
4 J. D. Bergados and T. T. S. Kuo, Nucl. Phys. A168 (1971) 225.
5 R. A. Broglia, C. Riedel, and T. Udagawa, Nucl. Phys. A169 (1971) 225.

j. Energy Dependence of the ^{3}He and ^{4}He Optical Potentials - H. H. Chang and B. W. Ridley

The elastic scattering of complex projectiles is generally described by potentials that are similar to the first order optical potential, the strength of whose real part is about n x ($U_{nucleon}$ at energy E/n) for a projectile with energy E containing n nucleons. The effect of exchange is expected to reduce the real strength below the first order value by a correction which increases with the density of the projectile, and which varies with energy in such a way as to render the net potential less strongly dependent on energy than is the nuclear optical potential[1].

In fitting ^{3}He and ^{4}He elastic data for ^{40}Ca and ^{58}Ni between 20 and 85 MeV, it has been observed[2,3] that the real parts of the optical potentials are nearly independent of energy for those families which correspond most closely with the first order strength. The present work extends the energy dependent analysis of the same ^{3}He and ^{4}He data to the case of more "realistic" potential families with $U_o \sim 130$ MeV, whose validity is beginning to be confirmed by measurements of high energy scattering in the backward hemisphere[4,5]. The effects of volume and surface forms for the imaginary potential are also investigated.

The data at all energies for a given projectile-target combination were fitted simultaneously by using the program OPTIM(M) with the following parameterization:

$$V(r) = -U(1 + e^{x})^{-1} - i(W_v - 1/4 W_s \, d/dx')(1 + e^{x'})^{-1} + V_{coul}(r),$$

$$U = U_o + U_1 E$$

and, either $W_v = W_{vo} + W_{v1}E + W_{v2}E^2$, $W_s = 0$,

or $W_s = W_{so} + W_{s1}E + W_{s2}E^2$, $W_v = 0$,

where E is the incident lab energy and $x = (r - r_R A^{1/3})/a_R$, $x' = (r - r_I A^{1/3})/a_I$.

For each class of potentials, a common set of geometrical parameters for ^{40}Ca and ^{58}Ni was established by simultaneous fitting of data for both nuclei, fixing only r_R at the value 1.10 fm. The energy dependent well depths were then found for each target nucleus separately. While the value r_R=1.10 fm gives satisfactory fits to ^{3}He data, this is not the case for ^{4}He, and subsequent individual fits to ^{4}He scattering consistently evidenced the need for larger values of r_R in the neighborhood of 1.25-1.30 fm for all potential families.

The optical potentials for ^{3}He are summarized in table II AVIII, and the fits to scattering by ^{58}Ni using the shallow potentials are shown in Fig. II A46. While the very weak energy dependence of U for potentials belonging to the deep (first order) family is confirmed, the shallow potential family exhibits a much stronger energy dependence which resembles that observed for nucleons by Becchetti and Greenlees[6].

Table II AVIII

Optical parameters for ^{3}He elastic scattering between 20 and 84 MeV lab energy. r_R=1.10 fm, r_{coul}=1.4 fm. Uniform standard deviation of 10% assumed on all points.

Target	U(MeV)	Type of W	W_v or W_s(MeV)	a_R	r_I	a_I	χ^2
^{40}Ca	143.1-0.34E	vol.	12.4-0.03E-0.E^2	0.847	1.72	0.726	10.0
^{58}Ni	135.6-0.20E	"	22.2-0.25E+0.002E^2	"	"	"	3.2
^{40}Ca	141.6-0.27E	surf.	19.5+0.12E-0.002E^2	0.853	1.308	0.751	12.0
^{58}Ni	138.0-0.15E	"	37.7-0.50E+0.003E^2	"	"	"	2.7
^{40}Ca	192.1-0.11E	vol.	12.9+0.12E-0.001E^2	0.739	1.63	0.839	9.0
^{58}Ni	181.7-0.05E	"	30.7-0.46E+0.003E^2	"	"	"	3.0
^{40}Ca	190.9-0.08E	surf.	16.9+0.18E+0.002E^2	0.763	1.22	0.807	8.5
^{58}Ni	182.9-0.02E	"	40.0-0.49E+0.003E^2	"	"	"	2.7

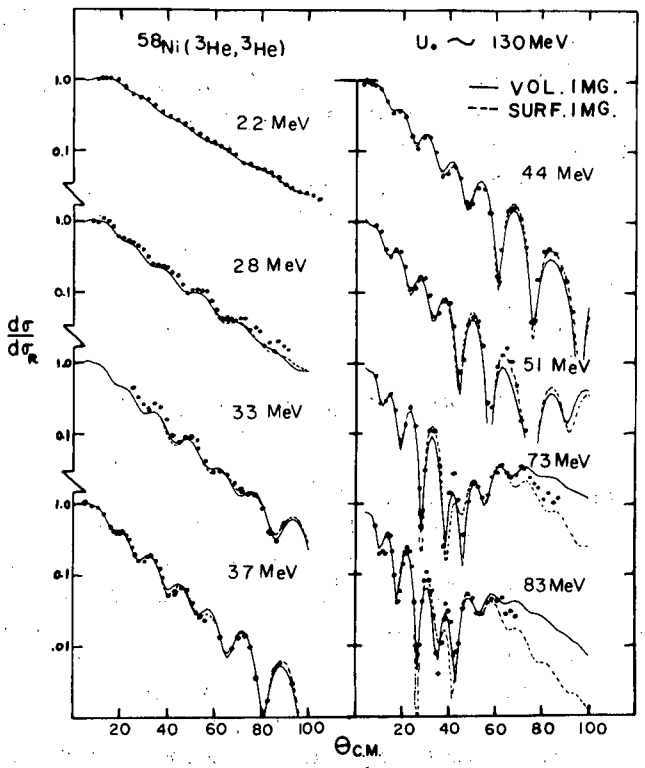

Fig. II A46 Optical model fits to ^{58}Ni(^{3}He,^{3}He) scattering data with the shallow potential family (U ~130 MeV).

These conclusions are not qualitatively dependent on the assumptions of surface or volume forms for the imaginary potential, which give almost equally good fits. If indeed the shallow potentials are more physically correct, then the associated nucleon-like energy dependence may reflect only the sensitivity of the existing data (θ generally $<90°$) to the potential in the nuclear surface region. Here the density effect is expected to be minimal. It is planned to extend the higher energy data into the backward hemisphere in the hope of learning more about the potential in the nuclear interior.

The optical potentials for ^{4}He are summarized in table II AIX. So far, only the volume imaginary form has been considered. Again we see that the very weak energy dependence of the deep potentials is replaced by a dependence resembling that for nucleons for the shallower family. The remarks concerning the similar behavior in ^{3}He scattering also pertain qualitatively to this case.

Table II AIX

Optical parameters for ^{4}He elastic scattering between 20 and 86 MeV lab energy.

Target	U(MeV)	W_v(MeV)	r_R	a_R	r_I	a_I	χ^2
^{40}Ca	139.0-0.37E	3.17+0.21E-0.001E^2	1.10	0.95	1.84	0.49	28
^{58}Ni	127.4-0.30E	5.98+0.07E-0.00E^2	"	"	"	"	28
^{40}Ca	179.7-0.23E	5.19+0.15E-0.00E^2	"	0.86	1.76	0.54	20
^{58}Ni	159.6-0.02E	12.0-0.09E+0.001E^2	"	"	"	"	19
^{40}Ca	174.8+0.00E	2.57+0.44E-0.002E^2	1.28	0.70	1.63	0.60	17
^{58}Ni	157.8+0.16E	14.8-0.05E+0.012E^2	"	0.67	1.67	0.46	10

Folded Potentials for ^{3}He and ^{4}He

A calculation of the density effect for ^{3}He and ^{4}He potentials along the lines of the work of Brueckner et al.[7] is in progress. As an interim study, first order optical potentials were constructed by folding the nucleon optical potential into the ground state wavefunction of the projectile[8]. The Irving-Gunn and Gaussian wavefunctions were chosen for ^{3}He and ^{4}He respectively, with parameters adjusted to yield the correct RMS charge radii. The proton and neutron optical potentials were those of Becchetti et al.[8]

The folded potential differs from the Woods-Saxon (W-S) form. A comparison with the familiar W-S parameters was achieved by fitting a W-S form to the folded potential by minimizing $(V_{fold}-V_{W-S})^2/(V_{fold}+V_{W-S})^2$ for the real and imaginary potentials separately. The

resulting W-S parameters are listed in table II AX. Differential cross sections calculated from the folded potentials are indicated by the solid lines in Fig. II A47. The representation of ^{4}He scattering is noticeably poorer than is the case for ^{3}He--an effect

Table II AX

Folded potentials approximated by Woods-Saxon potentials. ^{58}Ni is the target nucleus. The values inside the parentheses are the results of a two-parameter search.

Projectile	E_{lab}	U_v	r_R	a_R	W_v	W_d	r_I	a_I
^{3}He	37.4	149.1	1.21	0.76	3.06 (78.2)	23.0 (22.0)	1.32	0.70
^{3}He	83.5	124.6	1.26	0.83	12.9 (41.8)	8.7 (8.7)	1.42	0.69
^{4}He	24.7	192.1	1.26	0.78	0.92 (0.92)	53.2 (99.9)	1.27	0.61
^{4}He	52.4	182.2	1.26	0.78	5.20 (92.7)	35.8 (13.3)	1.35	0.60

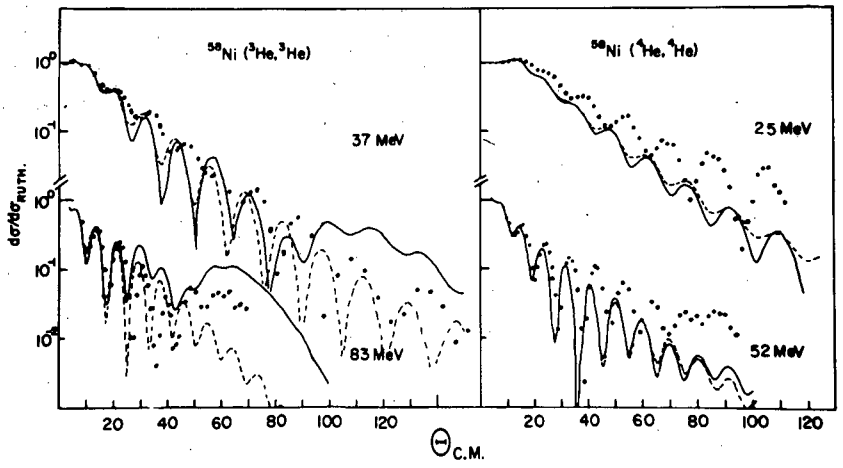

Fig. II A47 Predictions from folded potentials. The real potentials are fixed at the values calculated. The imaginary potentials are approximated by volume and derivative Woods-Saxon potentials. Solid curves represent initial potentials. Dashed curves represent fits obtained by varying W_v and W_s.

that may well be associated with a larger expected density correction for ^{4}He projectiles. The dashed lines result from a search on the W_S and W_V parameters using the real potential and overall geometry established by folding. Such a procedure is rationalized by the ignoring of projectile break-up in the simple folding procedure.

1 H. Wittern, Nucl. Phys. 62 (1965) 628.
2 B. W. Ridley, T. H. Braid, T. W. Conlon, Bull. Amer. Phys. Soc. 14 (1969) 1219.
3 T. W. Conlon, B. W. Ridley, T. H. Braid, Bull. Amer. Phys. Soc. 13 (1968) 650.
4 C. Fulmer, Conf. on Optical Potentials for Complex Projectiles, U. of North Carolina (1971).
5 W. T. Sloan, et al., Bull. Amer. Phys. Soc. 16 (1971) 601.
6 F. D. Becchetti and G. W. Greenlees, Phys. Rev. 182 (1969) 1190.
7 K. A. Brueckner, et al., Phys. Rev. 173 (1968) 944.
8 T. F. Smith and P. D. Kunz, private communication.
P. W. Keaton, Conf. on Optical Potentials for Complex Projectiles, U. of North Carolina (1971).

k. Elastic and Inelastic Proton and Alpha Scattering from ^{50}Cr - E. W. Stoub, R. J. Peterson, R. A. Ristinen

Beams of 22.86 MeV protons and 35.63 MeV alpha particles have been used to explore the excited states of ^{50}Cr. To optimize energy resolution in the proton spectra, a single turn extraction tune was used to yield an energy resolution of 40 keV (FWHM). Energy resolution in the alpha spectra was 90 keV. Good counting statistics produced spectra as shown (see Figs. II A48 and II A49). Measurements over angular ranges of 9° to 170° (lab) for protons and 7.5° to 120° for alphas yielded extensive angular distributions. DWBA calculations which used optical parameters fit to the elastic data allowed us to infer the spins and parities of several excited states. The optical model fits to the elastic data are shown in Fig. II A50, as are the comparisons of the data to the DWBA predictions for collective states. Table II AXI lists the optical model parameters for ^{50}Cr for both proton and alpha scattering. The measured energies of the first eleven excited states are consistent with those in the literature[1,2], (see table II AXII). Of particular interest is the lowest lying 3^- state at 4.05 ± .02 MeV found for the first time in these studies. This state was not observed in the ^{52}Cr(p,t)^{50}Cr reaction because of the proximity of a 0^+ state which dominates the (p,t) cross section[3]. Our assignment of 3^- to this state is made on the basis of the fits shown in Fig. II A50. Other new spin-parity assignments of 2^+ at 4.19 MeV and 4^+ at 3.90 MeV have been made. Further work is expected to provide many more spin-parity assignments and deformation parameters from both the proton and alpha particle scattering data. The sensitivity of the proton data to microscopic models will also be explored.

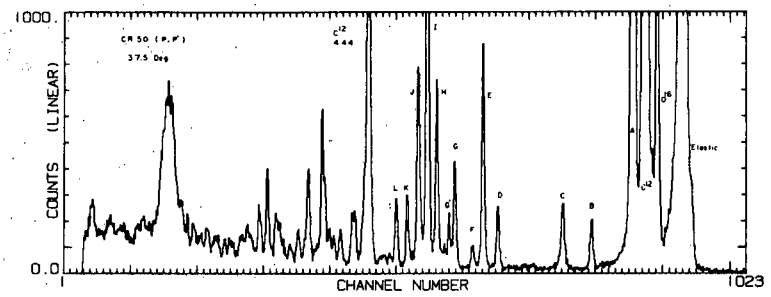

Fig. II A48 Proton spectrum. Lettered peaks may be identified by using table II AXII.

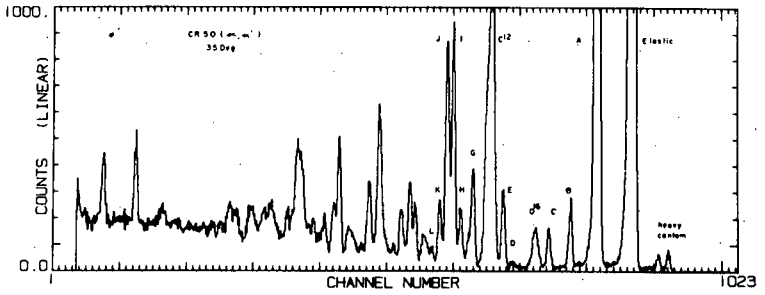

Fig. II A49 Alpha spectrum. Lettered peaks may be identified by using table II AXII.

Table II AXII

Peak Identification

Peak	Q_{exp}(keV)	Q_{known}(keV)
A	783	783
B	1430 (^{52}Cr 2^+)	1434
C	1886	1881
D	2923	2924
E	3160	3160
F	3321	3325
G	3611	3611
G'	3702	3698
H	3902	3895
I	4052	4052
J	4193	4193
K	4373	4369

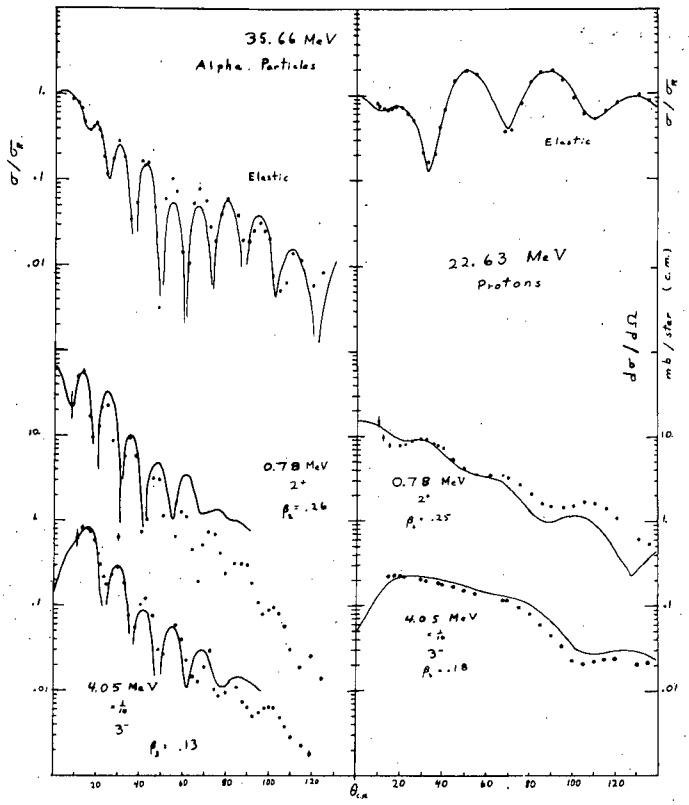

Fig. II A50 Elastic, 2^+ and 3^- data for both proton and alpha scattering, with optical model fits (see table II AXI for parameters) and DWBA calculations.

Table II AXI

Optical model parameters

Parameter	Proton	Alpha	
V_s	49.63	200	MeV
r_s	1.170	1.368	fm
a_s	0.732	0.619	fm
W_s	0.	15.18	MeV
W_D	8.09	--	MeV
r_I	1.179	1.728	fm
a_I	0.689	0.395	fm
V_{so}	7.24	--	MeV
r_{so}	0.956	--	fm
a_{so}	0.741	--	fm
r_c	1.20	1.40	fm

1 S. Raman, et al., private communication.
2 Nuclear Data Sheets, Vol. 3; 1970.
3 H. W. Baer, J. J. Kraushaar, J. R. Shepard and B. W. Ridley, Phys. Letters 35B (1971) 395.

2. Gamma-Ray Experiments

a. Studies in the β^+ Decay of Proton-rich Nuclei by the Pneumatic Shuttle ("Rabbit") Technique

The "rabbit" facility[1] has been used extensively during the last year. Its advantages are evident, as it allows a fast transfer (about 300 msec) of the sample, irradiated a few feet from the cyclotron, to a low-background counting area, 10 meters away. Nuclei with quite a short half-life can be observed that way. However, no detection selectivity is feasible; all the radioactive products present in the irradiated sample are observed, and γ-lines associated with a weak β-activity can go unnoticed in the large Compton background due to more abundant decays. Also, the cycling of the samples puts them under considerable mechanical stress, especially when returning at high speed to the counting area where they are stopped by a rubber bumper with a 1000 g deceleration. The making of targets with the suitable strength has required much attention. We have finally been able to use such materials as weak as recrystallized sulfur or as brittle as silicon. Gases enclosed in steel and tantalum cylinders sealed with tantalum foils and glued into polyethylene "rabbits" have also been successfully used. Nevertheless, the severe mechanical requirements still limit the range of available targets.

New information, essentially the observation of previously unreported β branches and the measurement of the corresponding log ft values, has been obtained for ten sd-shell proton-rich nuclei. The (p,n), (p,α), and (^{3}He,n) reactions were successively used to form the radioactive nuclei, as reported in the following sections. An attempt to use the (^{3}He,2n) reaction, which has a much lower cross section, to form other more proton-rich nuclei was unsuccessful. This difficulty prompted a systematic study of the total cross sections of ^{3}He-induced reactions on several sd-shell nuclei. The first results are also presented in this report.

---

[1] W. C. Anderson, Ph.D. thesis, Univ. of Colorado (1964) unpublished.

i. The β^+ Decay of A=4n+3, T_z=-1/2 sd-Shell Nuclei: ^{23}Mg, ^{27}Si, ^{31}S, ^{35}Ar, ^{39}Ca - C. Détraz, C. E. Moss, C. S. Zaidins

Many of our results were presented in last year's Progress Report. Since then, the absolute value of the β-branching ratios has been determined from the number of 511 keV annihilation γ-rays due to the β^+ decay of the nuclei under investigation. Also, the measured log ft values have been slightly improved, and upper limits

have been obtained for the branching ratios in the β decay of ^{39}Ca to several ^{39}K excited states. In the β decay of ^{31}S, a very weak branch was observed to feed the 3135 keV level of ^{31}P with a 0.025 ± 0.007% branching ratio. A complete report on these data has been published[1].

---

[1] C. Détraz, C. E. Moss and C. S. Zaidins, Phys. Letters 34B (1971) 128.

ii. The β^+ Decay of A=4n+1, T_z=-1/2, sd-Shell Nuclei: ^{25}Al, ^{37}K - C. Détraz, K. W. Johnson, C. E. Moss, C. S. Zaidins

Of all the sd-shell A=4n+1 nuclei, ^{25}Al and ^{37}K were the only ones for which several allowed β^+ branches had not been reported. In our experiment, these radioactive nuclei were formed in the (p,α) reaction on "rabbit" targets of natural silicon and calcium, respectively. The γ-lines following the β-decay were observed in a Ge(Li) detector and provided a signature of the various β-decay branches. One new branch was observed in the β decay of both ^{25}Al and ^{37}K. Improved upper values of the branching ratios are observed for the unobserved β branches. The results are summarized in table II AXIII.

Table II AXIII
Beta decay of ^{25}Al and ^{37}K.

Parent nucleus J_i^π, $T_{\frac{1}{2}}$(s)	Daughter nucleus	E_{xf} (keV) J_f^π	β^+ Branching ratio		Log *ft*
			this work	previous value	expt.
^{25}Al	^{25}Mg	585 $\frac{1}{2}^+$	$< 5 \times 10^{-4}$	$< 5\times10^{-3}$	> 6.5
$\frac{5}{2}^+$		975 $\frac{3}{2}^+$	$(4.1\pm1.7)\times10^{-4}$	$< 3\times10^{-3}$	6.25 ± 0.18
7.23		1614 $\frac{7}{2}^+$	$(9 \pm2) \times10^{-3}$ [a]	$(9\pm2)\times10^{-3}$	4.28 ± 0.10
		1960 $\frac{5}{2}^+$	$< 3 \times10^{-4}$	$< 7\times10^{-3}$	> 5.2
		2562 $\frac{1}{2}^+$	$< 7 \times10^{-5}$		> 4.8
		2738 $\frac{7}{2}^+$	$< 2 \times10^{-4}$		> 3.8
		2801 $\frac{3}{2}^+$	$< 9 \times10^{-5}$		> 3.9
^{37}K	^{37}Ar	1409 $\frac{1}{2}^+$	$< 2 \times10^{-4}$	$< (2.0\pm0.5)\times10^{-3}$	> 6.6
$\frac{3}{2}^+$		1611 $\frac{7}{2}^-$	$< 6 \times10^{-4}$	$< (1.7\pm0.5)\times10^{-3}$	> 6.1
1.23		2218 $(\frac{7}{2}^+)$	$< 1.5\times10^{-4}$	$\lessapprox 1\times10^{-3}$	> 6.4
		2491 $\frac{3}{2}^-$	$< 1.3\times10^{-4}$	$\lessapprox 1\times10^{-3}$	> 6.2
		2796 $\frac{5}{2}^+$	$(2.0\pm0.4)\times10^{-2}$ [a]	$(2.0\pm0.4)\times10^{-2}$	3.80 ± 0.09
		3171 $\frac{3}{2}, \frac{5}{2}$	$< 6 \times10^{-5}$		> 6.0
		3186	$< 1.2\times10^{-4}$		> 5.6
		3273 $\frac{3}{2}, \frac{5}{2}$	$< 1.1\times10^{-4}$		> 5.6
		3516 $\frac{3}{2}^-$	$< 2 \times10^{-4}$		> 5.1
		3526 $\frac{7}{2}$	$< 1.5\times10^{-4}$		> 5.2
		3602 $\frac{3}{2}^+, \frac{5}{2}^+$	$(3.4\pm0.6)\times10^{-4}$		4.76 ± 0.08
		3715	$< 5 \times10^{-4}$		> 4.4
		3751	$< 6 \times10^{-4}$		> 4.3
		3900	$< 1.2\times10^{-3}$		> 3.8
		3950	$< 7 \times10^{-4}$		> 4.0
		higher levels	$< 5 \times10^{-4}$		

[a]) The previously reported value is used for normalization.

Of particular interest is the observation of an allowed β-decay of ^{25}Al to the 975 keV state of ^{25}Mg, as according to the Nilsson model such a transition between states belonging to different rotational bands, although J-allowed, should be K-forbidden. This indicates a measure of K-mixing in these states. Also the observation of an allowed β-decay of ^{37}K to the 3602 keV state of ^{37}Ar restricts the spin and parity of the latter to $3/2^+$ or $5/2^+$. A report of this study has been published[1].

---

[1] C. E. Moss, C. Détraz, and C. S. Zaidins, Nucl. Phys. A170 (1971) 111.

iii. The β^+ Decay of A=4n+2, T_z=-1, sd-Shell Nuclei: ^{26}Si, ^{30}S, ^{34}Ar - C. Détraz, K. W. Johnson, C. E. Moss, C. S. Zaidins

The (^{3}He,n) reaction at 16 MeV on thick targets of natural magnesium, silicon and sulfur was used to produce the nuclei ^{26}Si, ^{30}S, and ^{34}Ar. Those are the only A=4n+2 nuclei for which there was still a lack of information as to possible allowed β^+ decays. In the case of ^{26}Si and ^{30}S, one γ-yielding β-branch had been observed and its log ft measured. This provided a convenient normalization for the absolute value of the branching ratios of weaker β branches observed in the present experiment. Table II-AXIV lists the new information obtained.

Table II XIV

Experimental results.

β^+-active nucleus	Daughter state		β^+ branching ratio	log ft
^{26}Si	^{26}Al	228 keV	$(6.3\pm0.3)\times10^{-1}$	3.56±0.03
		1058 keV	$(3.2\pm0.3)\times10^{-1}$	3.36±0.05
		1850 keV	$(4.8\pm0.5)\times10^{-2}$	3.58±0.05
		2072 keV	$(4.3\pm1.1)\times10^{-3}$	4.43±0.11
^{30}S	^{30}P	g.s.	$(1.94\pm0.10)\times10^{-1}$	4.37±0.02
		678 keV	$(7.75\pm0.10)\times10^{-1}$	3.482±0.011
		709 keV	$(5\pm2)\times10^{-3}$	5.7±0.2
		3020 keV	$(2.60\pm0.17)\times10^{-2}$	3.49±0.03
^{36}Ar	^{34}Cl	g.s.	$(9.68\pm0.10)\times10^{-1}$	3.45±0.04
		462 keV	$(4\pm3)\times10^{-3}$	5.6±0.3
		665 keV	$(1.4\pm0.4)10^{-2}$	5.01±0.13
		2581 keV	$(5\pm2)\times10^{-3}$	4.30±0.17
		3130 keV	$(9\pm3)\times10^{-3}$	3.58±0.14

Upper limits of the branching ratios of the unobserved β decays are listed in a more complete report prepared for publication[1].

The results of table II AXIV confirm that the 665 keV level in ^{34}Cl has $J^{\pi}=1^{+}$, and we assign $J^{\pi}=1^{+}$ to both the 2581 keV and 3130 keV levels in ^{34}Cl.

The strength of the pure Gamow-Teller $\Delta T=1$ β^{+} transitions can be compared to the analogous M1 γ-transitions in the daughter nuclei. If only the spin-dependent interaction is responsible for the M1 transition, Γ_{γ}(M1) and Γ_{β}(GT) should be equal. In the five cases where the results of table II AXIV allow a comparison, such is not the case. This indicates, as explained in more detail elsewhere[1], that the orbital contribution to the M1 transition is far from being negligible, as often assumed.

---

[1] C. E. Moss, C. Détraz, and C. S. Zaidins, Nucl. Phys. to be published.

iv. Search for the β-Decay Branches of Delayed-Proton Emitters to Bound States of the Daughter Nuclei, and a Measurement of Total Cross Sections for ^{3}He-Induced Reactions - C. Détraz, C. E. Moss, C. S. Zaidins, in collaboration with D. J. Frantsvog and A. R. Kunselman, Univ. of Wyoming

The emission of β-delayed protons by a whole series of A=4n+1, T_z=-3/2 nuclei, from ^{9}C to ^{49}Fe is now well documented (with the exception of ^{45}Cr). However, some of the β^{+} branches from these nuclei feed daughter states which are found for proton emission and decay by γ-ray emission. Only one such β-delayed γ-ray (a 810 keV line from the β^{+} decay of ^{33}Ar) has been reported so far[1]. We attempted a systematic search for these γ-rays by using the (^{3}He,2n) reaction on A=4n self-conjugated nuclei and by taking advantage of the fast transfer of the irradiated target allowed by the "rabbit" technique. For the three target nuclei used so far, ^{24}Mg, ^{28}Si and ^{32}S, this attempt has been unsuccessful and the searches for γ-lines could not be observed in the large Compton background due to much more intense activities. As a by-product, relative values of the total cross sections for several of the observed reactions have been extracted. The "rabbit" technique is a unique tool for such a study as it allows the simultaneous determination of the cross sections of all the reactions which lead to β-delayed γ-activity, even when the half-lives are as short as 100 ms. Consequently, this measurement is essentially free of

systematic errors.

Some preliminary results are listed in table II AXV (^{26}Mg target) and table II AXVI (^{28}Si target), for a 37 MeV ^{3}He beam losing about 20 MeV in the target. Only the bound states of the residual nuclei contribute to the quoted cross sections which have been normalized to a value of 1000 for the (^{3}He,d) or (^{3}He,pn) reaction.

Table II AXV

Residual Nucleus	^{25}Al	^{23}Mg	^{22}Mg	^{26}Si	^{25}Si
Lowest-threshold reaction	(^{3}He,d)	(^{3}He,α)	(^{3}He,αn)	(^{3}He,n)	(^{3}He,2n)
Cross section (arbitrary units)	1000	350	60	25	≤4

Table II A VI

Residual Nucleus	^{29}P	^{27}Si	^{26}Si	^{30}S	^{29}S	^{28}P	^{30}P	^{23}Mg
Lowest-threshold reaction	(^{3}He,d)	(^{3}He,α)	(^{3}He,αn)	(^{3}He,n)	(^{3}He,2n)	(^{3}He,t)	(^{3}He,p)	(^{3}He,2α)
Cross section (arbitrary units)	1000	900	20	25	≤2.5	≤3	≤35	60

[1] J. C. Hardy, J. E. Esterl, R. G. Sextro and J. Cerny, Phys. Rev. C3 (1971) 700.

v. The Radioactive Half-Lives of ^{20}Na and ^{36}K - C. Détraz, K. W. Johnson, C. E. Moss, C. S. Zaidins (in collaboration with D. J. Frantsvog and A. R. Kunselman, Univ. of Wyoming)

For both ^{20}Na and ^{36}K, two conflicting values of the half-lives have been given: 408±6 ms[1] and 451±2 ms[2] for ^{20}Na; 265±25 ms[3] and 345±5 ms[4] for ^{36}K.

We have remeasured these half-lives with the "rabbit" system. Emphasis was on the avoidance of systematic errors rather than on the achievement of very small statistical errors. The nuclei were produced via the (p,n) reaction at 27 MeV on ^{20}Ne and ^{36}Ar. One atmosphere of each gas was contained in steel cells sealed at each

end with 13 μm Ta foils. Each cell was mounted in a polyethylene carrier. After irradiation, 16 or 32 successive γ-spectra were recorded. We checked against sources of possible systematic errors such as unequal dead time in the successive spectra, or late arrival of the "rabbit" in the counting area. This was accomplished by feeding a pulser peak into the spectra, by mounting a ^{22}Na source on the "rabbit" and monitoring the 1275 keV line, and by monitoring a long lived γ-line in all the spectra. Half-lives were extracted by fitting the decays with a non-linear least-squares program which allowed up to two components of different half-lives. This was necessary in fitting the decay of the ^{20}Ne 1630 keV line, for instance, which is fed not only by the β^+ decay of ^{20}Na, but also by the β^- decay of ^{20}F formed in the $^{22}Ne(p,^3He)$ reaction.

In addition, and as a check of the system, the half lives of ^{28}P, ^{32}Cl and ^{40}Sc were measured. Table II AXVII summarizes the results

Table II AXVII

Radioactive nucleus	^{28}P	^{32}Cl	^{40}Sc	^{20}Na		^{36}K	
$T_{1/2}$(ms) previous values	270.3±.5	298±1	182.7±.8	408±6	451±2	265±25	365±5
$T_{1/2}$(ms) this work	277±9	291±5	183±3	446±8		342±26	

The confirmed higher value of the ^{20}Na half life gives a ratio $(ft)^+/(ft)^-$ of 1.062±0.037 for the mirror decays of ^{20}Na and ^{20}F to the 1630 keV state of ^{20}Ne. This value is more compatible with the empirical linear dependence[5] of $(ft)^+/(ft)^-$ with $W_o^+ + W_o^-$ than the value derived from the shorter half life of ^{20}Na.

1 J. W. Sunier et al., Phys. Rev. 163 (1967) 1091.
2 N. S. Oakey and R. D. Macfarlane, Phys. Rev. Lett. 25 (1970) 170.
3 R. E. Berg et al., Phys. Rev. 153 (1967) 1165.
4 A. A. Jaffe et al., Phys. Rev. C 3 (1971) 2489.
5 D. H. Wilkinson, Phys. Letters 31B (1970) 447.

b. The Search for ^{64}Ge and the Half-Life of ^{64}Ga - C. S. Zaidins, C. Détraz, C. E. Moss

The search for ^{64}Ge has become more important since the suggestion of several astrophysicists[1,2] that this nuclide may be involved in explosive nucleosynthesis in the late stages of stellar evolution. Several attempts to produce ^{64}Ge at other laboratories, via the reactions $^{58}Ni(^{12}C,^6He)$ and $^{54}Fe(^{16}O,^6He)$ have been so far unsuccessful, as has the attempt via the $^{40}Ca(^{28}Si,\alpha)$ reaction[3]. These, and

other studies, are also being carried out at the University of Texas and the University of California at Davis.

The experimental attempts for this past year at our laboratory have been a study of the $^{64}Zn + {}^{3}He$ reaction and its products. Early in this year, the excitation function of the $^{64}Zn + {}^{3}He$ reaction, looking only at the long-lived activity, was completed and a paper submitted for publication. The main result of this collaborative effort with the University of Wyoming was to realize that the ^{3}He induced reactions tend to be direct in nature, which does not favor the successful detection of a possible $^{64}Zn(^{3}He,3n)^{64}Ge$ reaction. One interesting result from this study is the discovery of two new activities with half-lives of about 2.5 and 7 hours. Each are seen in two different gamma transitions presumably following beta decays to excited states of the daughter nuclei.

The short-lived activities produced in the $^{3}He + {}^{64}Zn$ reaction were studied at energies of 25, 32, and 37 MeV. The preliminary analysis of this measurement does not indicate any detectable production of ^{64}Ge. It is possible that the compound-nuclear reaction $^{64}Zn(\alpha,4n)^{64}Ge$ will be favored in the E_{α}= 60-80 MeV range where measurements are being made at the University of California, Davis, cyclotron facility.

The one question that has been definitely answered this past year concerns the half-life of ^{64}Ga. Previous measurements indicated an anomalously long ^{64}Ga half-life in $^{64}Zn + {}^{3}He$ bombardments, when compared to that of $^{64}Zn(p,n)^{64}Ga$ half-life experiments. A very careful measurement of the 992 keV gamma ray, which accompanies the ^{64}Ga decay, with 32-multi-scaled spectra and a biased amplifier yielded a half-life of 159 ± 2 sec. This half-life is not only in excellent agreement with previously accepted values, but is the most accurate measurement yet made of this quantity. The responsible reaction is quite likely $^{64}Zn(^{3}He,t)^{64}Ga$.

Rather detailed calculations of the likely decay modes of ^{64}Ge to ^{64}Ga yield a range of possible half-lives of 20 to 2000 sec. These are almost certainly accompanied by a beta-delayed gamma ray from excited states in ^{64}Ga. Our current belief is that the failure to see such decays is more likely to be due to the <u>very</u> small cross-section $(^{3}He,3n)$ in this mass region, rather than a gross misunderstanding of the ^{64}Ge proposed decay scheme.

---

1 D. A. Arnett in an invited paper at the A.P.S. Meeting in Houston, Oct., 1970.

2 J. Truran, private communication.

3 C. N. Davids, private communication.

c. The Excitation Energy of the Second Excited State of ^{12}C - C. Détraz, C. E. Moss, C. D. Zafiratos, C. S. Zaidins, in collaboration with D. J. Frantsvog and A. R. Kunselman, Univ. of Wyoming

There has been much interest recently in redetermining the excitation energy of the second excited state of ^{12}C which enters as an intermediate state in the "triple alpha" reaction $3\alpha \rightarrow {}^{12}C$. The rate of the $^{4}He + {}^{8}Be \rightleftarrows {}^{12}C^{**}$ reaction, which constitutes one step in the process, depends very strongly on the energy of the ^{12}C state. For example, the stellar reaction rate changes by a factor of 5 for a 16 keV change of the excitation energy.

The most precise experiments previously reported involve inelastic scattering[1,2] and the reaction $^{15}N(p,\alpha)^{12}C$ [3]. A measurement of the energy of the γ transition from the second to the first excited state would provide the best value for the excitation energy. This transition has never been directly observed due to its small γ branching ratio[4], 3×10^{-4}.

The measurements we attempted involved the formation of ^{12}N, a β^+ emitter which has a 2.7% β^+ branch to the second excited state of ^{12}C and a half-life of 11 milliseconds.

The first measurement was carried out with a pulsed 27 MeV proton beam and a ^{12}C target of 200 mg/cm^2 (via the reaction $^{12}C(p,n)^{12}N$). The γ rays were detected in a 25 cm^2 Ge(Li) detector. The beam current had to be limited to less than 2 nanoamps in order to avoid "paralysis" of the detection system for over 100 millisec after the beam was turned off. This permitted the detection of the decay (4.439 MeV γ-ray) of the first excited state of ^{12}C which is populated with a 2.3% β branch in the ^{12}N decay. However, the severe limitation on beam current made the detection of the γ ray from the second excited state impossible in any reasonable time. The $^{10}B(^{3}He,n)^{12}N$ reaction was tried with a thin ^{10}B target, but even the first excited state decay was not seen under these conditions.

The second measurement was attempted by using a rotating wheel in air with a circumferential polyethylene $(CH_2)_n$ target of 150 mg/cm^2. The rotating wheel had an angular frequency of 3450 rpm. As a result, any area of the target appeared at the shielded detector less than 10 ms after irradiation. Lead shielding, 30 cm thick, permitted a beam of over 100 nanoamps of protons on target without exposing the detector to undue radiation. This beam intensity involved a production rate of ^{14}O in the air which created no health hazard outside the controlled area. The beam still had to be pulsed to eliminate the neutron background. The 4.44 MeV γ-rays were detected rather weakly in the presence of a background due to the buildup of a long-lived activity on the wheel. The approximately 20 min. half-life of this activity indicates a strong $^{12}C(p,pn)^{11}C$ inherent

background problem. Any further experiments must involve a target or targets which are not exposed continuously, but present a fresh area for beam irradiation with each cycle. Due to the expense of such a system no attempts at further measurements have been planned for the near future.

---

1 S. M. Austin, G. F. Trentelman, and E. Kashy, The Astrophysical Journal 163, 179-82 (1971).

2 M. Stocker, A. A. Rollefson, and C. P. Browne, Phys. Rev. C 4, (1971) 1028.

3 S. J. McCaslin, F. M. Mann, and R. W. Kavanagh, Bull. Am. Phys. Soc. 15 (1970) 1598.

4 D. E. Alburger, Phys. Rev. 124 (1961) 193.

3. Neutron Time-of-Flight Experiments

The fast neutron time-of-flight spectrometer described in last year's Progress Report and further described elsewhere in the present report has been used extensively for (p,n) reaction studies. A great deal of effort has been placed in a comprehensive survey of the (p,n) reaction with emphasis on understanding and exploiting the charge-exchange character of this reaction. The remainder of the effort has been directed toward nuclear spectroscopy, primarily the location of excited states in the 4n + 1 nuclei of the s-d shell.

Most of this year's work was carried out at E_p=23 MeV. The system has worked well, generally delivering one microampere average beams with a repetition rate of 4.5 MHz. Overall time resolution was consistently less than one nano-second. Flight paths ranged from 3 to 30 meters and overall FWHM energy resolution (dependent upon E_p, Q, and flight path) ranged from 30 keV to 200 keV.

a. Comprehensive (p,n) Reaction Survey - R. F. Bentley, J. D. Carlson, D. A. Lind, C. D. Zafiratos

Both the (p,n) and (^{3}He,t) reactions have excited considerable interest in recent years because a simple, one-step charge exchange mechanism may dominate in these reactions, at least for states of uncomplicated structure. If this is the case these reactions:

i. favorably populate isobaric analog states which, by virtue of their simplicity, are quite interesting

ii. provide a direct measure of the isospin dependence of the optical model potential

iii. provide excellent spectroscopic tools for the investigation of energy levels in the residual nucleus since the above mechanism is calculable and sensitive to J, π, and (to a lesser degree) upon configuration.

Considerable effort has also been placed in (^{3}He,t) studies, at this laboratory and many others, partly because of the technical difficulties of (p,n) measurements. However, agreement between DWBA theory and (^{3}He,t) measurements has never been as convincing as in single-nucleon transfer studies such as (d,p) or (^{3}He,d). Whether this indicates the presence of complex mechanisms, such as particle exchanges, or is due to the limitations of the optical model for complex projectiles is not clear. For this reason we chose to make a careful study of the (p,n) reaction where the optical model potentials are best founded and reasonably well understood. This reaction has the added advantage that nucleons are absorbed much less rapidly in nuclear matter than are mass-3 projectiles. The (p,n) reaction is thus much more sensitive to interior portions of the nuclear states involved.

At low bombarding energies the (p,n) reaction is dominated by a compound-nucleus reaction mechanism. However, at sufficiently high bombarding energies the decay of the compound nucleus is divided among so many channels that final states have compound-nucleus contributions much smaller than direct contributions. Clearly, the bombarding energy which divides the "compound" region from the "direct" depends upon the nuclei involved and the final states of interest.

We have obtained some evidence that a proton energy of 23 MeV is sufficiently large, for final states of simple configuration, to ensure a negligible compound-nucleus contribution. One piece of evidence is provided by the 1.6 MeV level of ^{54}Co which is formed in the ^{54}Fe(p,n)^{54}Co reaction. This level is strongly excited at 13 and 14.5 MeV, less so at 16 MeV, and is absent at 23 MeV. Our interpretation is that this level is a multi-particle, multi-hole state such as those which occur in the particle-hole conjugate nucleus ^{42}Sc. Such a state cannot be formed by a one-step process but is easily populated by a compound nucleus mechanism. Accordingly, its decrease of cross-section with increasing bombarding energy provides a measure of the region of non-negligible compound-nucleus yield.

Another piece of evidence is obtained by noting the depths of the back-angle minima observed in analog state angular distributions at E_p=23 MeV. These minima dip as low as 10 μb/sterad while most of the states of interest have cross-sections five or more times larger than this (except at minima in <u>their</u> angular distributions).

Our survey of the (p,n) reaction includes 35 target nuclei ranging in mass from ^{9}Be to ^{208}Pb. Fig. II A51 shows two examples of time-of-flight spectra acquired during this suvey. Fig. II A52 shows some angular distributions of analog state transitions. Our first efforts in analysis of the data have been directed towards:

i. a macroscopic model for analog transitions

ii. microscopic calculation of analog transition

iii. microscopic analysis of low-lying states of simple structure.

The subsequent sections of this report will discuss these topics separately.

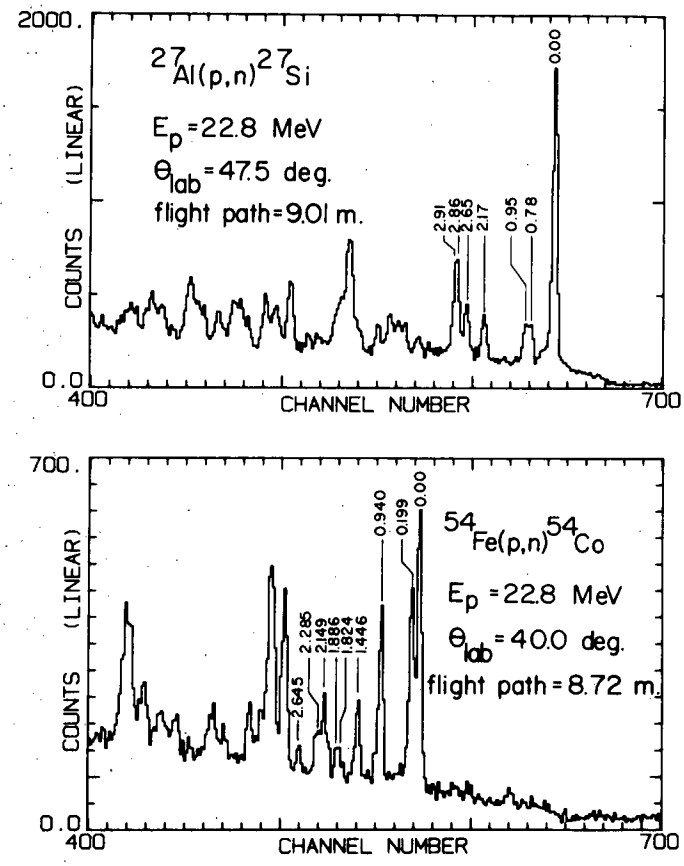

Fig. II A51 Time-of-flight spectra for the reactions ^{27}Al(p,n)^{27}Si and ^{54}Fe(p,n)^{54}Co. The time width per channel is approximately 0.3 ns.

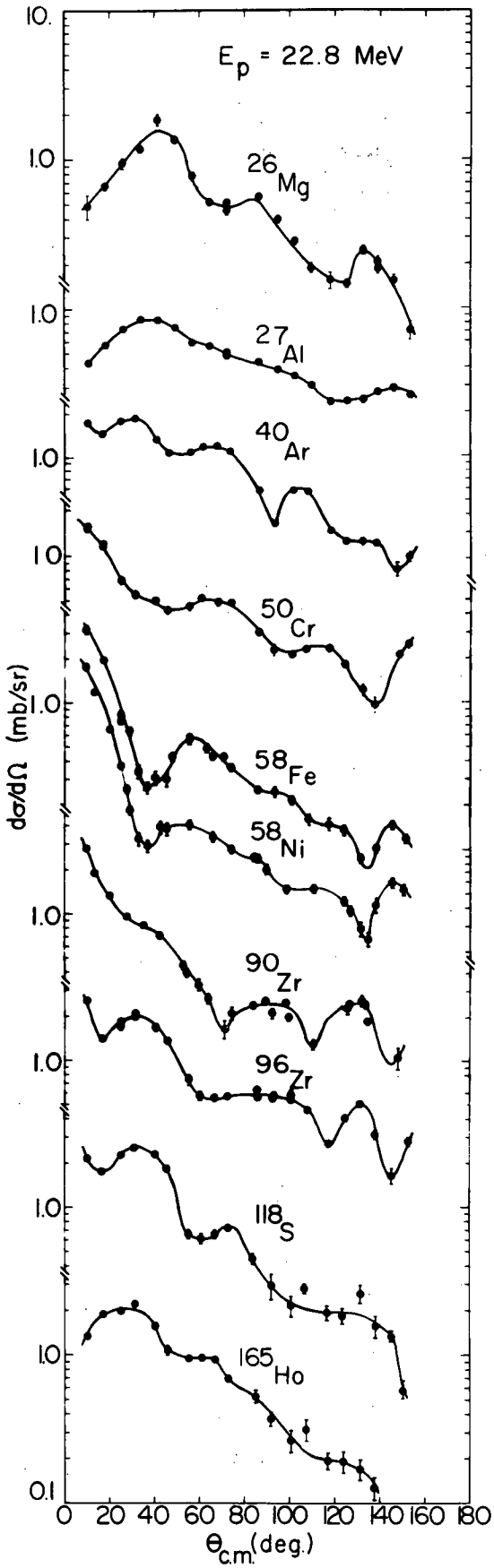

Fig. II A52 Angular distributions for analog transitions in ^{26}Mg, ^{27}Al, ^{40}Ar, ^{50}Cr, ^{58}Fe, ^{58}Ni, ^{90}Zr, ^{96}Zr, ^{118}Sn, and ^{165}Ho. The curve is to guide the eye.

b. Macroscopic DWBA Analysis of Isobaric Analog Transitions - J. D. Carlson, D. A. Lind, C. D. Zafiratos

Angular distributions of (p,n) reactions leading to isobaric analog states at E_p=23 MeV have been measured for 29 nuclei[1]. The targets studied were ^{9}Be, $^{25,26}Mg$, ^{27}Al, ^{31}P, ^{40}Ar, ^{49}Ti, ^{50}Cr, $^{54,56,58}Fe$, $^{58,61,62,64}Ni$, ^{64}Zn, ^{90}Zr, ^{93}Nb, ^{96}Zr, ^{96}Mo, $^{96,104}Ru$, ^{115}Sn, $^{117,118,119,120}Sn$, ^{165}Ho, and ^{208}Pb. Ground state (quasi-elastic) analog transitions were observed on all of these targets. Excited 2^+ analog transitions were also observed on all of the even mass targets with $A \leq 96$ except for ^{90}Zr.

A macroscopic DWBA analysis has so far been attempted for all of the nuclei with $A \geq 50$ by using the code DWUCK[2]. The proton and neutron optical parameters were taken from the compilation of Becchetti and Greenlees[3]. The analytic expressions used were their "best fit" expressions having the radius of the spin-orbit interaction equal to the real radius.

The Becchetti-Greenlees expression contains a complex isospin dependent term (real volume and imaginary surface) from which it is possible to write down a self-consistent isospin form factor.

According to Lane[4] the nucleon-nucleus interaction may be written as

$$U(r) = U_o(v) + 4U_1(r)\frac{\vec{t}\cdot\vec{T}}{A} \qquad (1)$$

The diagonal matrix elements of this expression give the proton and neutron potentials for elastic scattering

$$\langle t_3 = \pm 1/2, T_3 = 1/2(N-Z) | U | t_3 = \pm 1/2, T_3 = 1/2(N-Z) \rangle = U_o \pm U_1\epsilon \qquad (2)$$

where $\epsilon = N-Z/A$ is the asymmetry factor. One of the off-diagonal matrix elements gives the form factor for (p,n) reactions leading to isobaric analog states.

$$\langle t_3 = +1/2,\ T = 1/2(N-Z)-1 | U | t_3 = -1/2, T_3 = 1/2(N-Z) \rangle = 2U_1(\epsilon/A)^{1/2} \qquad (3)$$

Thus the form factor is given by

$$\text{Form factor} = \frac{2}{\sqrt{N-Z}}\ U_1\epsilon = \frac{2}{\sqrt{N-Z}}\ [V_1\epsilon + iW_1\epsilon] \qquad (4)$$

From the Becchetti-Greenlees expressions one can now take a complex U_1. For the real volume part of U_1 this is trivial. However, for the imaginary surface part a complication arises due to the fact that the imaginary geometry is different for the proton and neutron expressions. To take this difference into account a form factor of the following form has been used

$$\text{Form factor} = \frac{2}{\sqrt{N-Z}}\ [V_1(\text{real geometry})\epsilon + 1/2iW_1(\text{proton imaginary geometry}) + 1/2iW_1(\text{neutron imaginary geometry})] \qquad (5)$$

The V_1 and W_1 which one obtains are -24.0 MeV and +48.0 MeV respectively.

Figure II A53 shows the macroscopic DWUCK predictions with the above form factor and the corresponding data for 10 different targets. The predictions have not been normalized to the data. What is shown are the absolute calculations.

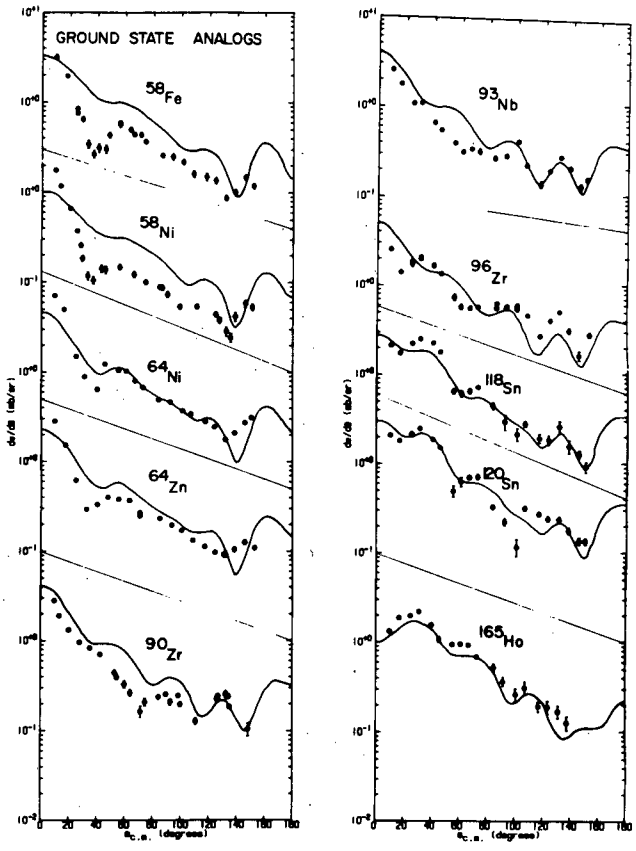

Fig. II A53 Comparison of ground state analog data with macroscopic DWBA predictions made by using a form factor derived from the isospin term in the Becchetti-Greenlees optical potentials.

Generally the absolute magnitude of the predictions is in good agreement with the data. Also, the DWUCK calculation does a good job at fitting the shape of the observed angular distribution for the heavier nuclei, $A \gtrsim 90$. It does not, however, fit the shape of the distributions for the lighter nuclei, particularly the large maxima at small angles. This difficulty appears to be rather general for nuclei with a small neutron excess ($N \approx Z$).

Attempts have been made with some success at empirically determining a form factor for the DWBA calculation which would give agreement with the data for the lighter nuclei. For the ^{58}Ni analog transition an acceptable fit has been obtained with a form factor the same as that given in eq. 5 except that the diffuseness had been

increased by 50% in both the real and imaginary parts. This had the effect of raising the small angle maxima. A comparison of these fits is shown in Fig. II A54 where the case with the form factor derived from Becchetti and Greenlees is labeled macro 1 and the case where the diffuseness has been increased 50% is labeled macro 2. Also shown in this figure is a microscopic calculation in which an $f_{7/2}$ neutron in ^{58}Ni was charge-exchanged via a Yukawa central interaction with the incident proton. The range parameter was 1 fm.

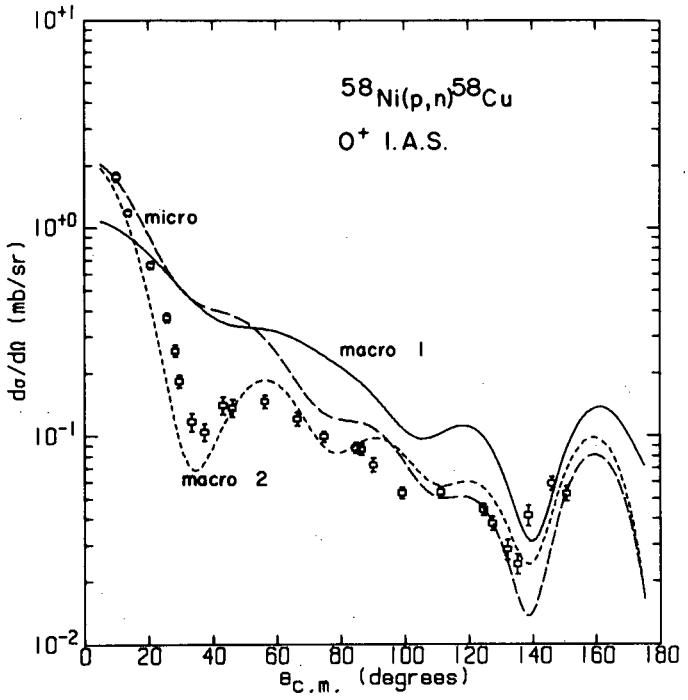

Fig. II A54 Comparison of $^{58}Ni(p,n)^{58}Cu$ (analog) data with both macroscopic and microscopic DWBA predictions.

Some macroscopic DWBA calculations have been done for excited 2^+ analog transitions with A=58,64. The form factor used in the DWUCK calculations for these L=2 transitions was simply the derivative of eq. 5. In Fig. II A55 are shown some DWBA predictions for 2^+ analog transitions. In this case the predictions have been normalized to the data. The calculations have roughly the same shape as the observed distribution. However, there is again a disagreement at small angles.

A rather interesting preliminary comparison of angular distributions has been made for analog transitions in nuclei belonging to the mass sequences A=58,64, and 96. It was found that within a constant A sequence the small angle minima became more pronounced as the neutron excess increased. A similar behavior could be obtained in

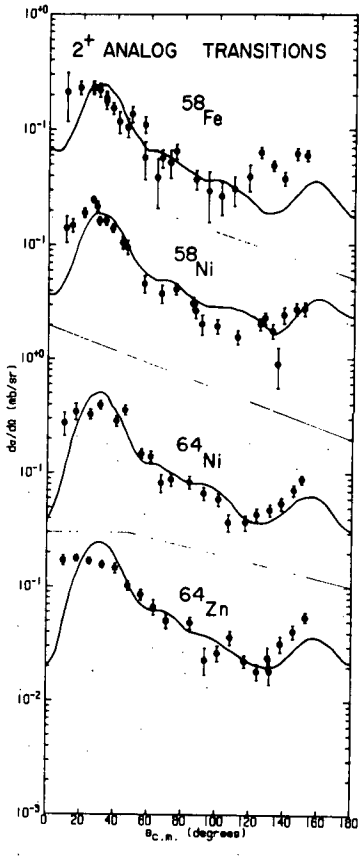

Fig. II A55 Comparison of macroscopic DWBA predictions for excited 2^+ analog transitions with data for ^{58}Fe, ^{58}Ni, ^{64}Ni, and ^{64}Zn.

the DWBA predictions by either increasing the radius or the diffuseness of the form factor over those of the optical potentials. Another systematic feature found in this comparison was that the minima in the angular distribution were in phase for nuclei having the same A. Finally, the absolute magnitude of the cross sections scale approximately as the neutron excess except at small angles.

---

1 R. F. Bentley, J. D. Carlson, D. A. Lind, R. B. Perkins, C. D. Zafiratos, Phys. Rev. Lett. 27 (1971) 1081.

2 P. D. Kunz, Univ. of Colorado, Boulder, private communication.

3 F. D. Becchetti, Jr., and G. W. Greenlees, Phys. Rev. 182 (1969) 1190.

4 A. M. Lane, Nucl. Physics 35 (1962) 676.

c. Microscopic Calculations of Analog Transitions -

R. F. Bentley and C. D. Zafiratos

Microscopic calculations have been completed for all the analog

transitions for which data have been analyzed and optical model parameters are available. Single configuration shell model wave functions have been computed in a Woods-Saxon well to give the appropriate separation energy. A real Yukawa interaction with ranges from 0.5 to 2 fm has been assumed. Reasonable fits to the data have not been obtained and extensive calculation on several transitions indicates that configuration mixing of the bound state wave function will not significantly improve the fits. Attempts are now being made to derive the form of an imaginary term in the microscopic interaction as suggested by Satchler[1].

---

[1] G. R. Satchler, Phys. Letters 35B (1971) 279.

d. Microscopic Analysis of Simple Non-Analog Transitions -

R. F. Bentley, C. D. Zafiratos

As in the case of analog transitions, microscopic calculations for transitions to $T_<$ states give unsatisfactory fits to the data. In the cases where the tensor force is allowed, its inclusion often improves the fits. Especially at large angles, however, the tensor force is not enough to achieve agreement with the data. See for example, Fig. II A56 where the effects of particle exchange should be small because of the low L transfer.

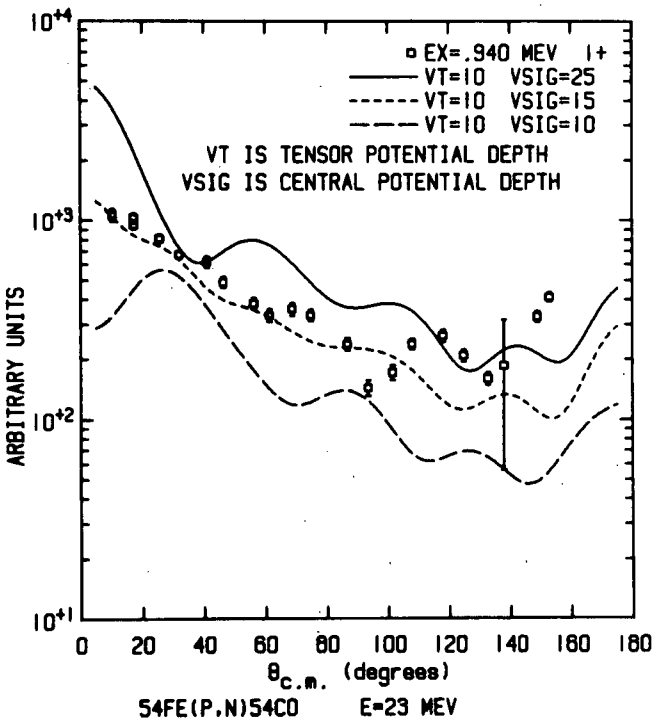

Fig. II A56 Cross section angular distributions showing data for the 1^+ state in ^{54}Co and three DWBA calculations with varying proportions of tensor potential included in the microscopic model.

Except for the tensor term, the interaction for these transitions is the same as for analog transitions. The derivation of an imaginary term in the microscopic interaction would therefore affect these calculations also.

e. Study of the (p,n) Reaction to Anti-Analog States -

H. Rudolph, C. D. Zafiratos, and R. F. Bentley

Recently Hinrichs et al.[1] have observed that the angular distributions of the (^{3}He,t) reaction proceeding to 0^+ anti-analog states do not appear to be characterized by zero orbital angular momentum transfer, i.e., comparison of the data for the analog and anti-analog transitions shows them to be exactly out of phase. Since this anomaly has as yet no explanation, it is of interest to investigate whether (p,n) angular distributions also exhibit this behavior. The observance or non-observance of the anomaly might indicate possible resolutions to the problem, e.g., if the (p,n) angular distributions are in phase, it is possible that present ideas regarding the (^{3}He,t) reaction mechanism may have to be restructured.

We have studied the ^{40}Ar(p,n)^{40}K and ^{56}Fe(p,n)^{56}Co reactions at 23 MeV incident proton energy. The energy resolution obtained at flight paths averaging 7.5 m was about 200 keV in the region of the anti-analog state. For ^{56}Co this resolution combined with the weak population of the anti-analog (<5% of the analog state for both nuclei) precluded the acquisition of useful data except at the longest flight paths (> 8 m). The data for ^{40}K anti-analog (shown in Fig. II A57) are also of insufficient quality to conclude whether an L=0 pattern is present or not. We are now planning to repeat the experiment with our new neutron TOF facility at a flight path of 12 m. This experiment should easily resolve the problem.

---

[1] R. A. Hinrichs, R. Sherr, E. M. Crawley and I. Proctor, Phys. Rev. Letters 25 (1970) 829.

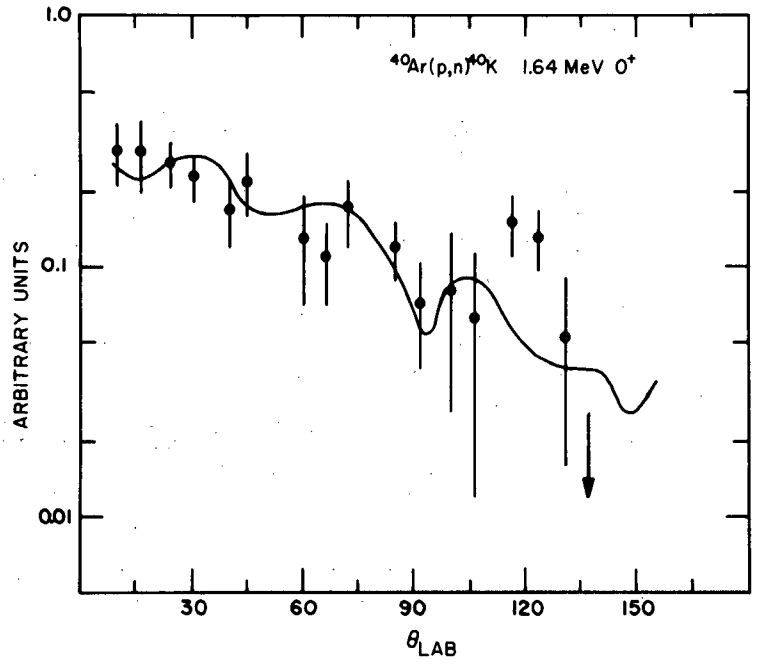

Fig. II A57 Angular distribution of the $^{40}Ar(p,n)^{40}K$ reaction to the anti-analog state. The solid line is a smooth curve drawn through the data for the 0^+ analog transition.

4. Other Activities

a. Trace Element Analysis by Detection of Characteristic X-rays - H. Rudolph, J. J. Kraushaar, W. R. Smythe, and R. A. Ristinen

Trace element detection and analysis have become especially important problems in recent years due to mounting public awareness of environmental pollution. Methods such as wet chemistry, neutron activation, atomic absorption spectroscopy, and atomic emission spectroscopy have long been used in this field. More recently the detection of characteristic x-rays produced by the passage of charged particles through matter[1] or by x-ray fluorescence[2] has proven to be an extremely useful and versatile tool in the detection of trace elements. In general, the method is low-cost and broad ranged, competing with and in many cases surpassing the sensitivity of the older methods of detection for most elements.

During the past year, we have been developing techniques for sample analysis by both the charged particle and x-ray induced methods. This report is designed as a summary of our results with special attention to types of hardware we have developed, sample preparation techniques and examples of systematic studies in which we are engaged.

I. Hardware

Most of our analyses up to the present have been done with a conventional cooled FET Si(Li) detector of 230 eV resolution at the iron K_α energy (6.4 keV). We plan to put into operation a guard ring-type Si(Li) detector[3] in the near future, which should greatly increase the sensitivity of the x-ray induced method.

In order to make quantitative measurements of trace element content, one must either have good target uniformity or a uniform flux beam, either of charged particles or x-rays. We have chosen to provide uniform beams. This allows a great deal of latitude in target preparation. A uniform flux of x-rays is rather easy to provide with most x-ray tubes and appropriate collimation. Charged particles, on the other hand, present a problem in that most beam handling equipment is designed to provide a good sharp focus rather than a uniform flux. We have solved the problem by allowing the focused beam to pass through a foil upstream of the target position and be diffused by small angle Coulomb scattering in the foil. This diffused beam has a radial shape which is roughly Gaussian, and one can adjust the uniformity of the flux on target by an appropriate choice of foil thickness and position and defining apertures. For a Gaussian shape it can easily be shown that the fraction of the incident beam which is passed through the collimators

is equal to the fractional variation in the current density of the beam from the center to the edge of a circular aperture. This is a handy reference for positioning the foil in order to get the desired uniformity in the flux.

The beam diffuser along with the irradiation chamber and target ladder assembly are shown in Fig. II A58. The chamber may be used with either charged particles or x-rays. The target

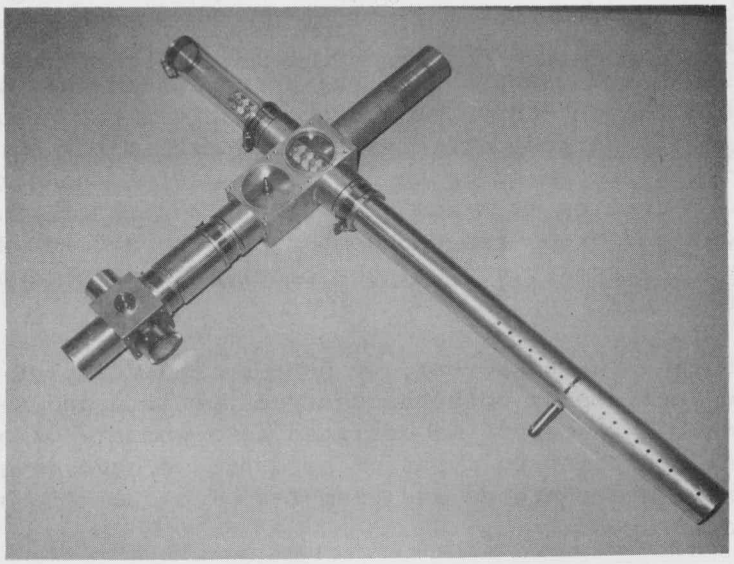

Fig. II A58(a) Irradiation chamber and associated hardware.

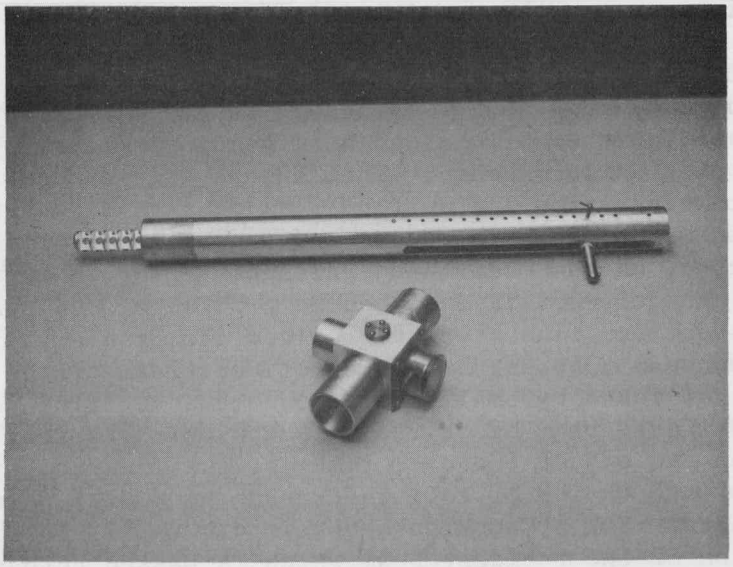

Fig. II A58(b) Target changer (above) and beam diffuser (below).

ladder accommodates up to sixteen target frames which are thin pieces of aluminum with 3/8" holes drilled through them. Thin mylar or formvar target backings are presently in use at this laboratory. Formvar has the advantage of being extremely thin ($\sim$ 15 $\mu g/cm^2$) and having high purity; commercial mylar frequently contains measurable quantities of iron, zinc and copper. It must be noted that the failure rate of formvar target backings is appreciable, and more care must be used in its handling during target preparation than with mylar, which is much more durable. We are, however, now using formvar whenever possible since the signal-to-noise ratio is greater for the thinner backing.

We have available at this laboratory a power supply and x-ray tube capable of 20 mA current at 75 kV. Because this high-intensity equipment was available, we have been able to run the same very thin targets used in the charged particle work for the x-ray excitation work, in contradistinction to the low power tube-thick target method reported by Giauque and Jaklevic [2]. We use filters of various metals and sometimes secondary radiators in order to monochromatize the bremstrahlung spectrum from the tungsten anode of the x-ray tube. A sliding ladder of filters is provided so that the incident spectrum may be adjusted for the range of elements of interest. For example, we have been using a tin filter in a study concerned with the detection of molybdenum. The x-ray set collimation provides a uniform flux of about 0.2" diameter at the target. This is the same beam size typically used with charged particles, which makes it convenient to use the same targets with either method.

II. Sample Preparation

We have developed a fairly simple technique for making targets from water residue. The idea is to feed a small droplet of water onto the target backing at a rate equal to the rate of evaporation of water from the droplet. The mechanism used (Auto-Dripper) is shown in Fig. II A59. A low speed (1 rph) high torque motor depresses the plate which in turn depresses the plungers on an array of nineteen hypodermic syringes. The target frames are mounted on a heated substrate in order to facilitate evaporation of the droplets. The amount of water used for each target is about 0.5 cc which may be deposited in eight hours with the Auto-Dripper.

Most organic samples are prepared by ashing. The sample may be dried in an oven if necessary, at about 100° C (typically overnight) and then the temperature is raised in 50° steps every half hour to between 550° and 650° C, depending upon the sample. The ashing is allowed to proceed at this temperature for about 10 hours. The ash is powdered and mixed thoroughly, and about 0.5 mg is weighed and deposited within the central 4 mm diameter area of the target backing. A low Z glue[4] is used to affix the material to the backing.

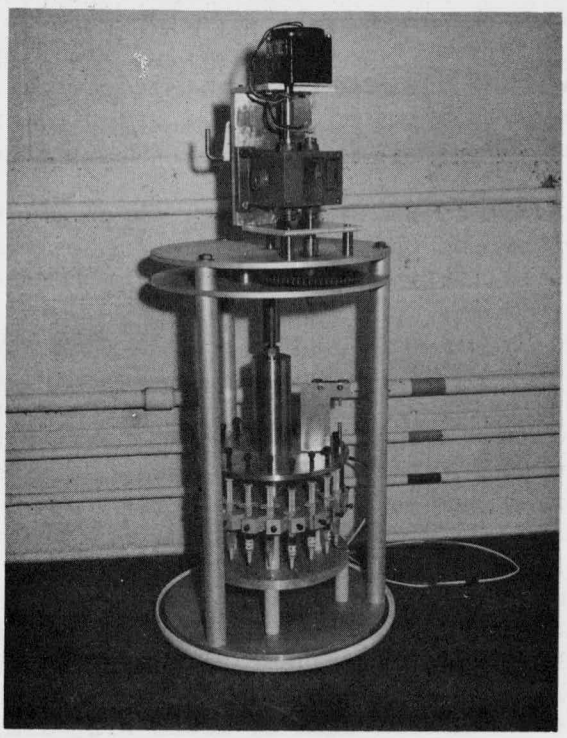

Fig. II A59 Auto dripper for making water residue targets.

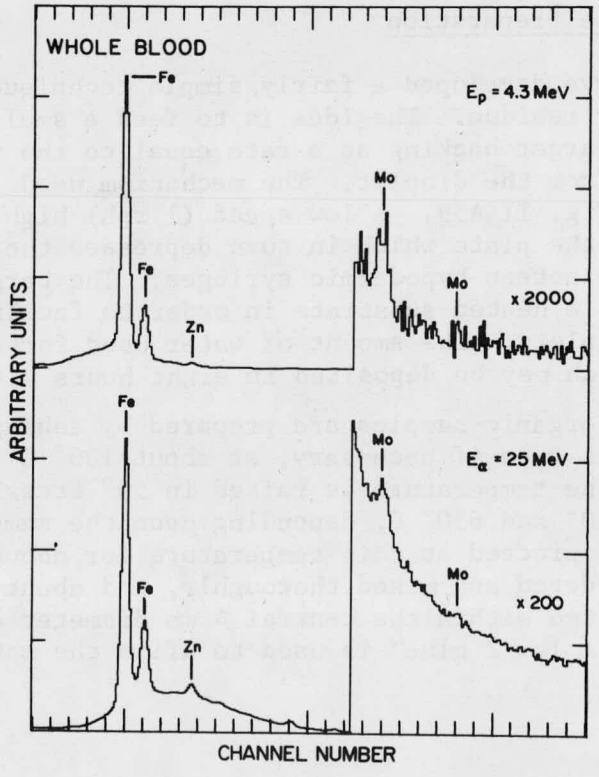

Fig. II A60 Whole blood sample irradiated by protons (upper) and alphas (lower).

We have used this technique for plants, bone, soft tissue and milk samples with great success. One may also ash whole blood and blood serum.

III. Investigations

A. Optimization of Particle Type and Energy

In Fig. II A60 the results of using protons and alphas as the bombaring particles are compared for a whole blood sample. The expanded portion of the figure clearly shows the better signal-to-noise ratio for protons. The concentration of molybdenum in this sample is about 80 ppB. For this type of sample the detection limit for elements with atomic number around forty is a factor of five to ten less than this.

The sensitivity of the method as a function of bombarding energy has been investigated, and the results for protons are illustrated in Fig. II A61. The water sample used to obtain these spectra is from a reservoir which supplies water to the city of Denver. The signal-to-noise ratio is in general best for the lowest proton energy (1.9 MeV). However, the cross section for x-ray production is lowest for this energy. The higher beam current which must be used at this energy combined with the larger energy loss of the protons in the

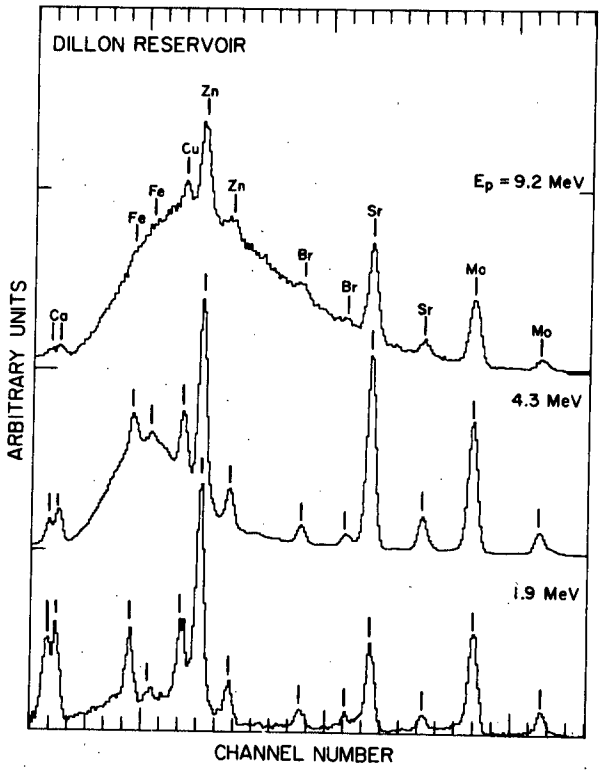

Fig. II A61 Energy dependence of proton induced x-rays.

target material tends to burn holes in the target. One can therefore not make use of the maximum count rate capability. Consequently, we have decided to use 4.3 MeV protons for our studies as a compromise between good signal-to-noise ratio and ease of processing large numbers of samples. This study shows that the high energies attainable with a cyclotron are not necessary for good trace element detection. Energies attainable with a single stage Van de Graaff accelerator would be sufficient.

B. Bremstrahlung Background

For most environmental measurements the important quantity to consider is not the absolute amount which can be detected but rather the minimum detectable relative amount when the element of interest resides in a matrix of other elements. The governing factor is then the background due to this matrix. Although characteristic x-rays from the elements of the matrix can be a problem, it is more often found that the continuum background causes the trouble.

One can easily see this in the water residue spectra in Fig. II A62. Without absorbers between target and detector (40 mil lucite in this case) the continuum background would be shown to rise very sharply at low energy. The amount of molybdenum in the three water samples ranges over about two orders of magnitude. Boulder city water contains about 2 ppB molybdenum. Note that in these spectra the height of the continuum is roughly proportional to the height of the calcium peaks.

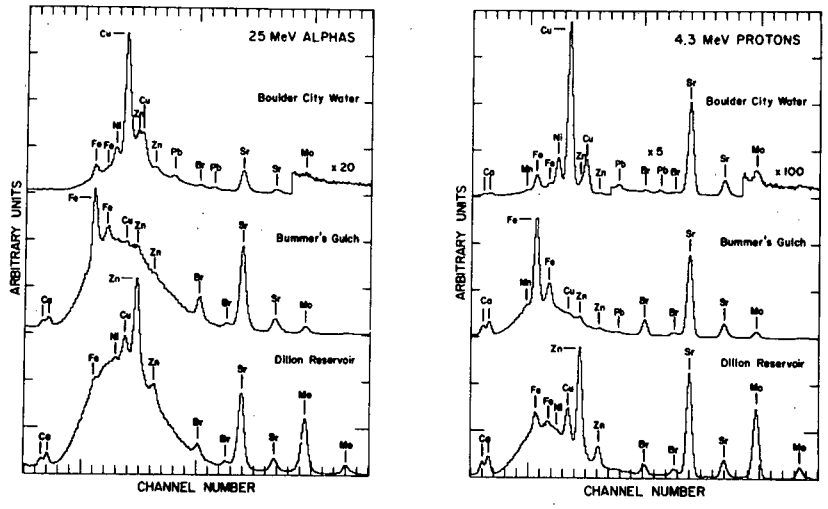

Fig. II A62 Spectra from three water residue samples. Note that the continuum height is roughly proportional to the calcium concentration.

We have called this background K-shell Bremstrahlung because the most important part (that at higher energy) appears to arise from Brehmstrahlung produced in the collision between the incident particle and a K-shell electron in an atom of the matrix. The variation of the endpoint energy of this Bremstrahlung spectrum with the atomic number of the matrix elements and the velocity of the incident particle has been experimentally determined and seems to correspond to a K-shell Bremstrahlung process.

C. Comparison with Other Methods

An attempt has been made to compare our results quantitatively with other methods of trace element detection. The spectrum shown in Fig. II A63 is from a sample of ashed mesquite plant provided by the United States Geological Survey in Denver. The sample was analyzed there by atomic emission spectroscopy. For most of the elements shown in the figure there was an overlap in results by the two methods. Table II AXVIII shows a comparison of the results.

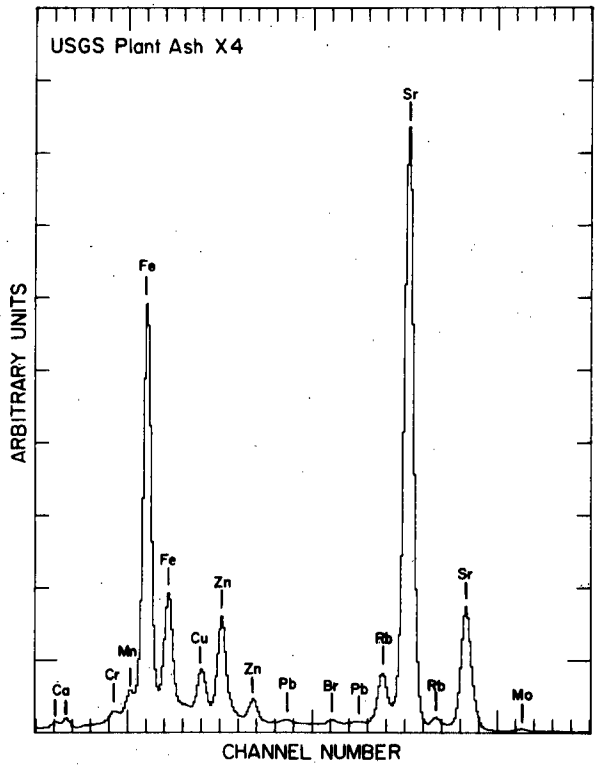

Fig. II A63 Ashed mesquite plant provided by the USGS in Denver.

The numbers all have an estimated error of 20%. The two columns have been normalized at iron. In all cases there is good agreement. It should be noted that the lower limits of detectability by atomic emission spectroscopy are in general greater than one part per million for organic matter, whereas the charged particle induced x-ray limits may be much lower than this.

Table II XVIII

Comparison of two methods of analysis.

ELEMENTS	QUANTITY (PPM) Charged Particle Induced X-rays a)	Atomic Emission Spectroscopy a)
Ca	21000	18000
Mn	590	500
Fe	5400	5400
Ni	(26)	32
Cu	390	280
Zn	730	500
Br	31	Not measured
Rb	530	Not measured
Sr	6400	>5000
Mo	60	83
Ba	260	230

a) Errors are ± 20%.

We have also made comparisons with wet chemistry techniques for determination of molybdenum. For this element the x-ray method has been probably the most sensitive technique. We have obtained good results for a series of water samples, and in addition are able to detect concentrations an order of magnitude smaller than by wet chemistry. Several plant ash analyses have also been compared, and agreement is good in all cases.

D. Multi-disciplinary Study of Molybdenum

We are also associated with an NSF-funded multi-disciplinary (Biology, Chemistry, Economics, Engineering, Geology, Medicine and Physics) study of the introduction, transport, and effects of molybdenum in the environment. Included in the study are stream and surface water surveys, soil and plant sampling, air sampling, laboratory experiments on plants and animals, and investigation of effects on human populations. The ultimate aims of the investigation are twofold: to model the processes by which molybdenum proceeds through the environment, possibly determining methods of decreasing its introduction if necessary, and to investigate its effects on living organisms both in the acute and clinical sense. As an example of one of the findings of the study, we have determined that when molybdenum is injected into rats, it tends to accumulate in the liver, kidney, and fatty tissue.

E. Trace Elements and Blood Dialysis

At the present time there are a large number of people who are being maintained on artificial kidney machines after total loss of kidney function. Statistics are mounting to indicate an abnormal

incidence of several types of bone disease in these patients. The dialyzing fluid used in the artificial kidney machines is generally made up from tap water, and since these patients are exposed to approximately 1000 L/week of this fluid, there is a suspicion that the high incidence of bone disease may be due to an imbalance of trace elements in the body introduced by the blood dialysis. We are presently working in cooperation with the VA hospital in Denver in an attempt to analyze the movement of trace elements across the membrane separating the patients' blood from the dialyzing fluid. We are also attempting to analyze tissue samples taken from deceased dialysis patients for trace element concentrations. One initial result is that the used dialysis fluid seems to have a large concentration of iron. This would be consistent with the fact that dialysis patients are generally iron deficient.

F. Medical Diagnosis

Our group is involved in the application of x-ray fluorescence techniques to general problems of medical diagnosis. There is much effort presently being expended on finding possible links between trace elements and disease. In Fig. II A64 are shown the spectra from whole blood samples provided by the University of Colorado Medical School. The disease being studied is Wilson's Disease which is manifested by an interference in copper metabolism and eventual deterioration of the liver cells. It is detected

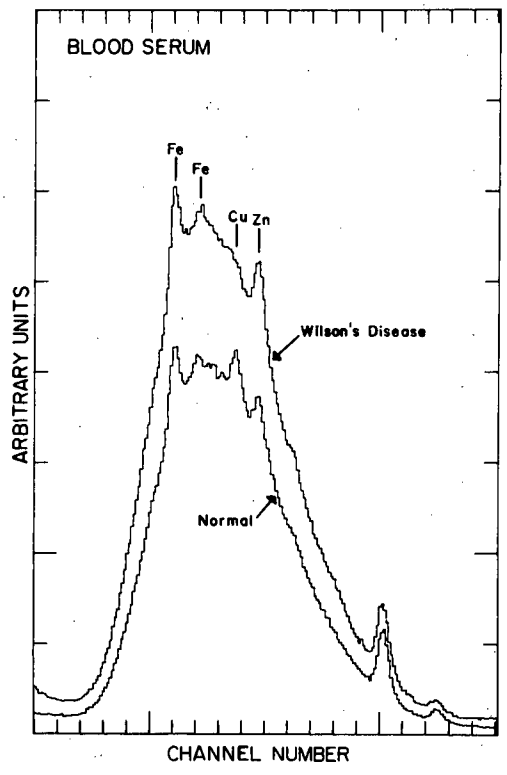

Fig. II A64 An illustration of the diagnosis of Wilson's Disease.

experimentally by a lack of copper in the blood serum as shown in the figure. Early diagnosis of the disease may be an important tool since it has an insidious onset, i.e., once clinical symptoms appear, the damage is irreversible. Investigation is presently continuing upon these lines.

G. Trace Elements in Milk

We are presently engaged in a survey of milk from dairy farms in the area in conjunction with the interdisciplinary molybdenum project and the Denver Board of Public Health. Our results show that the detection limits for trace elements in ashed milk are only slightly above what can be seen in water residue samples.

H. Impurities in Manufacturing Processes

Talks have been going on with a representative of the Dow Chemical Co., which operates the Rocky Flats installation for the AEC. They are interested in determining impurity content introduced during processing of radioactive materials. We have demonstrated that we can detect reasonably small amounts of elements such as iron, copper and zinc in a matrix made entirely of, say, uranium. Investigations are underway to determine the feasibility of on-line determination for quality control.

IV. Summary

The usefulness of the x-ray techniques for determination of trace amounts of the elements has been demonstrated in some detail. It is necessary, however, to discuss the absolute sensitivity of the method and the relative sensitivity when protons or x-rays are used as the source of excitation. In order to process large numbers of samples, irradiation times must be limited by some criterion, and sensitivities are quoted with this fact in mind. The standard runs which we make are 10 minutes for protons and twenty minutes for x-rays. In general, we interpose 0.04 inches of lucite as an absorber between the detector and the target. For protons, with this irradiation time and geometry, we obtain a sensitivity of no worse than 1 ppM of the target material for a range $25 \lesssim Z \leq 50$. This implies a sensitivity of 1 ppB for water samples and 10-100 ppB for most samples which can be ashed. These figures are quoted for a somewhat favorable background matrix, e.g., if a samples contains more than 50 ppM iron, then a concentration for cobalt of less than 2-3 ppM could not be measured due to the overlap of the iron K_β with the cobalt K_α line. Sensitivities will, of course, scale with the square root of the irradiation time.

We have attempted to compare in some detail the relative merits of proton and x-ray excitation. With a normal Si(Li) detector the irradiation times necessary with our x-ray equipment are sometimes as much as 4 to 6 times longer than for protons. Full time usage of either beam would then favor the use of protons. If, however, the background reduction obtainable through the use of a guard-ring detector[3] is at least a factor of 10, then the two types of excitation would be comparable on an analysis-time basis. This then implies that it is worthwhile to use charged particle beams only if the facility is readily available.

In conclusion, it has been established that the detection of characteristic x-rays for trace element analysis is a usable and competitive method. One can investigate a broad range of elements with good sensitivity simultaneously. Sample requirements are minimal; only a gram of material is sufficient. Analysis time is short enough to make the processing of large numbers of samples feasible.

---

[1] T. B. Johansson, R. Akselsson and S. A. E. Johansson, Nucl. Inst. and Meth. 84 (1970) 141.
[2] R. D. Giauque and J. M. Jaklevic, LRL-204 (July 1971).
[3] F. S. Goulding and J. M. Jaklevic, UCRL-20625 (May 1971).
[4] G. C. Electronics Polystyrene Q-dope diluted 100:1 in spectral grade toluene.

b. Outside Users of Cyclotron Facilities

The Nuclear Physics Laboratory has continued to encourage outside groups to make use of the cyclotron for educational or research purposes. Professor S. A. Watkins of Southern Colorado State College in Pueblo brought 15 advanced physics students to the laboratory for two days of nuclear physics experiments. Among other activities in the laboratory, they examined the use of x-ray fluorescence methods to determine the trace metals in the ink on currency.

Again last summer eight Hispano students from Denver spent every afternoon at the laboratory for four weeks. The students did a variety of interesting things, including an experiment with the cyclotron.

The cooperative program with the University of Wyoming has continued. Professor R. Kunselman and four graduate students are participating in the (p,n) and short-lived radioisotope studies that are described elsewhere in this report.

Professor James K. Kliwer of the Department of Physics at the University of Nevada is spending his sabbatical year at the Nuclear Physics Laboratory. He is involved in the x-ray fluorescence studies as well as some nuclear spectroscopic measurements. Professor Reinhard Graetzer from the Department of Physics at Pennsylvania State University is also spending the current academic year at the laboratory working on nucleon transfer reactions.

c. The Stable ^{50}Cr Red Blood Cell Survival Test - E. W. Stoub, R. A. Ristinen, and J. J. Kraushaar

The standard Red Blood Cell Survival test of Nuclear Medicine

has used radioactive ^{51}Cr as a tracer. Our study (the initial phases were described in last year's Progress Report) has substituted stable ^{50}Cr for ^{51}Cr to eliminate radiation exposure to the subject. Samples of blood are then activated by thermal neutron capture at the TRIGA reactor of the U.S.G.S. Center in Denver. Gamma ray spectrum analysis yields the time behavior of the chromium concentration in the blood of the subject, which indicates the red blood cell survival rates. Due to a high cross section for thermal neutron capture and the convenient 28 day half life, the gamma activity due to the decay of ^{51}Cr to ^{51}V at 320 keV is easily identified when Ge(Li) detectors are used.

The main difficulty in this experiment is the large fluctuation of the raw data, larger than statistics would allow. The cause of these fluctuations is assumed to be unstable metabolic conditions in the subjects, which were dogs. Given this assumption, a simple mathematical treatment yields a normalizing factor for each data point. This normalizing factor is the volume density of red blood cells for each blood sample. The resultant data have much more reasonable fluctuations, attributable to statistics and to uncertainties in volume measurements.

These investigations were presented at the 18th Annual Meeting of the Society of Nuclear Medicine, June 28-July 2, 1971, in Los Angeles. The work was carried out in collaboration with Dr. D. W. Brown of the C. U. Medical Center in Denver.

d. Nuclear Astrophysics - C. J. Hansen (JILA) and C. S. Zaidins

New interest in the $^{12}C + {}^{16}O$ stellar reaction rates and the appearance of low-energy cross-section data on this reaction[1] led to the derivation of expressions which may be used to calculate the astrophysical reaction rates and energy production of ^{12}C and ^{16}O mixtures. These expressions are

$$\langle\sigma V\rangle = 5.0 \times 10^{-7}\ T_9^{-2/3}\ \exp\left[-106.6\ T_9^{-1/3}(1 + 0.017\ T_9)\right] \text{cm}^3/\text{sec}$$

in the range $T_9 = 1.8$ to 4.2 (T_9 is the temperature in 10^9 K) and

$$\langle\sigma V\rangle = T_9^{-2/3}\ \exp\left[T_9^{-1/3}(-95.914 + 3.8344\ T_9 = 0.35254\ T_9^2)\right] \text{cm}^3/\text{sec}$$

over the larger range $T_9 = 2$ to 9 which were derived from least-squares fit to the data. There are still unanswered questions in the general astrophysical problems of ^{12}C and ^{16}O initial mixtures and $^{12}C + {}^{12}C$ and $^{16}O + {}^{16}O$ reaction rates. Their solution requires further data which may not easily be obtained for some time.

There was also an attempt to measure the precise excitation energy of the 2nd excited state of ^{12}C which is important in the stellar production of ^{12}C from ^{4}He. This work is described in the

"rabbit" section of this report.

---

[1] J. R. Patterson, B. N. Nagorcka, G. D. Symons and N. M. Zuk, Nucl. Phys. A165 (1971) 54.

e. Proposed Experiments at LAMPF - J. J. Kraushaar, R. J. Peterson, B. W. Ridley, R. A. Ristinen

Four proposals for experiments at LAMPF have been submitted (LAMPF numbers 46 through 49). We propose to use the high resolution pion spectrometer to study the elastic scattering of positive and negative pions at several energies from the deuteron. This experiment has been allocated 300 hours of beam time. We plan to study the scattering both of positive pions at about 150 MeV and protons of 800 MeV from a ^{89}Y target. One-hundred fifty hours of pion beam time have been allocated to this experiment. We also have submitted proposals for pion and proton scattering from several isotopes of nickel, but no time is yet assigned.

Our interest in scattering pions from the deuteron is to determine the extent of double scattering contributions to the cross section. A single scattering approximation is central to all optical model theories of pions scattered from complex nuclei, and we shall test this on the simplest complex nucleus.

The nucleus ^{89}Y exhibits several excited states populated by L=2 and L=3 transitions in scattering. We anticipate that the angular distributions to these states will be strikingly different in the inelastic scattering of 800 MeV protons, due to the fact that the short wave length, singular interaction, and low absorption of these projectiles will be very sensitive to details of the nuclear wave functions. Two general predictions for the scattering of pions make, however, contradictory statements on the sensitivity to the detailed wave function. The strong absorption at energies near the 3-3 resonance (~150 MeV in the lab) creates sharp diffraction structure in the angular distribution, and in comparison to strongly absorbed alpha particle scattering, we anticipate little sensitivity to the nuclear details. On the other hand, the p-wave interaction of the 3-3 resonance is manifested as a gradient in the operator causing the inelastic transition, and this operator does care about the detailed nuclear wave functions in the surface, and the data may be sensitive to the specific nuclear state. We have chosen ^{89}Y to test which assumption will be vindicated because of the existence of several states populated by the same L transfer, but with different wave functions.

It is anticipated that new research proposals will be submitted to LAMPF each year, and that an active users' research program will be followed.

B. Apparatus and Facility Development

1. Fast Neutron Time-of-Flight Spectrometer - R. F. Bentley, J. D. Carlson, D. A. Lind, C. D. Zafiratos

The neutron spectrometer described in this section has been under development for several years[1,2,3]. A peak of activity in its use was reached this past summer and spring when the system was in continuous use approximately two weeks out of every month. Its primary use was in the measurement of angular distributions from the (p,n) reaction in the angular range of 10° to 152°. This work was typically carried out at E_p=23 MeV with flight paths ranging from 7 to 10 meters. The system was also used for high resolution nuclear spectroscopy. In this work, flight paths ranged to 30 meters with an overall energy resolution as low as 30 keV FWHM. Various aspects of the neutron time-of-flight system are discussed below.

a) Beam Pulsing

The ion source gating system worked reliably as described in ref. 1 and 3 with one design change. At the higher repetition rates desirable when pulsing higher energy beams from the cyclotron, we often exceeded plate and/or grid dissipation capabilities of the Eimac 7211 planar triode in the power pulse amplifier. To reduce the ceramic-to-metal seal temperatures, the triode anode was clamped in a water cooled copper block. The triode has since operated 1000 hours without replacement.

b) Beam Transport and Target Chamber

The 6-inch diameter beam line installed last year has continued to perform well. Because of the small phase space occupied by a beam obtained from single turn extraction, no slits or apertures were needed in the beam transport system. This resulted in low backgrounds in the experimental area and gave excellent transmission through the system. Often 100% of the beam appearing on the first pop-in flag after the cyclotron deflector was transported to our target box on the 0 degree (no momentum analysis) beam line.

The target chamber was located in the center of the experimental area approximately 15 meters from the cyclotron. This location allowed maximum flight paths of 8-9 meters inside the building for detection angles from 10°-150°. The target chamber was fabricated from a 5-foot length of the 6-inch diameter aluminum beam pipe. Short lengths of 5-inch diameter pipe were welded perpendicularly above and below the target positions to accommodate up and down movement of a 5-position target rack (see Fig. II B4). Finally, to reduce the attenuation of neutrons from the target to the detector, one side of the 5-foot length was milled to 0.010-0.015 inch thickness in the horizontal plane. The attenuation due to the 0.010 inch

wall thickness was calculated to be, at most, a few percent and the attenuation due to air along the flight path was similarly of the order of a few percent.

c) Physical Layout and Shielding

A diagram of the basic lay-out of the T.O.F. system in the barn area is shown in Fig. II B1. The extracted beam from the cyclotron is taken down the zero-degree line and focussed onto a target located in the center of the barn area. The beam is then stopped in a Faraday cup one meter beyond the target. Heavy shielding around the Faraday cup had originally been eliminated entirely in favor of a shadow bar placed between the detectors and the Faraday cup. This was in keeping with the initial philosophy of holding all shielding to a minimum. With only light flooring, roofing, and walls in the barn area, it was hoped that, in the absence of shielding, backscattering of neutrons to our detectors would be minimized, reducing the time-of-flight background. Background studies were carried out to ascertain the effect of shielding immediately around the neutron scintillation detectors. The shielding did reduce background and the detectors were shielded as heavily as convenience and safety would permit. After these tests it was noted that wide background peaks in the time spectra appeared to be due to neutrons and γ-rays originating in the vicinity of the target and Faraday cup. It was then decided that perhaps some further local shielding was required beyond the shadow bar.

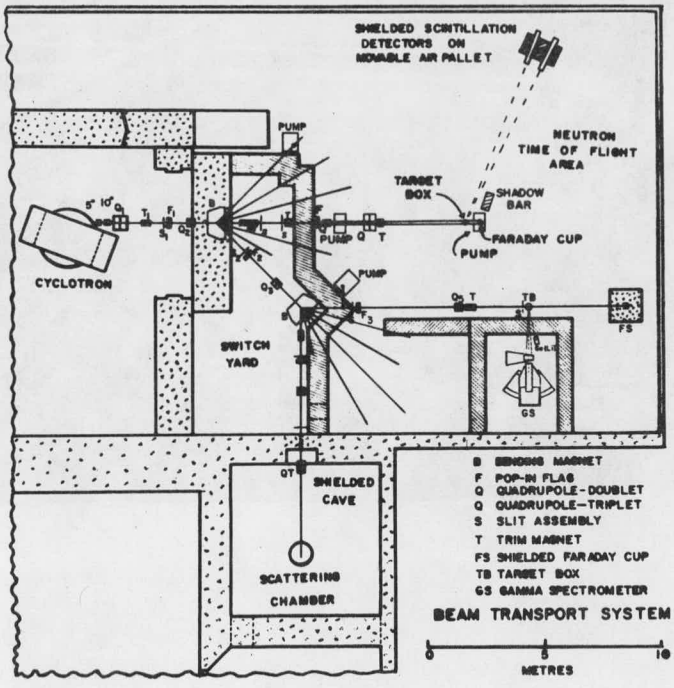

Fig. II B1 Layout of the neutron T.O.F. area in the barn.

Local shielding was provided in the form of 6-inch wide steel plates which were stacked along the detector side of the beam pipe in the vicinity of the Faraday cup and target. A gap was left in this shielding through which the detectors could view the target. This seemed to lower the background enough to be worth the inconvenience of stacking and unstacking the heavy steel plates.

Besides this local shielding a graphite baffle was installed approximately 0.5 meter upstream from the target. It was hoped that this baffle would eliminate any "halo" associated with the beam and cut down background due to protons striking the target frame and beam pipe. This also reduced the background by a small amount, and necessitated local shielding between it and the detectors.

Figures II B2, II B3, II B4, II B5 are pictures taken in the barn area which show the beam line, target chamber, Faraday cup, shadow bar, and shielding. Also seen in these figures are the monitor detector and the air pallet which supported the two primary detectors and their shielding. The monitor detector viewed the

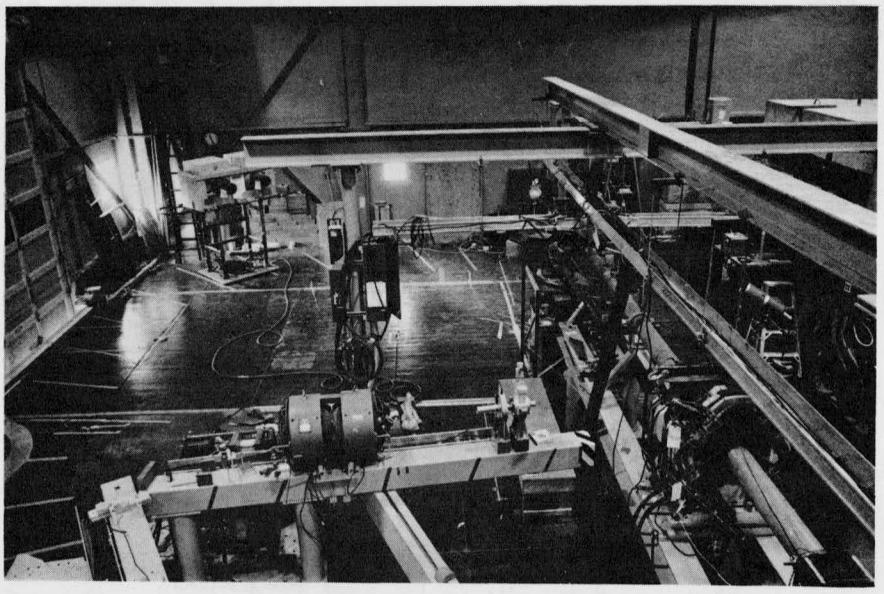

Fig. II B2 View of the neutron T.O.F. area from the switchyard roof. The T.O.F. beam line begins in the lower right hand corner. The detector cart is in the upper left. The marks on the floor were for positioning and alignment of the detectors.

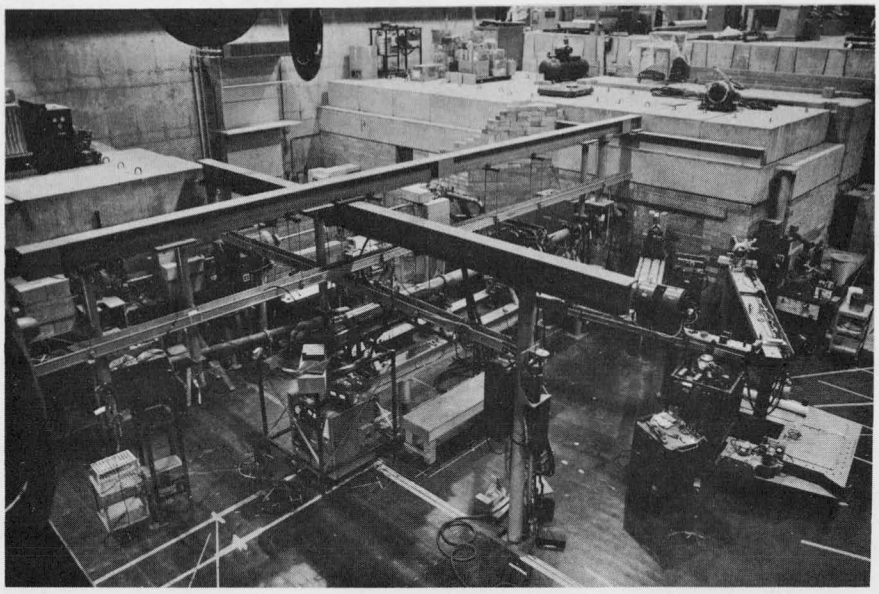

Fig. II B3 View of neutron T.O.F. area from the overhead crane. The T.O.F. line can be seen emerging from the switchyard in the center of the picture.

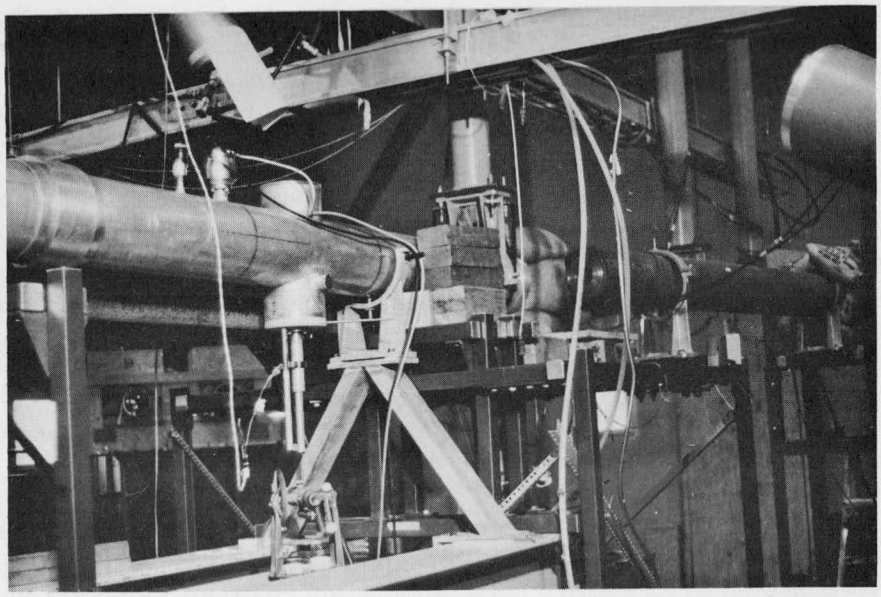

Fig. II B4 Close-up view of the target chamber and monitor shielding. The transit is for accurate measurement of detector angle.

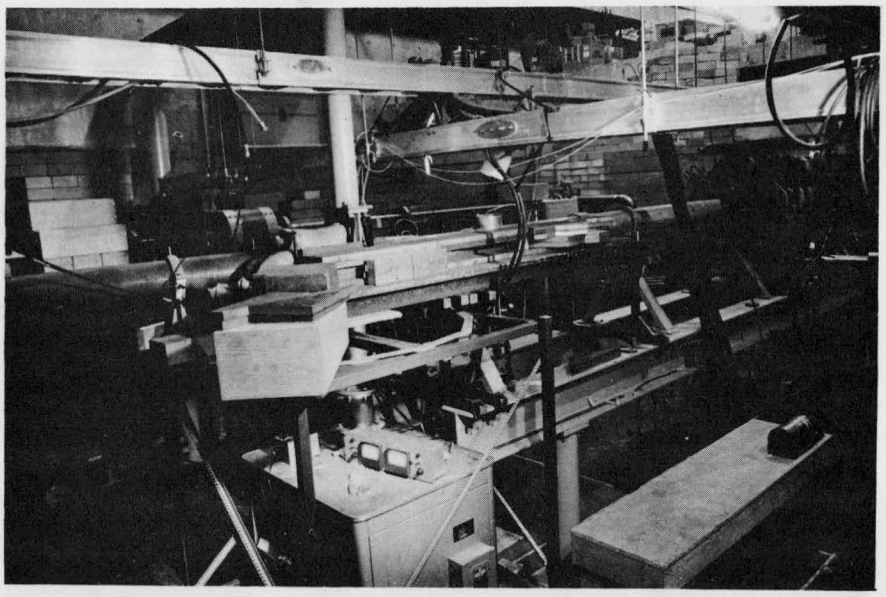

Fig. II B5 Another view of the target and Faraday cup region showing the shadow bar and local shielding.

target at a 10° scattering angle and 3-meter flight path on the opposite side of the beam pipe from the primary detectors. The cannon-like structure in the photographs is the monitor shielding. This shielding consisted of two concentric copper pipes inside a steel pipe with a steel collimating plug in the end. This, along with some iron shot stacked immediately around the detector and Faraday cup, proved to be an effective shield.

Figs. II B6 and II B7 show the two different detector arrangements which were used depending on the purpose of the experiment. In Fig. II B6 is shown the arrangement and shielding of the two primary detectors used for the measurement of angular distributions inside the barn. These detectors and their shielding could be moved by means of an industrial 3' x 4' air pallet. The air pallet was required to distribute the floor loading of the heavy shielding. The two detectors which will be described in detail below were located 6 feet above the floor in the plane of beam.

The detector shielding consisted of two 5-foot long brass pipes in which the detectors were placed. These pipes had a separation of about 0.75 meters which gave an angular separation of 5° to 10° depending on the flight path. The middle 2-foot length of these pipes immediately around the detectors was packed in bags of iron shot. These bags of shot were held in place and surrounded by 8 inches of boxed, borated paraffin on all sides. The boxes of paraffin were fastened together and supported on a steel table which was mounted on the air pallet.

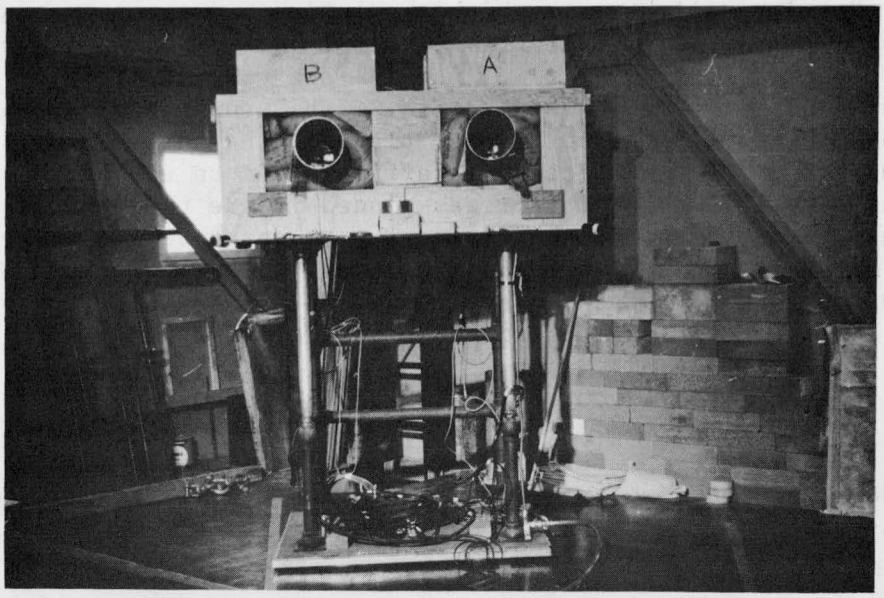

Fig. II B6 Neutron T.O.F. detector arrangement. An industrial air pallet supports the structure and provides mobility. Boxed paraffin and iron shot provide shielding.

Fig. II B7 Mobile detector cart for long flight path work. A housing of boxed paraffin on top of the tower provides local shielding around the detector. The top of the tower is equipped with a turntable to facilitate alignment of the detector.

For long flight path, high resolution spectroscopy, a detector had to be placed outside the building. For this purpose windows were put in the building wall at 18° and 55°. A 12-foot tower on a flat bed truck[4], as seen in Fig. II B7, supported the detector and shielding in the horizontal plane of the beam. Shielding consisting of boxed borated paraffin formed an enclosure on top of the tower. The detector was placed inside this enclosure in a thermally insulated brass pipe. The temperature was controlled by means of a thermostat and a heating tape wound around the pipe. The truck could be driven around the yard outside of the building to adjust flight path and detector angle.

d) Neutron Scintillator Detectors

The detectors which have been most extensively used consisted of a Lucite cell which contained NE 224[5] liquid scintillator and a RCA-4522 photomultiplier as shown in Fig. II B8. The NE 224 liquid

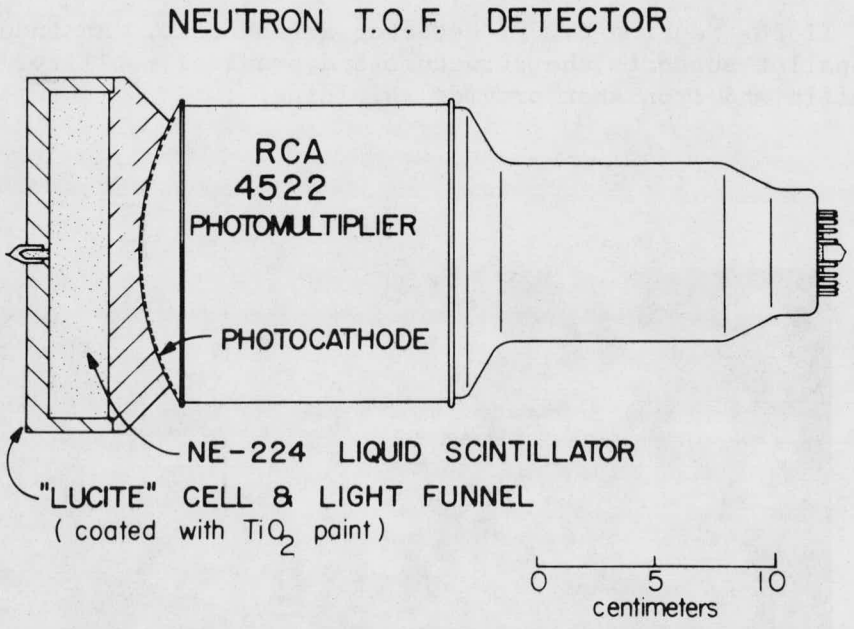

Fig. II B8 Scintillation detector used for the (p,n) reaction studies.

filled a volume 5.5 inches in diameter and 1.0 inch thick. The overall diameter of the scintillator cell, 6.0 inches, was larger than the diameter of the active area of the photocathode, 4.5 inches. To accommodate this, one face of the Lucite cell was formed into a conical light funnel. Further, the end of this funnel was machined to match the convex shape of the photomultiplier face. A layer of Dow Corning, 20-057, Optical Coupling Compound was used to optically connect the scintillator cell to the photomultiplier. The outside surfaces of the Lucite cell and light funnel were painted with a

TiO_2 reflective paint.

The photomultiplier and scintillator cell were wrapped in aluminum foil and plastic electrical tape. One layer of aluminum foil was connected to the photocathode and covered the entire scintillator end of the detector. This layer insured that there would not be any unwanted potential gradients in the vicinity of the photocathode to interfere with electron focussing. A double layer of electrical tape then insulated the entire detector. Finally, an outer layer of aluminum foil, which was grounded at the tube base, was provided for RF shielding.

The high-voltage dividers were provided in the form of Ortec 268 tube bases. These bases also contained a fast zero-crossover timing discriminator on the anode signal and a preamplifier for the dynode signal. A slight modification of the divider chain was necessary since the bases were designed for 58 AVP photomultipliers which contain a deflector grid not found in the RCA-4522. This modification involved shorting the resistor which controlled the deflector bias.

In order to reduce background in the T.O.F. spectra obtained with these detectors, it was necessary to employ neutron-gamma ray pulse shape discrimination techniques. NE 224 liquid scintillator has such pulse shape discrimination properties. It is necessary, however, to remove the dissolved oxygen to realize this.

Several techniques have been used to remove the dissolved O_2. One method involved lowering the vapor pressure of scintillator liquid by cooling and then pumping on the liquid with a vacuum pump. This method has been used only on glass scintillator cells. For the Lucite cells it was found that if argon was bubbled through the liquid for several hours it would effectively displace all of the oxygen and give good pulse shape discrimination. The circuitry involved will be described later.

The detector thresholds were set by setting the discriminator on the amplified linear signal at a level corresponding to some convenient multiple or fraction of the Compton edge from a ^{60}Co γ-ray source. Typically, twice the ^{60}Co Compton edge was used which is equivalent to the pulse output from a 5.65 MeV proton.

Measurements of the absolute neutron detection efficiency were recently carried out at the Los Alamos Scientific Laboratory Tandem Van de Graaff Accelerator. These measurements involved producing a neutron flux of a specific energy via the $^3H(p,n)^3He$ or $^3H(d,n)^4He$ reactions. The absolute flux was measured by using a proton recoil telescope[6]. The flux observed by the neutron scintillation detector was then measured and the efficiency calculated. The results of these measurements are shown in Fig. II B9. The curves shown have been interpolated between data points with the aid of curves obtained for similar detectors. The dashed

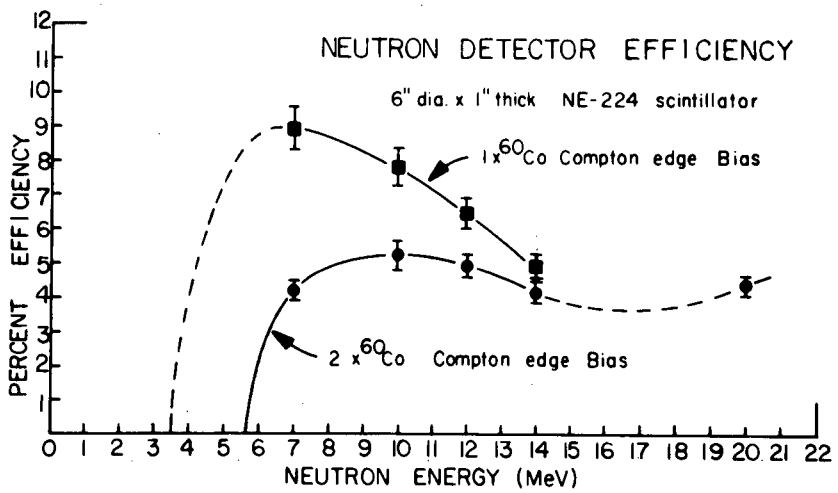

Fig. II B9 Neutron detector efficiency.

regions of the curves are places where the uncertainty in interpolation was rather high.

By using three scintillation detectors and running them in pairs to detect the two coincident γ-rays from ^{60}Co, the time resolution of the 6-inch diameter x 1-inch thick neutron detector was found to be 0.75 ns FWHM.

Several other detectors besides those described above have been used or tried. The monitor detector consisted of a 4-inch diameter by 1-inch thick glass cell filled with NE 224 mounted on a 58 AVP photomultiplier. A very elaborate rectangular slab scintillator utilizing long curved light pipes to view the scintillator from both ends was tried. This detector proved to have very poor neutron-gamma ray discrimination. This was attributed to inefficiency in light collection.

The largest detector which has been tried had a glass scintillator cell 8 inches in diameter and 1-inch thick. This detector worked quite well but was not used since it gave counting rates which were higher than needed when tried at an 8-meter flight path.

e) Electronics System

A simplified block diagram of the electronics system is shown in Fig. II B10. The system is designed to allow two main detectors and one monitor detector to be used simultaneously. The upper portion of the electronics diagram shows the circuity which sets the lower energy bias and handles the n-γ discimination for the two

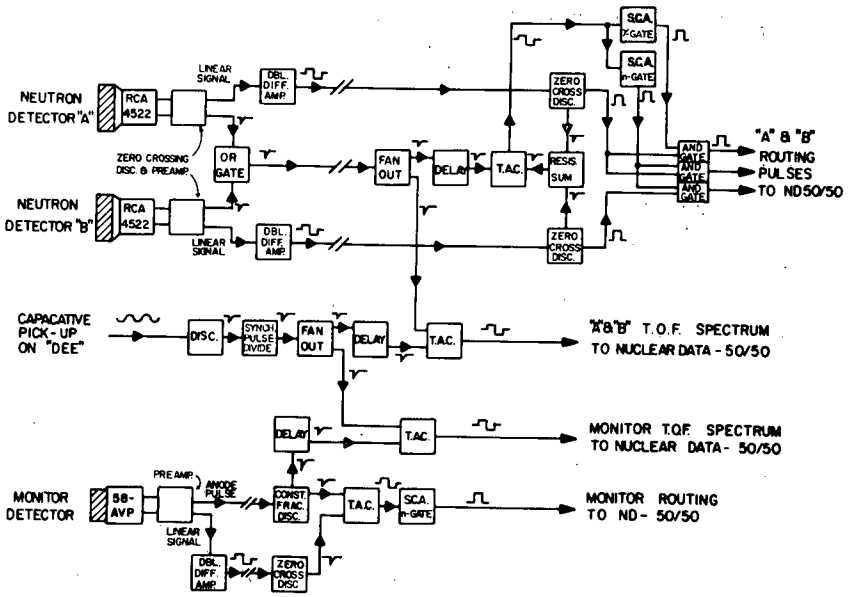

Fig. II B10 Block diagram of electronics system.

main detectors. The center of the diagram indicates how the time mark from the RF is obtained and used to generate the STOP pulse for the time-of-flight T.A.C. for all detectors. The monitor electronics are shown in the lower portion of the diagram.

The n-γ pulse shape discrimination relies on the fact that pulses for heavily ionizing particles, such as recoil protons, are made up of a short decay time component plus a long decay time component. For lightly ionizing particles, such as Compton electrons, the long decay time component is absent. When the linear signal from the photomultiplier is integrated, the rise time of the integrated signal is longer for neutron events than γ-ray events. If this signal is then doubly differentiated, the crossover point will shift as a function of the variation in rise time. To observe this difference, then, it is only necessary to detect the initiation of the event, i.e. via a fast disciminator on the anode pulse, and compare this with the time of crossover from an integrated and doubly differentiated linear signal. In Fig. II B11 is shown zero-crossover time distribution for the 6-inch dia x 1-inch thick NE 224 scintillator with PuBe as a source. It has been found that this n-γ discrimination is quite critically dependent on a number of factors. The most important are walk adjustment of the zero-crossover disciminator, count rate, bias, and RF pickup (from a local radio station) on the linear signal cables.

Routing into the ND50/50 multi-channel analyzer was employed

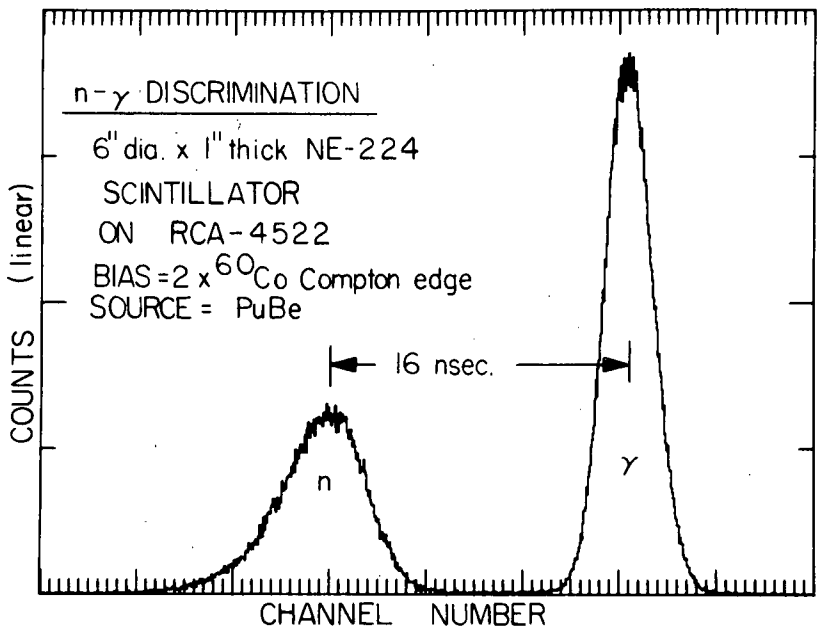

Fig. II B11 Zero-crossover time distribution for neutrons and gamma rays from a PuBe source as seen by the 6-inch diameter by 1-inch thick NE 224 scintillator.

to allow the storage of four spectra simultaneously. These spectra were the neutron gated T.O.F. spectra from all three detectors plus a γ-gated spectrum from one of the primary detectors.

f) Targets

Most of the targets used in the (p,n) studies were self supporting, enriched metal foils formed by standard cold rolling techniques. The thickness of these targets typically ranged from 3 to 5 mg/cm^2. Several gas targets were also used. The cell used to contain the gas is shown in Fig. II B12. This cell consisted of a 1-inch long by 1/2-inch diameter stainless steel tube, coaxial with the beam, with a filling port on one side. Natural Ni windows, .7 mg/cm^2, were held in place with brass flanges epoxied to the stainless steel tube. A graphite aperture shielded the epoxy joint from the beam. The gas pressure ranged from 1/4 to 1/2 atm.

The most difficult material to fabricate into a target was ^{96}Ru. This metal could not be rolled, evaporated, or electroplated into a foil due to its rather extreme properties of hardness, high melting temperature and insolubility in acid. The process which was finally used involved dissolving the metal in a NaOCl + NaOH solution. The NaOCl was then reduced with the addition of $Na_2S_2O_5$. This was then acidified with the addition of HCl. Addition of Mg powder caused

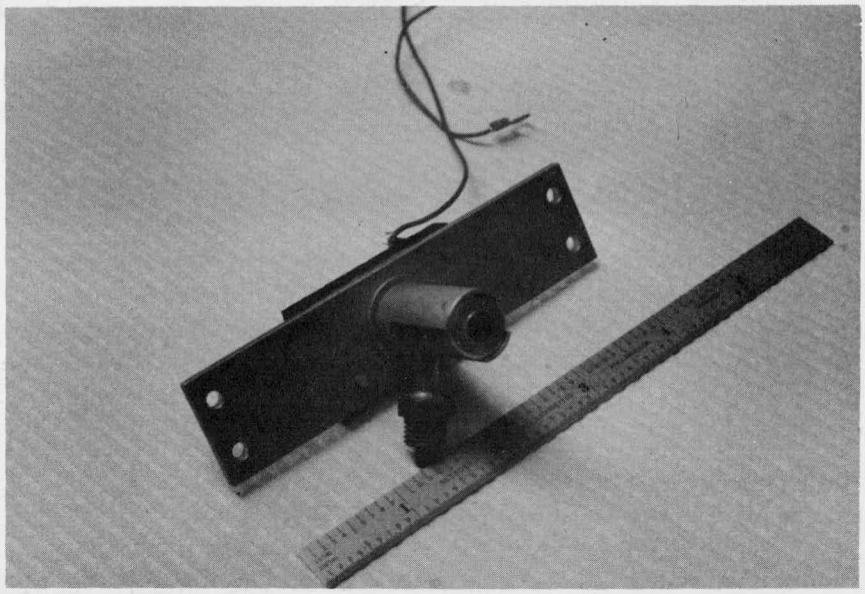

Fig. II B12 The gas target and frame used in the (p,n) studies.

the Ru to precipitate out of solution as a colloidal suspension. The suspension was centrifuged, decanted, and washed with water. It was decanted once more and added to methyl alcohol. An ultrasonic bath was necessary to disperse the lumps which had formed. This suspension was then centrifuged in a specially constructed tube having a .7 mg/cm^2 Ni foil on the bottom. After the excess alcohol was decanted, the suspension was centrifuged until all the alcohol had evaporated and the Ru metal was deposited uniformly on the Ni foil. The deposit was then held in place with a drop of Q-dope in toluene. A thin gold leaf overlay was added for further protection. A similar process was used to make a phosphorus target.

---

1 Univ. of Colo. Nuclear Physics Laboratory Progress Report (1969) pp. 93-104.
2 Univ. of Colo. Nuclear Physics Laboratory Progress Report (1970) p. 115.
3 Nucl. Inst. and Meth., R. F. Bentley, et al. 83 (1970) 2.
4 Obtained from Government Surplus list.
5 Obtained from Nuclear Enterprises, Ltd., San Carlos, California.
6 Gordon Hansen, LASL, private communication.

2. A Magnetic Spectrometer System - B. W. Ridley, R. J. Peterson, J. J. Kraushaar, R. A. Ristinen, D. Prull, E. Stoub, and S. Schery

a) Introduction

Several drawbacks of experiments which use solid state particle detectors may be overcome with a magnetic analysis system. The beam intensity which can be used with solid state counters is limited by the need for sharp resolution in the incident beam, and most of the cyclotron beam must be discarded on the analysis slits. Energy resolution of the spectra is further limited by the intrinsic resolution of the counters. Data collection rates for low-yield reactions are limited often by the intense elastic scattering that accompanies the reaction of interest.

A magnetic analysis system which uses the energy-loss, or dispersionless, condition may use a wide range of incident particle energies, and still produce good resolution for the specific final nuclear states. A beam preparation system, with dispersion D_1, places a beam of energy E_1 on the target. Reaction products with energy E_2 enter an analysis system with dispersion D_2 and magnification M_2. When the condition

$$D_1 = \frac{D_2}{M_2} \frac{E_1}{E_2}$$

is met, the spatial resolution of particles at the focus of the analysis system is independent of the spread in momenta of the incident beam. For direct reaction studies we usually do not have stringent requirements on the exact incident energy, and can easily endure the energy-averaging implicit in this scheme.

Reaction products of rigidity different from the beam follow different trajectories in the analysis system, and the intense elastic scattering flux may be disposed of at some distance from the detector. Reactions may then be studied even at a reaction angle of zero degrees.

A selection of magnetic trajectory also provides good particle identification. We have heightened this capability by allowing for electrostatic deflection in the axial direction between the reaction analysis magnet and its detector plane.

The cost of a magnetic analysis system is strongly dependent upon its acceptance, or solid angle. Recent measurements of the beam emittance from the cyclotron gave us the confidence to build a small aperture magnet system. The solid angle of the reaction analysis system was chosen to be about three times that presently used with counters. The factor of ten improvement in beam flux on target also provides a substantial gain in counting rate.

b) Design

The first design criterion is that the final dispersion be adequate for 5 keV resolution with a multiwire proportional chamber. This necessitated a 4-meter separation between the analysis magnet and detector. There is no room in our experimental area to rotate such a large analysis system, so we will instead swing the beam about the target for angular distribution measurements. Figure II B13 shows a view of a model of the spectrometer system.

The beam from the cyclotron enters a circular entrance aperture, then is collected by a long quadrupole, which transforms the beam from the symmetric slit to an asymmetric beam diverging from a virtual source that is narrow in the dispersion plane. The first dipole bends the beam by 45 degrees to a focus midway to the second dipole. Aberrations are not corrected at this focus, but the focus will be of aid in determining the beam energy and in tuning up.

The second dipole bends the beam down to a focus on the axis of the original beam. The entire assembly rotates about this axis. Aberrations are corrected at the target spot to nearly one part in 10^4, $(\Delta p/p)$. The entire cyclotron beam is spread on the target (the dispersion was selected so as to use existing mounted targets), but the position and momentum of each particle are highly correlated. Table II BI lists a summary of the optical elements.

The reaction products from the target enter a quadrupole lens system known as the zoom lens. This is composed of four quadrupole elements, which enable one to keep a sharp virtual object in coordinates x and in y at some fixed points, maintain the y magnification at unity, and vary the x magnification from 0.6 to 3.2. This allows a wide range of nuclear reactions to be studied. The virtual objects are placed so as to optimize the solid angle. At present, we are making do with existing quadrupoles, although some limits on solid angle and maximum rigidity particles are encountered.

The particles emerging from the zoom lens enter a 90 degree dipole magnet, which performs the momentum-analysis on the reaction products. This magnet is on a lower floor of the building and its focal plane is located beneath the entrance to the beam swinger system. The vacuum can is baffled and water cooled to allow the primary beam to be lost on it.

All particles populating a specific final state are focussed to a point on the focal plane, whatever may have been the energy of the projectile which initiated the reaction. A multiwire proportional counter at the focal plane collects the spectrum.

The design of this system was accomplished by using a home-made ray tracing machine to determine the geometry of the dipole. The apparatus is described elsewhere in this Progress Report. We strove for a solution with the minimum number of curved edges, and no higher than second order curvatures anywhere. This optical design was then

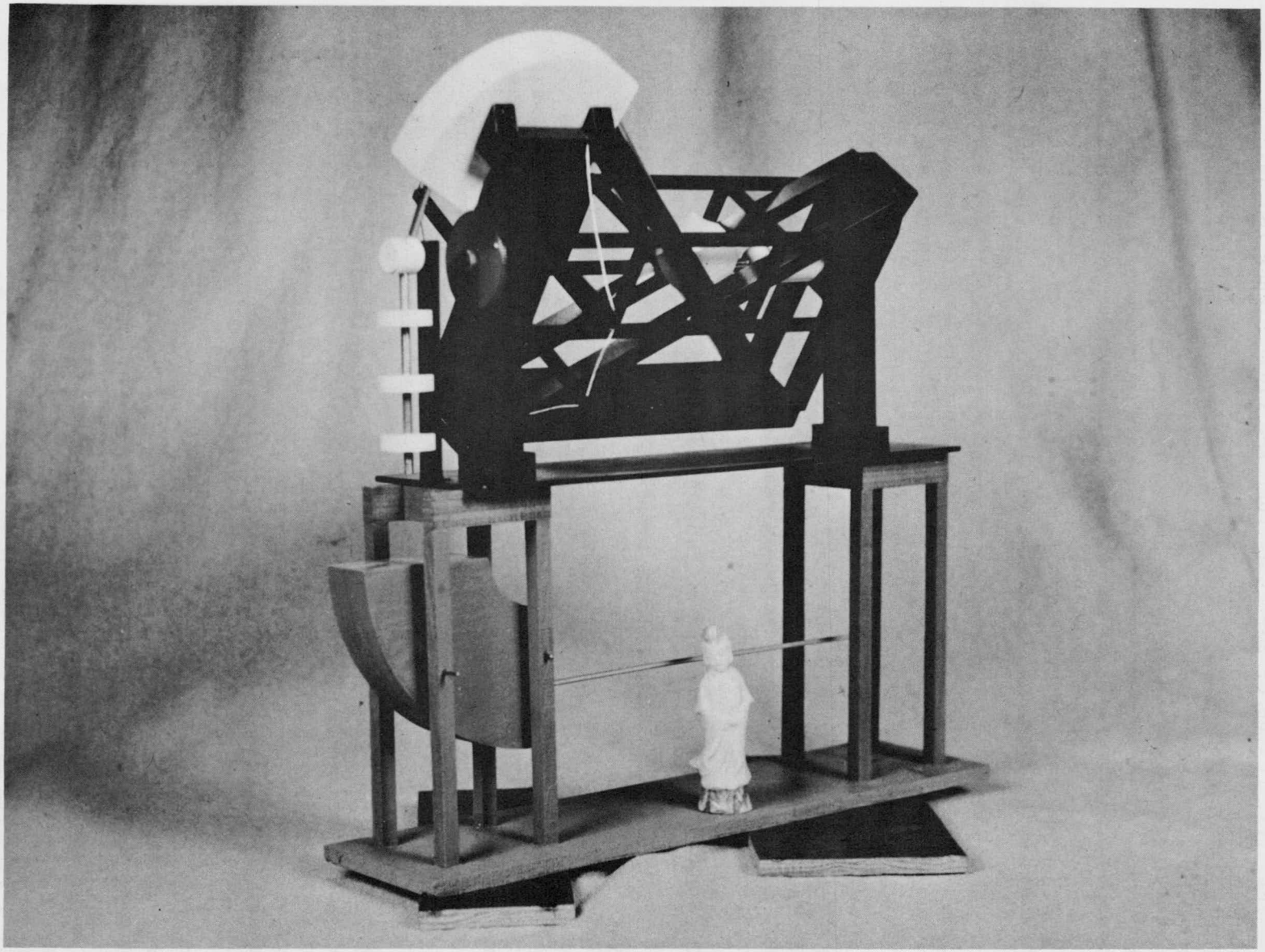

Fig. II B13 This model of the magnetic analysis system shows the swinger oriented to study reactions at an angle of about fifteen degrees. The incident beam enters from the right and the spectrometer focal plane is beneath one of the two tables which support the beam swinger. The figurine has a scale height of six feet.

TABLE II BI

Summary of the magnetic analysis system.

Entrance Slit	2 mm radius	
45° Dipole	Gap	3.80 cm
	Ampere-turns	700 x 48
	Radius	0.914 m
	Iron	3500 lbs.
	Copper	400 lbs.
135° Dipole	Gap	3.80 cm
	Ampere-turns	700 x 48
	Radius	0.914 m
	Iron	10,000 lbs.
	Copper	650 lbs.
On the target	Dispersion	3.64 m
	Magnification	0.126
	Spot size	0.8 x 1.5 cm
90° Dipole	Gap	4.5 cm
	Ampere-turns	600 x 84
	Radius	1.22 m
	Iron	16,500 lbs.
	Copper	1,800 lbs.
	Solid angle	0.8×10^{-3} ster.
On the detector	D = 6.71 m	

completed through use of the code TRANSPORT, good through second order in all dimensions.

An advantage of the beam swinger design is that it can be used for neutron time-of-flight studies as well as for charged-particle spectroscopy. In the energy-loss tune, the difference in path lengths leads to a range of arrival times on the target. By retuning the entrance quadrupole and changing the entrance slit, a tune may be found that cancels differences in path lengths, and 0.5 nsec bursts on the target may be obtained.

A set of fixed neutron counters may then be used, and angular distributions run by swinging the beam. The counters may then be shielded more efficiently than if they were movable.

c) Field Mapping and Ray Tracing

The actual fields of the magnets are unlikely to be precise to

one part in 10^4 due to machining tolerances, and the ultimate resolution could not then be as good as designed. We are developing a device for measuring the fields, and a computer code which uses the measured field to ray trace the actual trajectories. We intend to adjust the external field clamps to provide the correct focus and resolution, because the field is relatively insensitive to tolerances in the clamp edges.

The field mapping apparatus for the 45° and 135° magnets has been built. The apparatus consists of a high-strength aluminum alloy hoop. The angular positioning is controlled by a stepping motor, and the radial and vertical positioning are controlled by means of dowel pins and shims. The points of constraint are the center of the hoop and a teflon skid beneath the field measuring probe. This system of constraints enables a very stable positioning of the probe. Preliminary studies with a model magnet indicate that the probe can be repositioned with an error of less than 0.001 inch.

The absolute radial positioning of the probe is limited primarily by the ability to measure the radii to reference points on the hoop (distances of about 37"). To date, from caliper measurements, these radii are known ±0.004 inch. The absolute axial positioning will be determined by the known tolerances of the magnet surface on which the teflon skid rides.

The field measuring probe used with this apparatus is a temperature compensated Hall plate device made by the F. W. Bell Co. The output of the Hall plate is analyzed by a Bell Co. model 640 gaussmeter and the resulting signal is amplified by a D.C. amplifier for use by an analog-to-digital converter. Preliminary studies of the Hall plate electronics and magnet power supply indicate that resolution and stability of about 1 part in 10^4 are being obtained.

It is planned to make a grid of measurements of the axial component of the magnetic field in the median plane of the magnets, and then use interpolation procedures in combination with Maxwell's equations to get field values at other points. Several interpolation programs have been written which use both two dimensional Lagrangian interpolation (6 and 10 points) and parameterized special functions for the fringe fields. To date, 10 point Lagrangian interpolation has given the best results. By using a half-inch grid of data in regions of the median plane where the field is changing 1500 Gauss/inch, interpolation with an average error of three Gauss has been obtained.

A ray tracing program designed as an aide in eliminating aberrations is essentially complete. The program traces rays through either one or two dipole bending magnets with a given number of uniform field regions. The magnets are oriented relative to a fixed laboratory coordinate system and an assumed bending radius for the central ray in each of the uniform field regions is supplied. A data table giving positions of the effective hard edge

at each fringe field region is either supplied as input (for instance from the measurements of the field mapping device) or computed for a given straight or circular edge. The input rays are defined by giving initial coordinates and angles in the laboratory system plus the percentage change in momentum from the central ray. The program calculates the exact solution for the projection of this ray in the median plane under the hard edge model and then corrects this solution by perturbations to second order caused by the finite fringe field extent and vertical motion. The ray is plotted in an x,z coordinate system, where z is the distance along the central ray and x is the displacement normal to the central ray (Fig. II B14). Future modifications will be to include quadrupole fields, an extension to three magnets, and a calculation of hard edge positions from field mapping data.

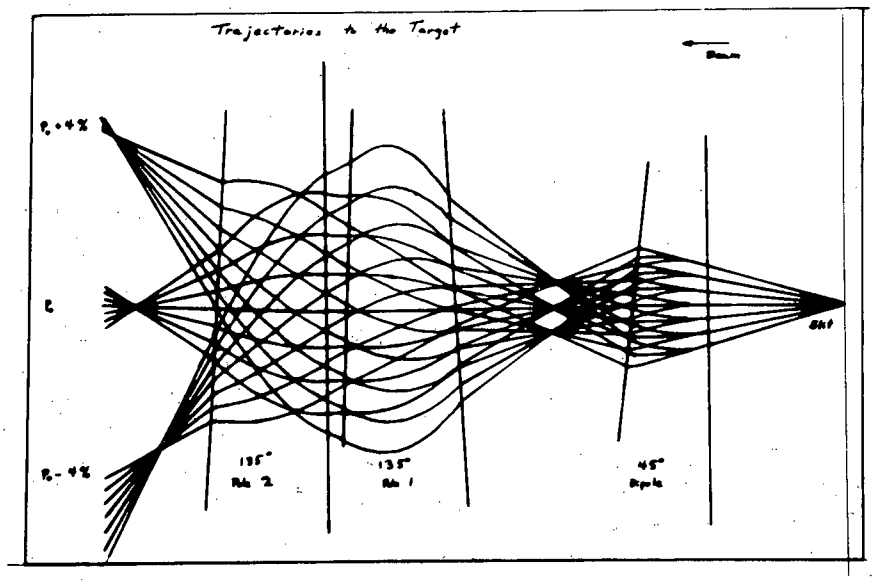

Fig. II B14 The trajectories of particles with momenta P_o and P_o ±4% are shown from the circular entrance slit, through the 45° and 135° magnets, and onto the target. This is the output from the ray-tracing code described in the text.

The first and second order matrices describing the magnet system may be entered into a Monte Carlo code to generate spectra under a variety of conditions. Figure II B15 shows such an example, using the beam through the entire system, with two values of the solid angle of the reaction product analysis magnet.

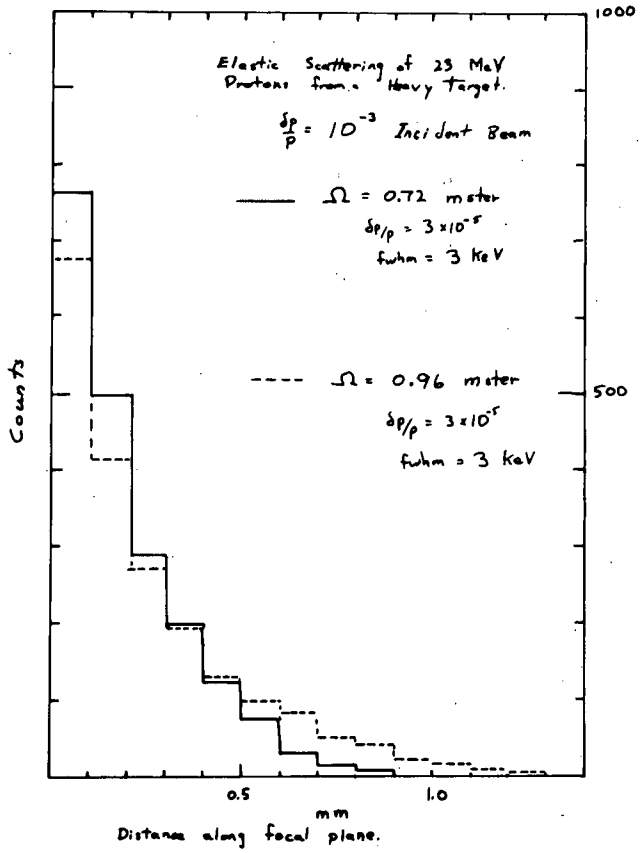

Fig. II B15 Two spectra of particles from the target to the detector are shown as generated by a Monte Carlo method from the designed field. The zoom lens is included, and an incident momentum spread of 10^{-3} is used. It is seen that the larger solid angle does not worsen the FWHM resolution, but does add tails to the peaks.

d) Multiwire Proportional Counter

A multiwire proportional counter is being built for position-sensing of particles incident on the spectrometer focal plane. The active area of the chamber to be used initially, which is being built at Lawrence Berkeley Laboratory, is 30 cm in the radial direction by 7 cm in the axial direction, with electrode spacings of 2 mm center-to-center in both directions. A phase compensated electromagnetic delay line readout system[1] will, by its interpolation characteristics, allow spectra to be taken with FWHM resolution corresponding to a fraction of the wire spacing, or to better than 0.5 mm in this chamber.

Current work is directed toward the construction and testing of the proportional chamber and associated electronics and to the design and testing of a mount for the proportional chamber. The

mount must provide for positioning of the chamber in vacuum, with rotational and translational degrees of freedom for optimum orientation under different conditions of spectrometer focussing.

e) Schedule

Design of this system began in November 1970, and contracts for the first magnets were let on March 1971. The 45 degree magnet arrived in October, 1971.

The modifications of the barn area to accommodate the system are complete, the swinger assembly is complete, and many pieces of vacuum plumbing, magnet supports, slits, etc. have been fabricated.

The magnets will be installed following field mapping. An energy loss system is difficult to tune, because there is no sharp focus anywhere except at the final detector. After the system is running, we anticipate spending several months looking for optimum resolution. For many experiments this will be limited by target thickness.

We will then have a spectrometer system with up to 5 μA on the target, a solid angle of 0.8 msr, a resolution of 10-15 keV FWHM, built-in particle identification, and capable of studying reactions down to zero degrees.

---

[1] R. Grove, I. Ko, B. Leskovar, and V. Perez-Mendez, UCRL 20255

3. Mechanical Ray Tracing in Spectrometer Design - D. E. Prull, B. W. Ridley, R. J. Peterson

A modified version of an instrument described by Klank, Lind, and Johnson[1] (as derived from an idea of Green and Berkley[2]) for designing uniform field spectrometers was extremely useful in the design of split-pole dipole bending magnets. The modifications were made to ray trace through three connected uniform field regions, rather than just one as in the original design of the instrument.

The instrument traces exact trajectories, free of aberrations in two dimensions. A sketch of the instrument is shown in Fig. II B16 and shall be referred to in the following description. The field region has a uniform magnetic field B_1, with a corresponding bending radius ρ_1, between the pole tips, and a field B_2 in the gap with corresponding bending radius ρ_2. This geometry is typical of modern split pole magnets. Momentum deviation from the central ray is given by $\pm \Delta\rho_1/\rho_1 = \pm \Delta\rho_2/\rho_2$.

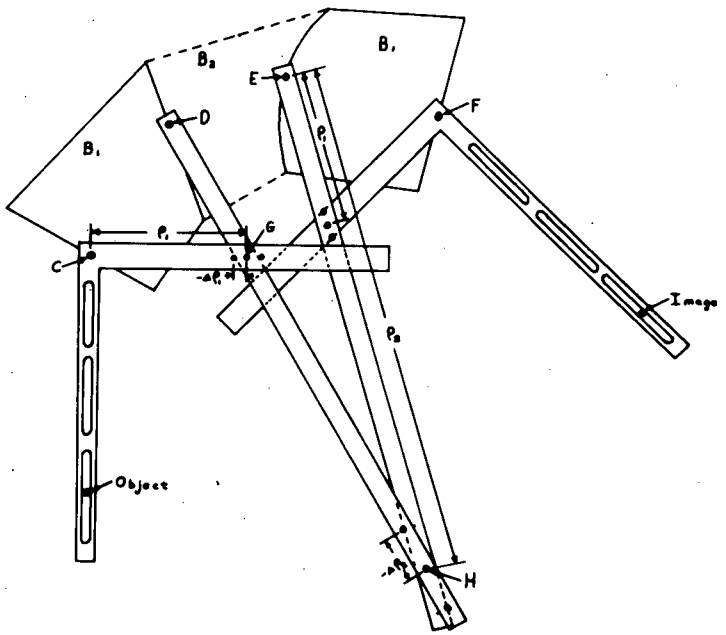

Fig. II B16 A mechanical ray tracing instrument. Details of its operation are discussed in the text.

The instrument is made from two carpenter's squares and two long strips of aluminum. Holes were drilled at C, D, E and F for plexiglass windows, each with a small hole suitable for a pencil lead. The pivots, such as G, were located a distance ρ_1 (or $\rho_1 \pm \Delta\rho_1$) from the center of the plexiglass windows. At G the

aluminum strip was drilled and tapped while the holes in the carpenter's square were drilled to fit a machined screw head with close tolerance. The other pivots were similarly made, with the holes at H being a distance ρ_2 (or $\rho_2 \pm \Delta\rho_2$) from the center of the plexiglass windows on the aluminum strips.

If three faces of the magnet are given, screws are placed at the desired object and image. The pencil lead then traces the required fourth face. If all four faces are given, exit trajectories can be drawn by removing the image screw and fixing the object at the desired location for each of the three different momenta. If the image position is given, the required entrance trajectories can be drawn by removing the object screw.

We used this instrument to find the desired optical solutions with the simplest edge geometry of the dipoles. This is much more rapid and intuitive than solving by a computer code.

---

[1] B. Klank, D. A. Lind, and R. R. Johnson, Nucl. Instr. and Meth. 67 (1969) 61.

[2] A. E. S. Green and R. J. Berkley, Rev. Sci. Instr. 37 (1966) 414.

4. Electronics Maintenance and Development - L. A. Erb

Cyclotron

Improvements are continually being made to the cyclotron. Some of these are summarized here.

Magnet System

The main magnet regulator electronics were revised to take advantage of a few developments to help improve machine stability. A one-volt water cooled current shunt was installed which replaced a 200 mV air cooled shunt which was used for sensing the main magnet current. An all solid state chopper stabilized operational amplifier with superior frequency response and gain has replaced the older vacuum tube model. Voltage feedback was added to increase system stability. Overall performance has improved due to these modifications.

The valley coil shunts were modified to incorporate both voltage and current feedback in an active regulator. Previously the shunts were an open loop variable current sink without feedback.

Additional magnet shunt inputs were added to the digital voltmeter monitoring system. All of the magnet currents in the cyclotron and beam transport systems can now be monitored on the DVM.

RF System

A final amplifier overcurrent detector was added to the automatic dee voltage regulator to reduce the number of overcurrent faults on the system due to parasitic oscillations. This addition has reduced but not eliminated the problem.

Fire Alarm

The building smoke and fire alarm detector system has been expanded to also protect the upper and lower vault areas. Originally the alarm system protected only the control room with its machine control, data acquisition, and data processing equipment.

The air circulation equipment within the areas of the building protected by the fire detection system has been modified so it is automatically turned off if the alarm sounds. This precaution will slow the spread of a fire.

^{3}He System

Final installation and wiring of the automatic portion of the ^{3}He system has been delayed by the spectrometer project. Manual operation is possible now and it is being used in this mode.

Beam Transport System

Bending magnet number one stability has been greatly improved by the installation of a new operational amplifier. Bending magnet number two is scheduled for similar modification when time allows.

A four-inch quadrupole power supply has been rebuilt to better its stability. Some of the changes include operational amplifier modification, ground loop elimination, and signal lead shielding.

The number of available one degree magnet stations were increased to accommodate the additional magnets being used. A further expansion of station capability is forthcoming.

Data Processing System

The PDP-9 computer has given us relatively good service this past year. This low cost data reduction capability has more than paid for itself by allowing a greater number of experiments of greater complexity to be accomplished with little increase in manpower or cost. The only aggravating hardware problems encountered this year were with the memory and teletype. A redesign of the central processor primary power distribution and switching circuitry was necessary due to a faulty set of push-on lug connections but down time due to this failure was minimal.

The PDP-8L computer has performed very well with only a minor teletype problem giving trouble.

All of the laboratory pulse height analyzers have performed without major problems this year. A PDP-8L with ADC was housed in the lab this summer for repair and program development. It was used in part for detector calibration and resolution checking which is a somewhat menial task for such a powerful machine, but it was productive for periods in which it was not used for software development.

Spectrometer

The new spectrometer is requiring a variety of major power supplies. New supplies are being built to supplement those already available. Several 300-, 600-, and 750-amp regulated supplies are required.

New supply construction incorporates advanced versions of the post-regulator technique. The usual military surplus voltage regulated supplies are being used to supply large quantities of power. Post-series transistor regulators do the actual current regulation. The voltage regulated supplies have been modified to track the load by maintaining a fixed voltage drop across the regulator transistors. Narrow load resistance tolerances are thus eliminated by this technique.

The beam swinger will be rotated about its beam input axis by a variable speed electric motor drive. The motor initially will have only local and remote controls for speed and direction. Eventual computer control is expected. This equipment is now being readied in our shop.

Magnetic field checks must be made on the spectrometer magnets upon their delivery to insure proper quality construction and magnetic field shape. To accomplish this we are using a computer-positioned Hall probe Gaussmeter. The PDP-9 Calcomp controller has been adapted to generate forward and reverse drive pulses to command a stepping motor drive. Circular paths can be mapped automatically by using this technique. The external analog output of the Gaussmeter is presented to the ND-50/50 ADC for digitizing. Mass storage of data is done on mag tape for later analysis. Minimal expense and manpower is utilized by using this system.

NIM Modules

The major projects of this year have left little time to expand the ERBTEC NIM module line. A second model 220 dual signal processor was completed, as was a count-rate meter.

X-Ray

Modifications were made on the X-ray machine power supply to allow lower tube currents and thus lower counting rates for critical experiments.

5. Heavy Ion Gas Cells - R. A. Emigh

A need arose for a gas cell which could be used for (^{3}He,^{7}Li), (^{3}He,^{7}Be), and similar experiments, and which would not have as much energy straggling as the gas cells available at the Colorado Nuclear Physics Laboratory. This need required that the gas cell have as thin an exit window for scattered particles as possible. It was determined that it would be easiest to design and build two different cells, one for small scattering angles and one for large scattering angles.

The cells were constructed of copper and brass. The entrance and exit windows for the beam were 3.12 mgm/cm^2 thick Havar foil. The heavy ion exit window was made of Formvar, an organic film floated on water. Formvar can be made in thicknesses of about 10 μgm/cm^2 to 500 μgm/cm^2 without too much difficulty. For both cells a thickness of 100 μgm/cm^2 was used in order to minimize straggling and still be thick enough to allow 0.2 atmosphere of pressure inside the gas cell.

a) Large Angle Gas Cell

The main body of the large angle gas cell, shown in Fig. II B17, was machined from circular copper stock and shaped to fit in the existing scattering chamber target holder. The Havar foil was epoxied between the body of the gas cell and a brass frame. This was done for both the entrance and exit windows for the main beam.

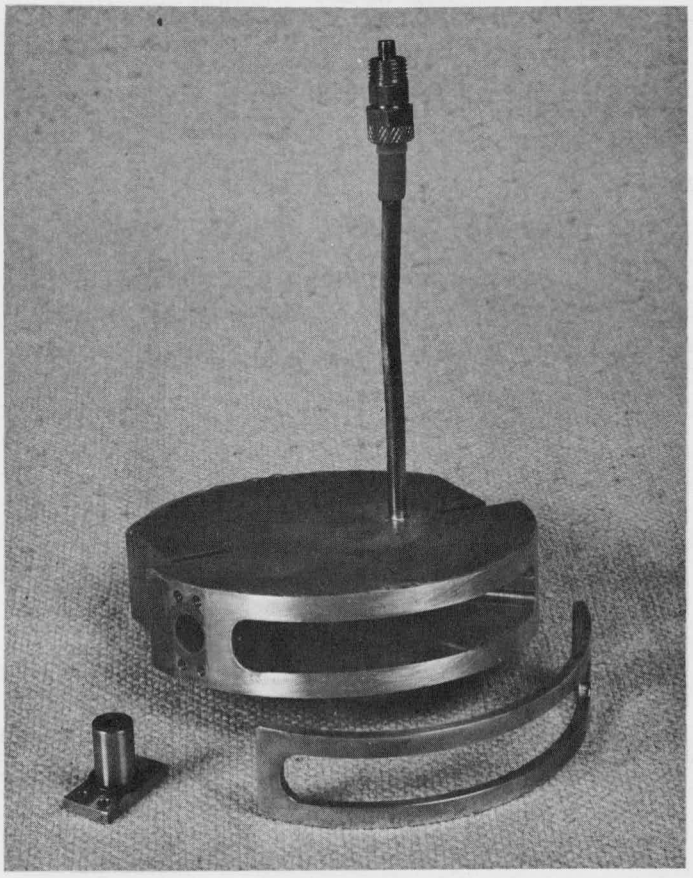

Fig. II B17 Large angle gas cell with exit window holder at bottom left and one of the brass beam frames at right. Havar is epoxied between cell body and frame.

The holder for the scattered particle exit window is a brass plug that has a small opening at one end (7/64 inch x 3/16 inch). Formvar was placed over this opening. The Formvar adhered to the plug so no external means were needed to assure that the Formvar would not become detached. An O-ring seals the plug to the body of the gas cell.

The plug penetrates into the gas cell so that the Formvar exit window will be as close as possible to the center of the target. This configuration cuts down on straggling since the scattered ions travel a shorter distance through the target gas than they would if this window were at the outside radius of the gas cell.

One can obtain data at scattering angles from 23° to 157° in the laboratory with this cell. The cell has been used with no difficulties for extended periods of time in a scattering chamber with 0.1 atmosphere of various types of gases inside the cell.

b) Small Angle Gas Cell

The main body of the small angle gas cell shown in Fig. II B18 was made from a six-inch length of two-inch I.D. copper tube. Two holes with fittings were placed in the side of the copper tube to allow gas to flow through the gas cell. A brass plate which would

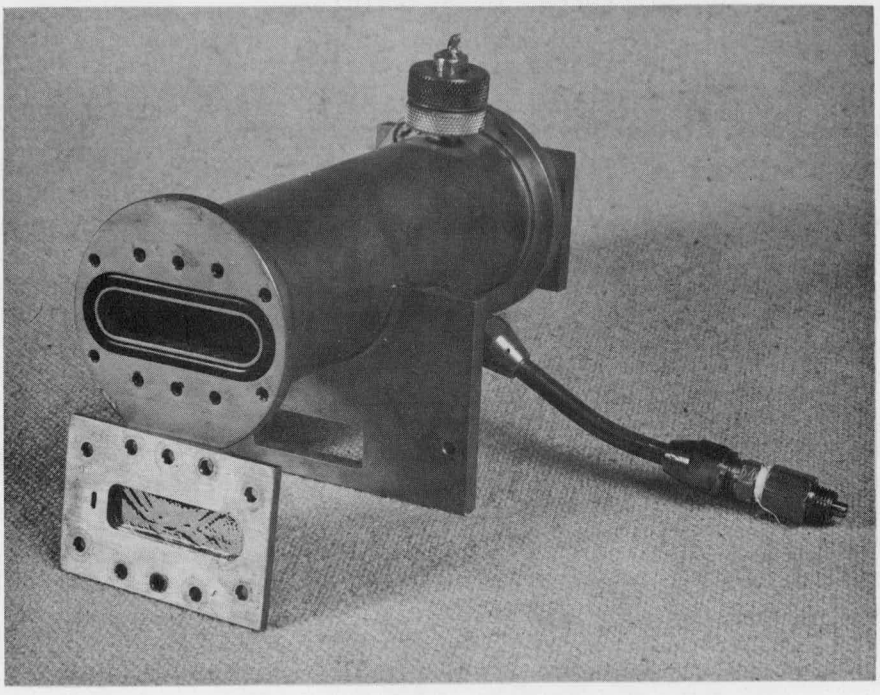

Fig. II B18 Small angle gas cell with one of the beam frames. This beam frame has Havar epoxied on the back and contains the small Formvar window.

attach to the target holder in the scattering chamber was brazed onto the copper pipe. Brass end plates with oblong openings and O-ring grooves were brazed onto the ends of the pipe. Finally, two window frames were machined from brass. One of the beam frames had an opening which matched exactly with the opening in the end plates. Havar was placed over the end plate opening and the frame was bolted down on the Havar.

The other window frame was made slightly different from the first frame as there are two openings. One opening is the same as the oblong end plate opening except that it is not as long and is squared off. The second opening for the exit of reaction products is small (1/16 inch x 3/16 inch) and is placed near the squared off part of the first opening. Havar is epoxied onto the large opening and Formvar is placed over the small opening. The frame is then firmly attached to the end plate with screws. The O-ring assures a vacuum tight seal.

By using the small angle gas cell one can obtain laboratory scattering angles of 5° to 33° in the forward direction and 147° tO 175° in the backward direction. This cell has been run at 0.03 atmosphere with no problems.

6. Heavy Ion Source Development - R. A. Emigh, D. A. Lind, C. D. Zafiratos, C. S. Zaidins

In response to interest in reactions which could be induced by heavy ion beamsat the University of Colorado cyclotron, a program has been recently initiated to develop a heavy ion source. Specifically, a lithium beam is wanted in order to study excited cluster states by direct multiple particle transfer to a target nucleus (see University of Colorado Nuclear Physics Laboratory Progress Report (1969)). Similarly, one would like to be able to obtain carbon and nitrogen beams in sufficiently high charge states and in quantities large enough to be useful.

First a study was made on the two ion sources presently available at the University of Colorado cyclotron. Both sources are standard cyclotron ion sources and differ only in where gas is leaked into the chimney. In the source generally used, the gas is fed in at the bottom near the filament. Thus electrons and gas particles enter the chimney from the same opening at the bottom. The other source has the gas introduced into the chimney opposite the exit slit (center feed).

Both ion sources were run with alpha particles at 28 MeV. For a given gas flow the filament current, arc current and arc voltage were varied (these parameters are not independent of each other). The beam current was measured at the cyclotron extraction radius.

The center feed ion source was run three different ways; normally, without the source cap (button), and with two high permeability iron slugs in the chimney. The cylindrical iron slugs, with holes drilled down the center in order to allow electrons to enter the chimney, were placed on either side of the gas opening in the chimney. It was believed that the iron slugs would cause a magnetic bottle to form and thus keep the gas localized in a small volume near the exit slit. The bottom feed ion source was run only in its normal configuration.

As expected, it was found that the lower the filament current, the higher the beam current for a given arc current. The highest current beams were produced from the center feed ion source operating in its normal state. The bottom feed ion source produced almost as well, but the two modifications of the center feed source did poorly in comparison.

The most significant observation was that the beam current increased with increased arc power. The highest beam currents in all cases were obtained when the maximum power from the arc power supply was applied.

We plan to build a pulsed power supply with a maximum power output of from five to ten kilowatts at a 10% duty factor. The average power would be less than one kilowatt which the existing ion sources can handle. Therefore, no immediate modifications of the existing ion sources are anticipated at this time.

7. Polarized ^{3}He Target - R. H. Ware and B. W. Ridley

It has been proposed that ^{3}He which has been polarized by optical pumping of the 2^3S_1-2^3P transition[1] could be used with the regular cyclotron ion source to produce a polarized ^{3}He beam[2]. A step preliminary to the above is the development of an optically pumped polarized ^{3}He target.

The optical pumping apparatus here has successfully produced polarized ^{3}He. Scattering experiments have been performed with a glass target cell containing unpolarized ^{3}He. The target cell design includes thin glass beam entrance and exit windows (.1 mm) and permits observation of angular distributions through thin glass walls (.2 mm) from 25°-155°. Techniques have been developed for cleaning and filling the glass target cells at the high purity levels required for optical pumping. Design of a non-magnetic scattering chamber for use with glass cells containing polarized ^{3}He has begun. It is anticipated that scattering data from a polarized target will be collected soon.

---

1 F. D. Colgrove, L. D. Schearer, and A. K. Walters, Phys. Rev. 132 (1963) 2561.

2 Univ. of Colo. Nuclear Physics Laboratory Progress Report (1969).

8. Neutron Energy Spectra from Bonner Spheres - C. S. Zaidins and J. B. Martin

The project, described in the 1968-1970 Technical Progress Reports, of reliably measuring neutron dose rates, was successfully completed during this year. An article on the methods used to obtain the neutron energy spectrum and dose equivalent rate data has been submitted to the Health Physics Journal, and two computer codes have been made available to interested labs.

The method used in obtaining the neutron energies and fluence rate is based on the unfolding of the data obtained from a Bonner Multisphere system, described in the 1970 Technical Progress Report. The counts in each sphere C_i are related to the neutron flux density, $\Phi(E)$ by

$$C_i = \int R_i(E)\ \Phi\ (E)\ dE$$

where $R_i(E)$ is the energy dependent response function for each sphere. The basic problem that needed to be solved was the deconvolution of the integral to find $\Phi(E)$.

The basic approach to the problem involved the choice of a linear approximation model for $\Phi(E)$ of the form

$$\Phi(E) \approx \sum_{j=1}^{N} A_j\ f_j\ (E)$$

where $F_j(E)$ is an appropriately chosen function, N is the number of energy intervals and the A_j are linear coefficients to be determined. Thus the set of simultaneous equations, one for each sphere,

$$C_i = \sum_{j=1}^{N} A_j R_{ij}$$

becomes the mathematical system to be solved. The R_{ij}'s can be calculated from the $f_j(E)$'s by

$$R_{ij} = \int R_i(E)\ f_j(E)\ dE$$

for any choice of an $f_j(E)$ set.

The details of our method involve a "histogram" or "step function" model for the $f_j(E)$ choice over some number of energy intervals from 10^{-2} eV to 20 MeV. The number of intervals, N, chosen vary from six to ten in the cases we tried.

The methods of solution of the simultaneous equations relating the A_j's and the C_i's fell into two categories, linear least squares and linear programming. The least squares technique involved the use of the program NFLS which we developed in such a way to insure no negative flux intervals. The linear programming method used a very standard approach but was modified to use various subsets of the spheres to generate solutions and then average the results so

as to weight all spheres in an equal manner. This program, NFLP, needed the averaging technique because it was not feasible to solve for all the spheres at one time. The two methods agreed very well in their results but the calculated uncertainties were higher for the NFLP program due to the averaging technique.

Once the values and uncertainties can be found for the A_i's, the dose equivalent rate, total neutron fluence, average energy and median energy can be easily found. The output of both programs includes the differential energy spectra, the above listed quantities of interest, and a plot of the fraction of the integral flux below the energies of interest. The programs are not difficult to use on even a smaller computer such as the PDP-9.

Typical results of the process are shown in Figs. II B19, II B20, and II B21. In Fig. II B19, the integral spectral shape of a PuBe source is shown for both a shielded and unshielded configuration. Fig. II B20 shows the dose equivalent rate as a function of distance from a thick Be target bombarded by 1 μamp of 27 MeV protons and Fig. II B21 shows the distance dependence of average and median neutron energies from the same target. The system hardware and analysis techniques are now available for routine use in monitoring neutron exposure conditions in this laboratory.

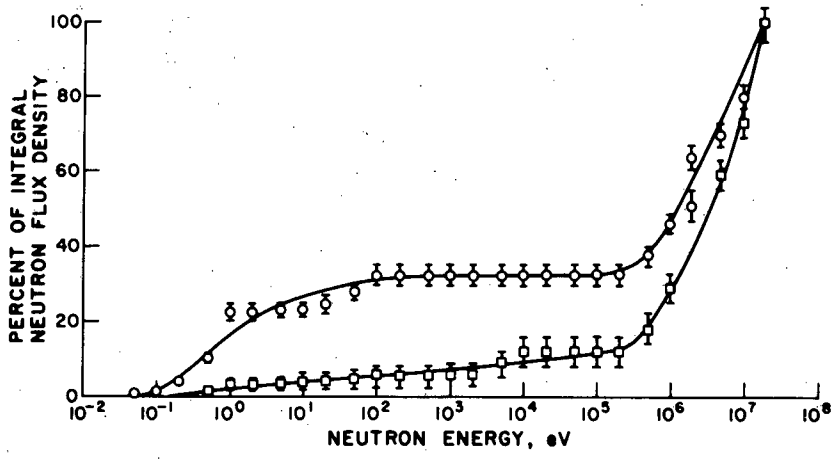

Fig. II B19 The percentage integral neutron flux density as a function of energy, from a PuBe neutron source. The lower curve is from the source unshielded and the upper curve is with an 18 cm thick paraffin moderator.

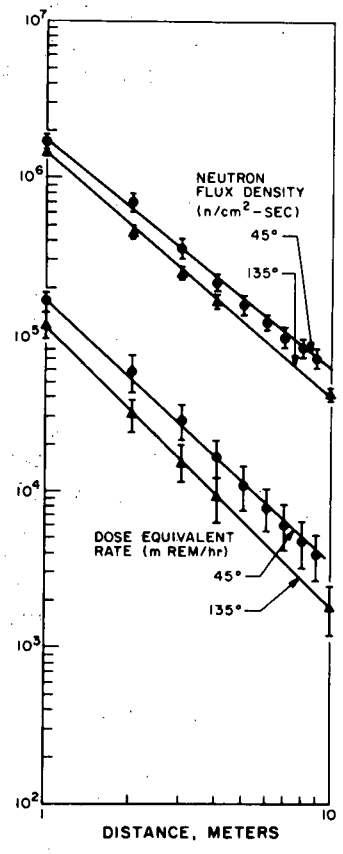

Fig. II B20 The neutron dose equivalent rate and neutron flux density produced by a 1 μA beam of 27 MeV protons on a thick Be target, measured at varying distances along lines at 45° and 135° with respect to the beam direction.

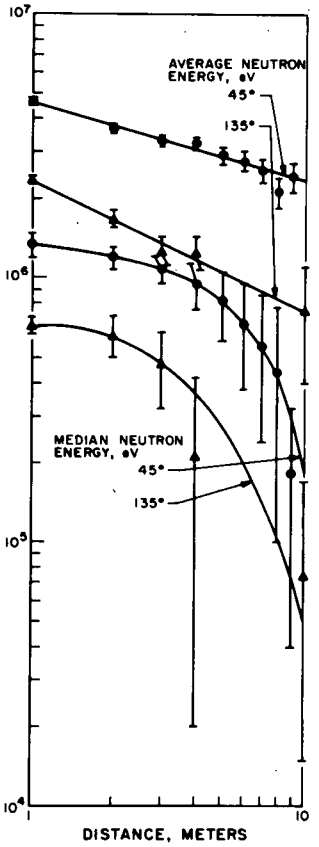

Fig. II B21 The average and median neutron energies from a thick Be target bombarded by a 1 μA beam of 27 MeV protons, measured at varying distances along lines of 45° and 135° with respect to the beam direction.

9. Data Processing--Additions to the PDP-9 Computer System -

D. H. Zurstadt

A Tektronix model 611 storage display scope has been added to the PDP-9 computer system. This display unit, along with interfacing to the computer, was purchased directly from Digital Equipment Corporation and has proven to be reliable and useful. With the addition of a light hood, the scope can be used comfortably under normal room lighting conditions. As was originally hoped, the storage capabilities of the 611 scope make possible displays of almost unlimited complexity with good resolution. Cursors can be displayed in "live" or "non-store" mode and moved about in a very acceptable fashion by using the computer console switches, thus forming a basis for interactive usage. One desirable improvement on this setup would be to interface a junction box containing switches, buttons, and perhaps "joysticks" to control the cursors.

The basic alphanumeric display subroutines supplied by Digital Equipment Corporation are being used without significant modification, but a general purpose graphics software package has been developed to help support the use of the display scope for data reduction. Provision is included for generating alternate output on the Calcomp incremental plotter under the standard device-independent keyboard monitor system.

10. Data Processing--PDP-9 Programming Developments

SPECTR - D. H. Zurstadt

This program, which incorporates all of the operations required for handling and reducing large numbers of multichannel spectra, has undergone somewhat continuous modification. Many of the modifications are related to computer or user efficiencies, but major new developments have been the addition of interactive display routines on the storage scope and least-squares Gaussian peak extraction capabilities.

The new scope display options enable the user to view an entire multichannel spectrum, or a preselected segment thereof, with the number of events (or counts) displayed vertically on a linear, log, or square root scale and the channel number displayed horizontally. In a number of discrete steps, the user may then zoom in or scan to the right or left along the spectrum to locate the region of immediate interest in his analysis. This zooming process is aided by the use of movable cursors displayed on the scope as well as by a small inset display of the entire spectrum, which indicates the region being displayed in the full scale detail. After the proper region of interest is located, it is possible to prescribe interactively, again using the movable cursors, initial parameters for the least-squares Gaussian peak extraction process. First a background is

estimated and drawn in for the region of interest. Then peaks within the region may be selected for the fitting procedure to follow.

The least-squares Gaussian peak extraction is based on initial background and peak parameters prescribed either via the interactive display process outlined above or via direct Teletype input. In either case, a variety of options all having typical default values make the setup both simple to use and flexible. Each fit is based on:

a) a background which may be predefined, fixed, or variable and

i) constant,
ii) linear,
iii) parabolic, or,
iv) exponential;

b) peak locations, each of which may be fixed, variable, or fixed relative to another peak location which in turn may be fixed or variable;

c) peak widths, each of which may be fixed, variable, or linked to vary identically with that of another peak or set of peaks; and

d) peak skewing terms, each of which may be zero for no skewing, fixed, variable, or linked to vary identically with that of another peak or set of peaks.

From one to ten peaks may be fit simultaneously for each region; the PDP-9 requires from 30 seconds to 20 minutes to complete a fit, depending on the complexity of the problem. Output may include parameter values from iteration to iteration during the fitting, final parameter values with error estimates, peak areas with error estimates, search convergence information, and a printer plot of the final fit superimposed on the original data.

Chaining - D. H. Zurstadt

A number of modifications to a special program segmenting system have been made which make it possible to handle segments in a more random manner and to automatically call and return from segments to an arbitrary number of levels.

PICSY - D. H. Zurstadt

Modifications have been made to the PICSY program input and control system to separate less frequently used sections of coding from the main sections and to incorporate more frequently used subroutines in the main body of coding. This generally results in smaller space requirements for those program segments which use the input/output system.

PLOTXS - G. W. Edwards and R. F. Bentley

Program PLOTXS was developed for the PDP-9 system for the purpose of generating hard-copy plots of differential cross sections on the incremental plotter (Calcomp). Fig. II B32 shows the type of plot produced.

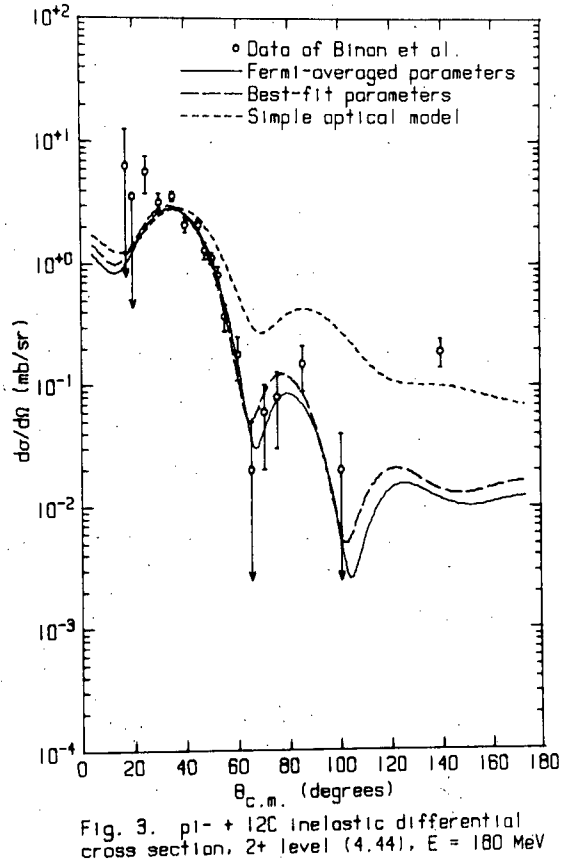

Fig. 3. pi- + 12C inelastic differential cross section, 2+ level (4.44), E = 180 MeV

Fig. II B22 A plot of differential cross sections produced with the program PLOTXS, showing a set of experimental cross sections with error bars and three theoretical fits to the data.

The program accepts user commands from the on-line teletype to specify such options as the physical size of the plot, the title, labels for the horizontal and vertical axes, the range of the abscissa (up to 180 degrees) and ordinate (up to 18 decades), the types of lines and symbols to be plotted, notes identifying the various lines and symbols, etc. Experimental and theoretical cross section data are read from punched cards or from DECtape. The plot thus specified may, at the user's option, be plotted on the display scope for examination and emendation prior to plotting on the Calcomp.

A user option has been incorporated into DWUCK which punches the elastic and inelastic differential cross sections in a format suitable for use with PLOTXS. Thus experimental cross sections and theoretical DWBA cross sections may be quickly and conveniently plotted for experimental records, publications, theses and illustrated lectures.

11. Monochromator for X-Ray Fluorescence Analysis - D. A. Lind

A simple curved crystal X-ray monochromator was designed and built. The device is designed to use Bragg reflection from lattice planes of graphite, silicon, or germanium depending on the wavelength range desired. Detection can be done with either a solid state detector, a proportional counter, or NaI scintillator. The device has been fabricated but has not yet been tested.

12. Detector Manufacture - R. A. Ristinen

For the fifth consecutive year, the needs of the laboratory for lithium-drifted detectors, both silicon and germanium, have been entirely met by in-house manufacture. As has been true since the beginning of lithium-drifted detector manufacture, the identification and procurement of crystals of good quality has been a key element in the manufacture of detectors. We have not yet achieved an entirely satisfactory method of purchasing germanium or silicon of reliably uniform and excellent quality.

One small detector was made of pure intrinsic germanium obtained from General Electric. This detector was made by a method similar to that which we use for Si(Li) detectors. The detector has given excellent energy resolution and tests are now being done on its durability with respect to temperature cycling and room temperature storage. Further manufacture of detectors of pure intrinsic germanium will probably continue.

13. General Cyclotron Improvements - A. B. Phillips

Improvements having to do with electronics are covered in the section on Electronics Maintenance and Development.

In November, 1970, the old helium-3 recycling system for the ion source broke down, and the new system was put into operation. In spite of the fact that the automatic controls for the new system have not been installed, the original charge of three liters of helium-3 is still in use after approximately 1400 hours, or ten months, of operation. We had been using about sixteen liters of gas, about $2,500.00 worth, per year on the old system.

In April, 1971, the smoke detection system was extended to cover the cyclotron vault and subvault. This protection had been recommended in the annual AEC Fire and Industrial Safety Inspection.

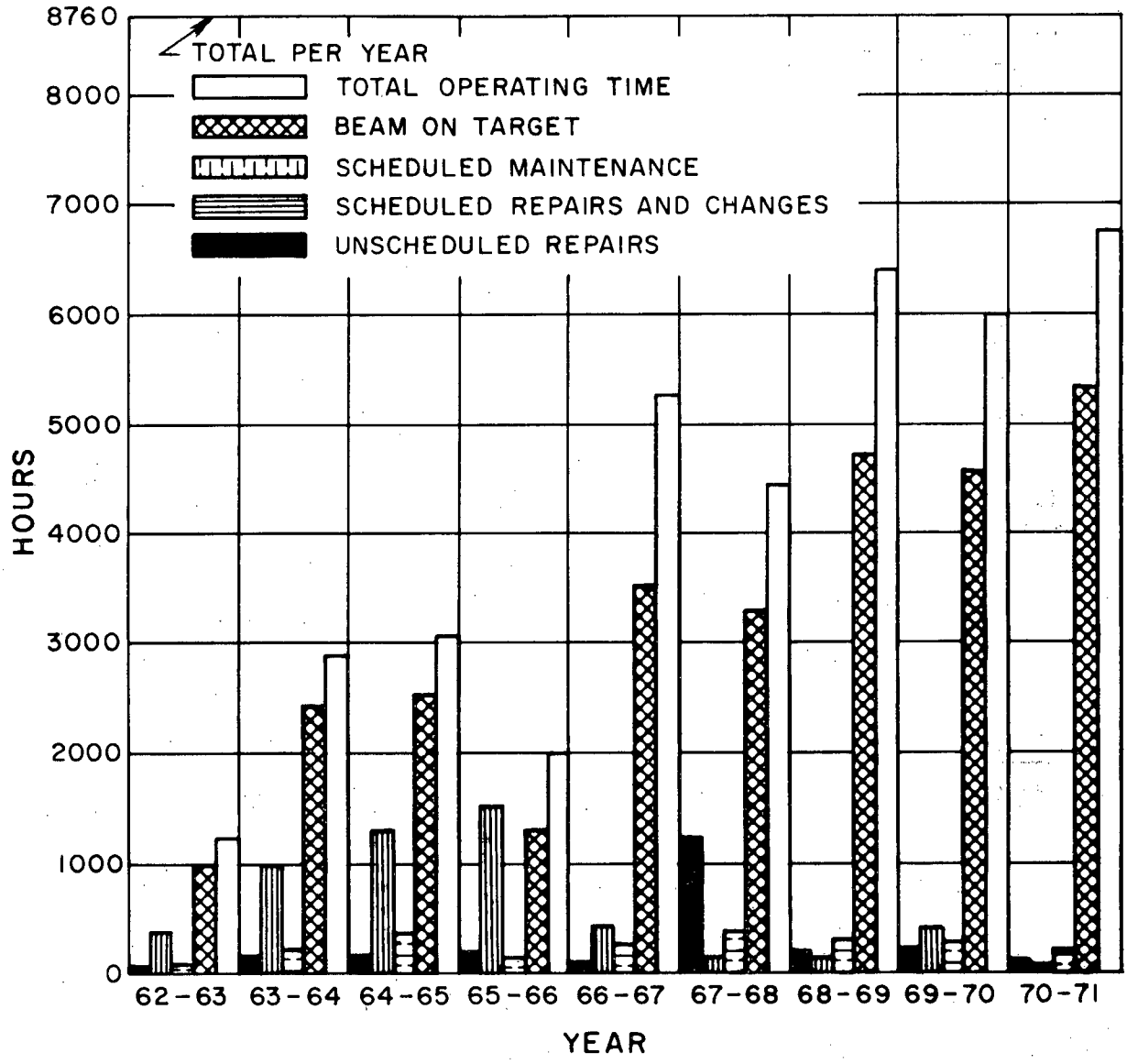

Fig. II C1 Operating history of the cyclotron. Data are based on annual periods running from September 1 through August 31.

C. Cyclotron Operation - A. B. Phillips

Operation for the period 1 September 1970 to 31 August 1971 is covered below. Table II CI shows hours of cyclotron operation by purpose. Table II CII shows hours of cyclotron operation by type of particle accelerated. The 35-hour discrepancy represents hours of testing when no beam was used.

Of the 8760 hours in the year, the cyclotron was in use for 6725 hours, or 77% of the year. Actual beam-on-target time was 5793 hours, or 86% of cyclotron running time.

The cyclotron was out of commission for a total of 387 hours during the period. Two-hundred and three hours were used for routine maintenance, 31 hours for scheduled repairs, 100 hours for unscheduled repairs, and 53 hours for a planned change in the experimental set-up.

Table II CIII is a list of scheduled visitorsto the laboratory during the period. The history of cyclotron operation is shown in Fig. II C1.

TABLE II CI

HOURS OF CYCLOTRON OPERATIONS - PURPOSE

Month	Cyclotron Development & Test	Research		Radionuclide Production		Subtotal Hrs/mo.
		Staff	Collaborate	Staff	Outside	
Sept. 70	---	549	---	---	---	549
Oct. 70	14	630	---	---	---	644
Nov. 70	---	632	---	---	---	632
Dec. 70	20T	527	---	---	---	547
Jan. 71	15T	579	---	---	---	594
Feb. 71	---	595	---	---	---	595
Mar. 71	---	701	---	---	---	701
Apr. 71	---	495	---	---	---	495
May 71	---	514	---	---	---	514
June 71	---	609	---	---	---	609
July 71	---	594	---	---	---	594
Aug. 71	---	286	---	---	---	286
Totals	14 + 35T	6711	---	---	---	6760

TABLE II CII

HOURS OF CYCLOTRON OPERATION - PARTICLE

Month	Protons 4-27.3 MeV	Deuterons 4-16 MeV	H_2^+ 4-18 MeV	^3He 16-44 MeV	^4He 3-28 MeV	Other	Sub-Total Hr/mo.
Sept. 70	351	---	20	158	20	---	549
Oct. 70	261	28	12	212	131	---	644
Nov. 70	201	18	---	315	98	---	632
Dec. 70	228	---	---	141	158	---	527
Jan. 71	337	23	---	189	30	---	579
Feb. 71	212	---	6	315	62	---	595
Mar. 71	467	40	---	181	13	---	701
Apr. 71	296	---	---	199	---	---	495
May 71	448	---	18	48	---	---	514
June 71	493	24	5	65	22	---	609
July 71	500	---	---	94	---	---	594
Aug. 71	175	---	---	111	---	---	286
Totals	3969	133	61	2028	534	---	6725

TABLE II CIII

SCHEDULED VISITORS - 9/1/70 to 8/31/70

Date	No.	From
10/2/70	6	THE SCHOOL, Boulder, Colorado
10/7/70	30	Fairview High School, Boulder, Colorado
10/9/70	25	Health Phys. Soc. & Indus. Hygiene Ass'n.,Colo.
10/28/70	75	Univ. of Colo. Physics 112 class
11/18/70	30	Univ. of Colo. Grad. Students Orientation
12/12/70	15	Univ. of Colo. Denver Center Physics class
2/27/71	20	Colo. Jr. Academy of Science, Longmont, Colo.
3/11/71	75	Univ. of Colo. Physics 112 class
3/15/71	15	Southern Colo. St. College, Pueblo, Colo.
4/2/71	30	Soc. Nuclear Medicine Tehnicians, Denver, Colo.
4/17/71	15	Univ. of Colo. Denver Center Physics class
4/30/71	40	Univ. of Colo. Physics 215 class
5/4/71	100	Univ. of Colo. Physics 202 class
5/19/71	15	Univ. of Northern Colo. Physics class, Greeley, Colo.
5/26/71	25	Colo. College, Intro. Physics class, Colo. Spgs., Colo.
6/28/71	15	Hispano program, U. of Colo. Nuclear Physics Lab
7/22/71	60	Summer Conf. High School Students, U. of Wyoming, Laramie, Wyoming
8/3/71	35	NSF Conf. H.S. Students, Colorado College
8/10/71	10	Radiation Biology class, Ft. Collins, Colo. (CSU)
Total	636	

III. THEORETICAL PROGRAM

A. Inelastic and Charge-Exchange Scattering of Pions from Nuclei

G. W. Edwards and E. Rost

Encouraging progress has been made in a theoretical investigation of two types of direct pion-nuclear reactions: Inelastic scattering to excited collective states of the target nucleus, and single and double charge exchange reactions leading to isobaric analog states of the residual nucleus. Calculations have been carried out both in the distorted-wave Born approximation (DWBA) and in the coupled-channels formalism.

The distorted-wave program DWUCK has been extensively modified to carry out DWBA calculations of inelastic scattering (π,π') and the single charge exchange reaction (π^+,π°) for incident pion kinetic energies spanning the 3,3 resonance region (100 MeV $\lesssim T_\pi \lesssim$ 300 MeV). The pion-nuclear optical potential is taken to be of the Kisslinger form[1], with optical model parameters derived directly from pion-nucleon phase shifts[2]. Inelastic transitions are obtained by deforming the optical potential, so that the non-spherical part of the potential connects the nuclear ground state to excited collective states. Results of the inelastic scattering calculations have been reported[3]. Good fits to the ^{12}C inelastic scattering data of Binon *et al.*[4] are obtained at forward angles, provided that one retains the p-wave term in the optical potential. A consistent set of deformation parameters, comparable in magnitude to those obtained from electron and nuclear inelastic scattering, has been obtained for the 2^+ (4.44) and 3^- (9.64) excited states of ^{12}C.

DWBA total cross sections for the reaction $^{91}Zr(\pi^+,\pi^\circ)^{91}Nb^*$ have been calculated and are presented in Fig. III-1 as a function of incident pion kinetic energy. Experimentally, this reaction can be carried out by observing the proton decay of the isobaric analog state in ^{91}Nb, as has been done with the (p,n) reaction on the same nucleus[5]. The (π^+,π°), results are of a very preliminary character, since we have not yet established the energy region in which we expect the DWBA treatment to be valid.

To investigate the accuracy of the DWBA treatment, and to calculate the double charge exchange reaction (π^+,π^-), a coupled channels program CHOPIN has been written to treat pionic reactions. The DWBA inelastic scattering results are generally corroborated by the coupled channels calculations. Differential cross sections for the double charge exchange reaction are shown in Fig. III-2, and the total cross sections as a function of energy is shown in Fig. III-3. When the Kisslinger optical potential is expressed in terms of separate (and different) neutron and proton nuclear densities, we find that the charge exchange cross sections are very sensitive to the neutron and proton densities.

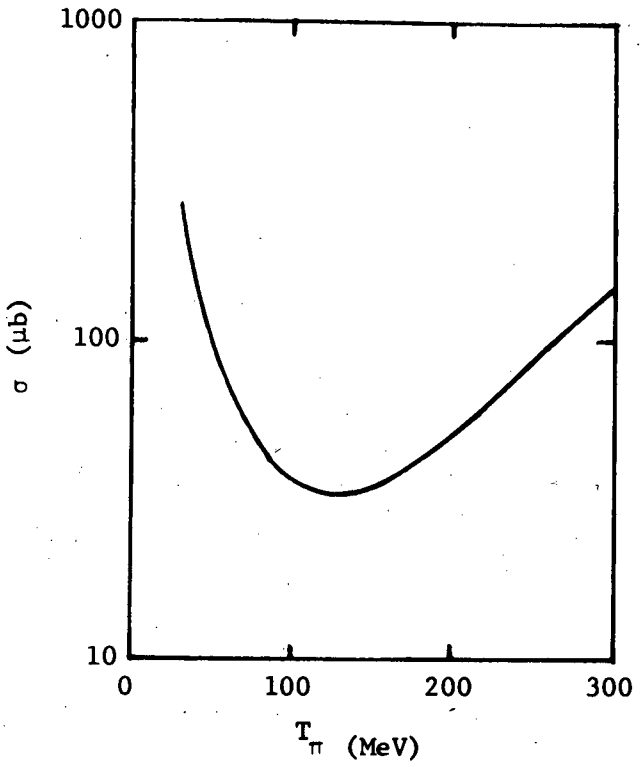

Fig. III-1 $^{91}Zr(\pi^+,\pi^\circ)^{91}Nb^*$ total cross section for excitation of the isobaric analog state in ^{91}Nb.

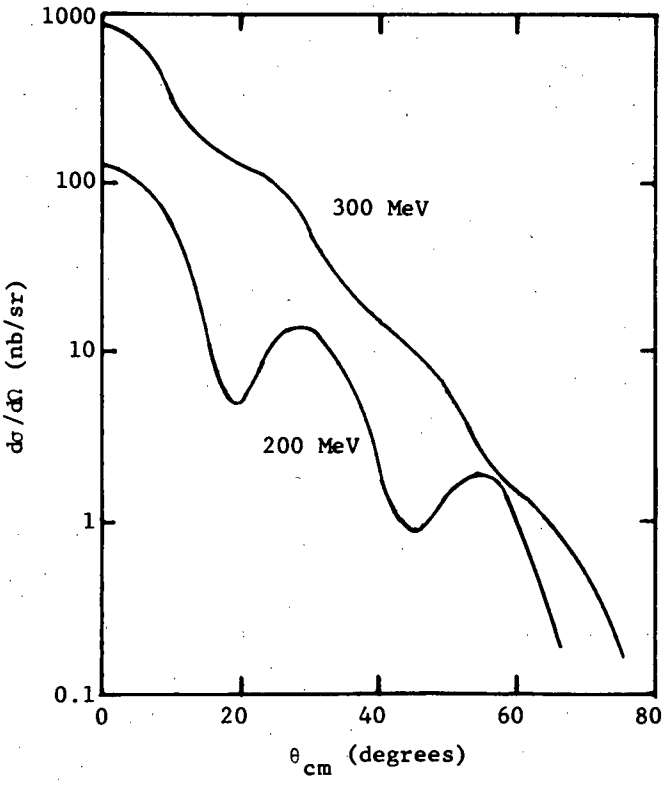

Fig. III-2 $^{93}Nb(\pi^+,\pi^-)^{93}Tc^*$ differential cross section at 200 MeV and 300 MeV incident pion kinetic energy.

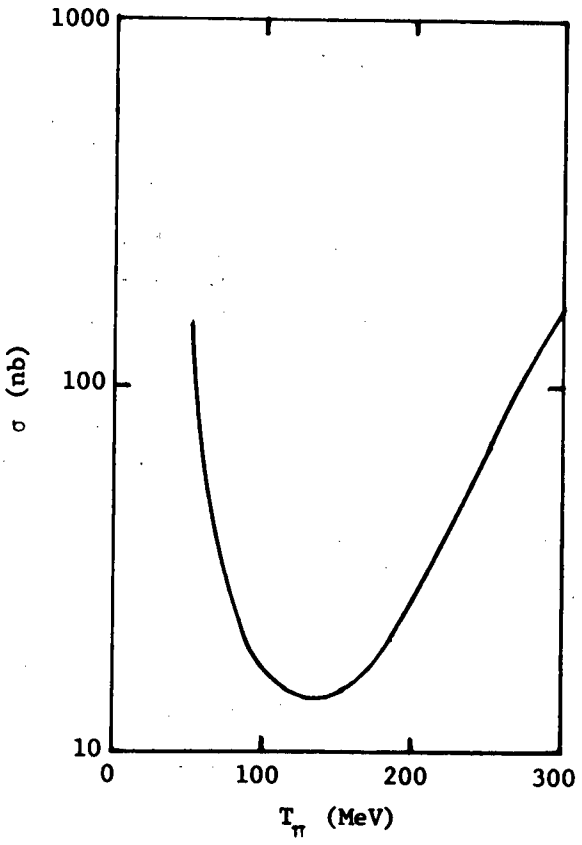

Fig. III-3 $^{93}Nb(\pi^+,\pi^-)^{93}Tc^*$ total cross section for excitation of the double isobaric analog state in ^{93}Tc.

We feel confident that the analysis of appropriate meson factory experiments will yield definitive information on the shape of the neutron density distribution.

---

1 L. S. Kisslinger, Phys. Rev. 98 (1955) 761.

2 See E. H. Auerbach et al., Phys. Rev. 162 (1967) 1683, Eqs. 25 and 26. We use phase shifts given by L. D. Roper et al., Phys. Rev. 138 (1965) B190.

3 G. W. Edwards and E. Rost, Phys. Rev. Letters 26 (1971) 785. See also an erratum, Phys. Rev. Letters 26 (1971) 1354.

4 F. Binon et al., Nucl. Phys. B17 (1970) 168.

5 A. I. Yavin et al., in Isobaric Spin in Nuclear Physics, J. D. Fox and D. Robson (eds.), New York, Academic Press, 1966, p. 584.

B. Puzzling Levels in ^{44}Sc - S. Pittel

The first two excited states in ^{44}Sc at 68 keV and 146 keV are not excited in any simple direct reactions. This suggests a fairly complex nature for these levels, surprising in view of the general success of the $f_{7/2}^n$ picture for other nuclei in this region. Further evidence for the complex nature of these two states comes from gamma ray measurements, e.g. the 146 keV level decays almost completely to the 68 keV level rather than to the 2^+ ground state.

A series of particle-hole shell-model calculations have been carried out to try to provide a consistent explanation for these levels. In the first calculation, a 5-particle, 1-hole configuration space was used together with realistic two-particle matrix elements. The results suggest that one of the two levels (probably the one at 68 keV) could have spin 1^-. Its structure would then be consistent with its non-observation in the various direct reactions.

A calculation has also been carried out to estimate the energy and structure of the lowest 6p-2h state. The results suggest that a $J^\pi=0^+$, T=1 state could lie very low in energy, and might perhaps be the mechanism for the 146 keV state. This state would be very pure, since the $(1f_{7/2})^4$ configuration has no J=0, T=1 state. If this is indeed the structure of the 146 keV level, it should be observable in the ^{46}Ti(p,^{3}He) reaction with an L=0 pattern.

C. 0^+ States in ^{44}Sc and the ^{46}Ti(p,^{3}He) Reaction - S. Pittel and E. Rost

Recently Sherr[1] has attempted to study 0^+ levels in ^{44}Sc by means of the ^{46}Ti(p,^{3}He) reaction. He finds a state at 2.8 MeV, the 0^+ analog of the ^{44}Ca ground state. He also finds a possible state at 4.75 MeV, with a strength about 1/5 to 1/10 that of the 2.8 MeV level. This state is probably the analog of the 1.9 MeV 0^+ state in ^{44}Ca. No evidence for the 0^+ T=1 state is observed.

We have attempted to explain the relative strengths to these levels, as well as the shape of the 2.8 MeV angular distribution by using a mixed-configuration DWBA analysis. The two T=2 states were considered to be mixtures of 4p and 6p-2h configurations. A simple shell-model calculation was carried out and the resulting wave functions used in Distorted Wave calculations. The shape of the 2.8 MeV angular distribution is reproduced adequately. Relative corss sections (at 10° c.m.) of $\frac{\sigma_{DW}(2.8\ \text{MeV})}{\sigma_{DW}(4.75\ \text{MeV})} \approx 4$ were obtained.

The 0^+ T=1 state should be nearly a pure 6p-2h state. With this assumption, we performed DWBA calculations assuming it to lie at 0.15 MeV (at the position of the puzzling level discussed in sect. B) and at 0.66 MeV (degenerate with a known 1^+ level). Both calculations predict a cross section at 10° approximately 1/10 that of the transition to the 2.8 MeV level, possibly explaining its non-observation.

---

[1] R. Sherr, private communication.

D. Mechanism for Extending the ^{20}Ne Rotational Band - S. Pittel

The possibility of extending the ^{20}Ne rotational band past the 8^+ limit implied by the simple shell model[1] has been investigated. $J^\pi=10^+$ states were constructed by lifting a single nucleon from the 2s-1d shell into the unbound $1g_{9/2}$ orbital. The lowest 10^+ state resulting from a diagonalization of the energy matrix was predicted at 21.9 MeV. This is in good agreement with the position expected from an extrapolation of the excitation energies of the lower band members. The transition strength from this state to the 8^+ band member was calculated and found to be strongly enhanced, supporting the hypothesis that this is an appropriate mechanism for extending rotational bands. The results of these calculations have been published in Physics Letters.

---

[1] e.g. A. Arima et al., Nucl. Phys. A108 (1968) 94.

E. Calculation of ^{55}Mn in an Extended Shell Model Basis - S. Pittel

The principal stimulus for this calculation is the observation of a previously unknown and unexpected $1/2^-$ state in ^{55}Mn (described elsewhere in this Progress Report).

The observation of a $1/2^-$ level at such a low energy is not predicted by previous theoretical investigations of ^{55}Mn. McGrory studied this nucleus within the framework of the spherical shell model[1]. He considered ^{55}Mn as an inert ^{56}Ni core, plus two neutrons distributed among the $2p_{3/2}$, $1f_{5/2}$, and $2p_{1/2}$ orbitals, and three proton holes in the $1f_{7/2}$ shell (i.e. a 2 particle-3 hole (2p-3h) configuration space). This calculation has been redone by employing Kuo-Brown matrix elements, including core polarization corrections calculated relative to a ^{40}Ca core[2]. The results (labeled 2p-3h) are compared to the experimental spectrum in Fig. III-4. The agreement is good except for the absence of a $1/2^-$ state corresponding to observation.

In order to provide an explanation for the missing level the above shell-model calculation has been extended to include a limited set of 3p-4h states. In an isospin scheme, the possible 3p-4h states are:

$$(T_p,T_h)T = (3/2,1)5/2;\ (1/2,2)5/2;\ (3/2,2)\ 5/2.$$

By using a monopole force to represent the particle-hole interaction[3], one finds that the most important 3p-4h states should be those with $(T_p,T_h)T = (1/2,2)\ 5/2$. The basis used by McGrory was thus extended to include those proton excitations into the $2p_{3/2}$, $1f_{5/2}$, and $2p_{1/2}$ orbitals with this isospin structure.

It has been noted recently[4] that the splitting between the $2p_{3/2}$ and $1f_{7/2}$ single particle levels (hereafter called $\Delta\epsilon$) should be treated as a parameter whose variations reflect the influence of

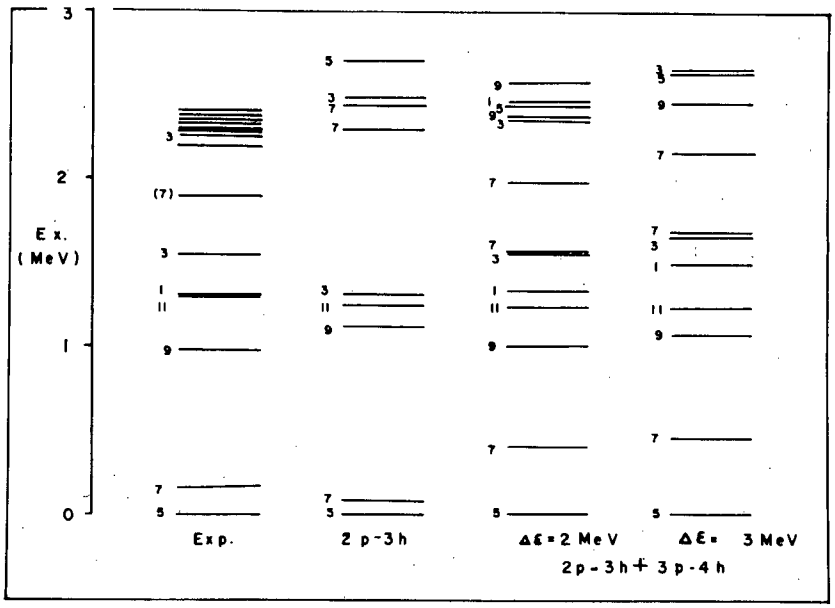

Fig. III-4 The experimentally observed spectrum of ^{55}Mn is compared to theoretical predictions as described in the text. Each state is labeled by twice the total spin (2J).

neglected particle-hole configurations. In Fig. III-4 are also shown the spectra calculated by using $\Delta\epsilon$=2 MeV and 3 MeV. The similarity of these spectra indicates an insensitivity to $\Delta\epsilon$ in this calculation. The spectrum with $\Delta\epsilon$=4 MeV is also very similar to the results in Fig. III-4.

These calculations do produce a $1/2^-$ state near the observed position, and at the same time still reproduce all the other low-lying levels. For $\Delta\epsilon$=2 MeV (for which all subsequent results will be given) the $1/2^-$ level is 42% 2p-3h and 58% 3p-4h.

The 3p-4h components involve some promotion into the $2p_{1/2}$ orbital, and one might expect the $1/2^-$ state then to be populated by proton stripping on ^{54}Cr. If a weak coupling wave function for the ^{54}Cr ground state of the form

$$[\phi^{J_p=0}(f_{7/2}^{-4})\ \phi^{J_n=0}(^{58}\text{Ni g.s.})]^{J=0}$$

is assumed, then the proton stripping spectroscopic factor $(2J+1)C^2S$ for the lowest $1/2^-$ state of ^{55}Mn is predicted to be only .030. This is in agreement with the non-observation of this transition in a recent study of the ^{54}Cr(^{3}He,d)^{55}Mn reaction[5]. Much of the $2p_{1/2}$ strength is to the $1/2^-$ level calculated at 2.47 MeV. The calculated spectroscopic strengths to other ^{55}Mn states are in good agreement with experiment.

[1] J. B. McGrory, Phys. Rev. 160 (1967) 915.
[2] T. T. S. Kuo and G. E. Brown, Nucl. Phys. A114 (1968) 241.
[3] R. K. Bansal and J. B. French, Phys. Letters 11 (1964) 145.
[4] e.g., P. Federman and S. Pittel, Phys. Rev. 186 (1969) 1106, and Nucl. Phys. A139 (1969) 108.
[5] J. Rappaport et al., Nucl. Phys. A123 (1969) 627.

F. Shell-Model Study of the Titanium Isotopes - S. Pittel

Previous shell-model investigations of the titanium isotopes have assumed that the valence nucleons occupy the $1f_{7/2}$ orbital[1]. Experimental data from direct reaction studies and gamma-ray measurements indicate the necessity of extending the configuration space. A similar situation existed in the spectroscopy of the calcium isotopes. Pure $(1f_{7/2})^n$ calculations[1] were unable to reproduce many of the level properties, but extended calculations including an active $2p_{3/2}$ orbital have provided an excellent description of these isotopes[2].

With this in mind, we have begun a detailed shell-model study of the titanium isotopes, including up to two nucleons in the $2p_{3/2}$ orbit. To keep the shell-model bases to a manageable size, we permit only neutron excitations into the $p_{3/2}$ orbit. Furthermore, only those two neutron excitations in a relative J=0 state are considered. Even with these minimum extensions of the configuration space, energy matrices as large as 113 x 113 must be evaluated.

Computer programs have been written to calculate and diagonalize the various energy matrices. These programs have been tested and preliminary results on ^{45}Ti have been obtained. The results indicate definite improvement over the pure $(1f_{7/2})^n$ calculations.

[1] J. D. McCullen et al., Phys. Rev. 134 (1964) B515.
[2] P. Federman and S. Pittel, Nucl. Phys. A155 (1970) 161.

G. The ^{51}V(^{3}He,t) Reaction - S. Pittel and E. Rost

Sherr[1] has recently studied the population of $7/2^-$ states in ^{51}Cr via the ^{51}V(^{3}He,t) reaction. In addition to the $7/2^-$ ground state, other $7/2^-$ levels are known at 2.31 and 6.64 MeV. The 6.64 MeV level is the analog of the ^{51}V ground state. For a $7/2^- - 7/2^-$ transition, many LSJ values can contribute, the total angular distribution being an incoherent sum of them. The experimental data suggest that the analog state transition is dominated by L=0, while the other two transitions show little or no trace of L=0 transfer.

We have studied these transitions by using $f_{7/2}^{11}$ wave functions and a Distorted Wave analysis. Energy spectra and wave functions for ^{51}Cr and ^{51}V were obtained by employing $f_{7/2}^2$ interaction energies

inferred from the ^{42}Sc spectrum.[2] Excited $7/2^-$ states in ^{51}Cr are predicted at 2.35 and 6.50 MeV in excellent agreement with experiment. Form factors for LSJ transfer to these two levels and the ground state were calculated, and the results used in DWUCK. It was found that when (LSJ) = (000), the only transition with a non-zero form factor was the transition to the analog state. Incoherent addition of the various LSJ contributions, assuming an arbitrary relative normalization of the even to odd J transfers, gives excellent reproduction of the shapes and magnitudes of the three angular distributions.

---

[1] R. Sherr, private communication.
[2] J. J. Schwartz et al., Phys. Rev. Letters 19 (1967) 1482.

H. Optical Model Potential Depth for Deuterons - P. D. Kunz

The first order expression for a non-local deuteron optical potential has been derived from the non-local neutron and proton optical potentials. The potential has been reduced to an equivalent local potential by the technique of Fiedeldey[1]. The results show that the depth of the potential in the interior of the nucleus can be found in terms of using the nucleon-nucleus depths at half the kinetic energy of the deuteron plus a correction term due to the internal motion of the deuteron which reduces the depth by about 8%.

---

[1] H. Fiedeldey, Nucl. Phys. 77 (1966) 149.

I. Nuclear Excitation of Giant Dipole and Quadrupole Resonances -

P. D. Kunz and J. Bang

The magnitudes of the cross sections for the excitation of the giant dipole and quadrupole resonances have been estimated by using the collective model of Bohr and Mottelson[1]. By using sum rules and a form factor suggested by Zimanyi[2] et al. the strengths of the inelastic scattering cross section can be estimated. The agreement of the strength of the dipole excitation in ^{40}Ca for 180 MeV protons is rather good as shown in Fig. III-5.

---

[1] A. Bohr and B. Mottelson, Lecture notes, unpublished.
[2] J. Zimanyi, I. Halpern, V. A. Madsen, Phys. Lett. 33B (1970) 205.
[3] H. Tyren and Th. A. J. Maris, Nucl. Phys. 4 (1958) 662.

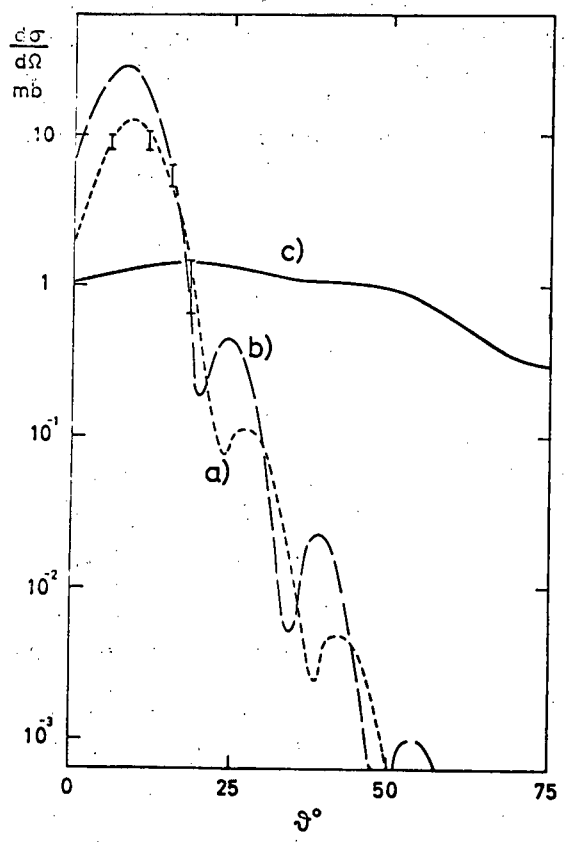

Fig. III-5 Cross section for scattering of protons from ^{40}Ca exciting the giant dipole state. Curves a and b are for 180 MeV protons with a radius parameter of 1.20 F and 1.30 F respectively while curve c is for 40 MeV protons and a radius parameter of 1.30 F. The data are from the 180 MeV experiments of Tyren and Maris[3].

J. Microscopic Form Factor for (p,α) Reactions - P. D. Kunz

The method of Bayman and Kallio[1] for obtaining the two-nucleon transfer form factor may be extended to the zero range form factor for the three-nucleon transfer case by the assumption of an alpha particle wave function of the form, $\exp(-k^2\Sigma r_{ij}^2)$. The first step of the procedure reduces the two-neutron wave function to its center of mass coordinate, and the second step integrates out the remaining coordinate between the proton and the center of mass of the di-neutron by modifying the Bayman-Kallio prescription to allow for different mass particles. Work is continuing on testing the method against experimental data.

---

[1] B. F. Bayman and A. Kallio, Phys. Rev. 156 (1967) 1121.

K. Computer Code Developments - P. D. Kunz

The computer code DWUCK has been extended to include a wider range of angular momentum transfer and partial waves without increase in size of memory needed for the program. Also a provision has been

made for the coherent summing of the transition amplitudes. The internal angular momentum algebra has been changed to correspond with that of Satchler[1]. In addition the finite range effects[2] for two nucleon transfer reactions have been added.

---

[1] G. R. Satchler, Nucl. Phys. 55 (1964) 1.
[2] E. Rost and P. D. Kunz, Nucl. Phys. A162 (1971) 376.

IV. PUBLICATIONS AND REPORTS

A. Published Articles

Rotational States of ^{158}Dy, ^{164}Er, ^{168}Yb, and ^{174}Hf Excited by Evaporation Reactions. J. H. Jett and D. A. Lind, Nucl. Phys. A155 (1970) 182.

Nuclear Reaction Measurements with ^{1}H, ^{2}H, ^{3}He, and ^{4}He Incident on Silicon Detectors. T. R. King, J. J. Kraushaar, R. A. Ristinen, Rodman Smythe, and D. M. Stupin. Nucl. Instr. and Meth. 88 (1970) 17.

Rotational Levels of Deformed Even-Even Nuclei. P. M. Abraham and E. Rost, Nucl. Phys. A162 (1971) 173.

Study of Isobaric Analog Ground States for Several Nuclei Using the (^{3}He,t) Reaction. W. L. Fadner, R. E. L. Green, S. I. Hayakawa, J. J. Kraushaar, and R. R. Johnson, Nucl. Phys. A163 (1971) 203.

Spectroscopy of States in ^{91}Zr from Gamma-Ray Transitions Observed in the $^{88}Sr(\alpha,n\gamma)^{91}Zr$ Reaction. J. E. Glenn, H. W. Baer, and J. J. Kraushaar, Nucl. Phys. A165 (1971) 533.

Study of the Excited States of ^{46}V Using the (^{3}He,t) Reaction. W. L. Fadner, L. C. Farwell, R. E. L. Green, S. I. Hayakawa, and J. J. Kraushaar, Nucl. Phys. A162 (1971) 239.

Isospin Dependence of the Mass-3 Optical Potential from the Comparison of Triton and Helion Elastic Scattering. P. P. Urone, L. W. Put, H. H. Chang, and B. W. Ridley, Nucl. Phys. A163 (1971) 225.

Finite Range Corrections in Two-Nucleon Transfer Reactions. E. Rost and P. D. Kunz, Nucl. Phys. A162 (1971) 376.

A Quadrupole Lens Reaction Products Spectrometer System. R. E. L. Green and D. A. Lind, Nucl. Instr. and Meth. 94 (1971) 93.

Small-Angle j-Dependence of (α,p) Reactions. J. E. Glenn, C. D. Zafiratos, and C. S. Zaidins, Phys. Rev. Letters 26 (1971) 328.

Beta Decay of ^{23}Mg, ^{27}Si, ^{31}S, ^{35}Ar, and ^{39}Ca. C. Détraz, C. E. Moss, and C. S. Zaidins, Phys. Letters 34B (1971) 128.

Optical Model Analysis of 38 MeV ^{3}He Elastic Scattering Extended into the Backward Hemisphere. P. P. Urone, L. W. Put, B. W. Ridley, and G. D. Jones, Nucl. Phys. A167 (1971) 383.

Comments on "Shapes of Angular Distributions of (^{3}He,t) and (p,n) Transitions to 0^{+} Anti-Analog States". E. Rost, Phys. Rev. C3 (1971) 2491.

The $^{19}F(^{3}He, ^{6}Li)^{16}O$ Reaction at 40 MeV: A Study of the Multi-Particle, Multi-Hole Structure of ^{16}O Excited States. C. Détraz, C. E. Moss, C. D. Zafiratos, and C. S. Zaidins, Nucl. Phys. A167 (1971) 337.

Mechanism for Extending the ^{20}Ne Rotational Band. S. Pittel, Phys. Letters 34B (1971) 555.

Isospin Purity at High Excitation Energies as Evidenced by Cross Correlations of Mirror Channel Fluctuations. C. Détraz, C. E. Moss, C. D. Zafiratos, and C. S. Zaidins, Phys. Rev. Letters 26 (1971) 448.

π-Carbon Inelastic Scattering Near the 33 Resonance. G. E. Edwards and E. Rost, Phys. Rev. Letters 26 (1971) 785.

Beta Decay of ^{25}Al and ^{37}K. C. E. Moss, C. Détraz, and C. S. Zaidins, Nucl. Phys. A170 (1971) 111.

Non-direct $^{26}Mg(^{4}He, ^{6}He)^{24}Mg$ Reaction at 35 MeV. R. J. Peterson, H. W. Baer, H. H. Chang, and B. W. Ridley, Phys. Rev. C4 (1971) 278.

New 0^{+} States in ^{50}Cr Observed via the (p,t) Reaction. H. W. Baer, J. J. Kraushaar, J. R. Shepard, and B. W. Ridley, Phys. Letters 35B (1971) 395.

The $^{39}K(^{3}He, ^{3}He)^{39}K$ and $^{39}K(^{3}He,d)^{40}Ca$ Reactions at 29.3 MeV. M. E. Cage, R. R. Johnson, P. D. Kunz, and D. A. Lind, Nucl. Phys. A162 (1971) 657.

Comparison Between the $(^{3}He, ^{7}Be)$ α-Pickup Reactions on ^{40}Ca and ^{40}Ar. C. D. Zafiratos, C. Détraz, C. E. Moss, and C. S. Zaidins, Phys. Rev. Letters 27 (1971) 437.

New (p,n) Reaction Studies at E_p= 23 MeV. R. F. Bentley, J. D. Carlson, D. A. Lind, R. B. Perkins, and C. D. Zafiratos, Phys. Rev. Letters 27 (1971) 1081.

The Rate of the $^{12}C + ^{16}O$ Reaction. C. J. Hansen and C. S. Zaidins, The Astrophysical Journal 168 (1971) 317.

Optical Model Potential Depth for Deuterons. P. D. Kunz, Phys. Letters 35B (1971) 16.

SPECTR - A Program for Handling and Analyzing Multichannel Pulse Height Spectra. D. H. Zurstadt, Proceedings of the DECUS Fall Symposium (1970) 263.

PICSY - A Program Input and Control System. D. H. Zurstadt, Proceedings of the DECUS Fall Symposium (1970) 143.

A Faster, More Compact Chaining Procedure for the PDP-9. D. H. Zurstadt, Proceedings of the DECUS Fall Symposium (1970) 241.

A Fractional Turn Injector Cyclotron. Rodman Smythe, Fifth International Cyclotron Conference, R. W. McIlroy, Ed., Butterworths, London (1971), p. 95-100.

The $^{28}Si(^{3}He,2p)$ and $^{12}C(^{3}He,2p)$ Reactions at 40 MeV. D. M. Stupin and R. A. Ristinen, Nucl. Phys. A173 (1971) 286.

B. Articles Submitted for Publication

Beta Decay of ^{26}Si, ^{30}S, and ^{34}Ar. C. E. Moss, C. Détraz, and C. S. Zaidins, submitted to Nuclear Physics.

Energy Dependence in $(^{3}He,t)$ Transitions to Isobaric Analog Ground States. W. L. Fadner, J. J. Kraushaar, and S. I. Hayakawa, submitted to Physical Review.

Investigation of the Mechanism of ^{3}He-Induced Four-Nucleon Pick-up Reactions. C. Détraz, C. D. Zafiratos, C. E. Moss, and C. S. Zaidins, submitted to Nuclear Physics.

A Study of Excited States in ^{58}Cu, ^{54}Co, ^{50}Mn, and ^{46}V. N. S. P. King, C. E. Moss, H. W. Baer, and R. A. Ristinen, submitted to Nuclear Physics.

The $(^{3}He,^{6}Li)$ Reaction on Several Nuclei in the Region A=10 to 27. I. K. Oh, C. S. Zaidins, C. D. Zafiratos, and S. I. Hayakawa, submitted to Nuclear Physics.

An Unexpected $1/2^{-}$ State in ^{55}Mn. R. J. Peterson, S. Pittel, and H. Rudolph, submitted to Physics Letters.

Investigation of the $^{26}Mg(p,t)^{24}Mg$ Reaction at $E_p = \sim 26$ MeV. J. R. Shepard, J. J. Kraushaar, and H. W. Baer, submitted to Physical Review.

An Investigation of the Excited States of ^{50}Mn and of Energy Dependent Effects in the $^{50}Cr(^{3}He,t)^{50}Mn$ Reaction. W. L. Fadner, J. J. Kraushaar, and L. C. Farwell, submitted to Nuclear Physics.

A Study of the $^{113}In(^{3}He,d)^{114}Sn$ Reaction at 37.7 MeV. M. E. Cage, P. D. Kunz, R. R. Johnson, and D. A. Lind, submitted to Nuclear Physics.

Structure of ^{62}Zn Studied through the (p,t) Reaction at 27.5 MeV. L. C. Farwell, J. J. Kraushaar, and H. W. Baer, submitted to Nuclear Physics.

Excitation Energies of Levels in ^{16}F, ^{20}Na, and ^{24}Al. C. E. Moss and A. B. Comiter, submitted to Nuclear Physics.

The $(p,n\gamma)$ Reaction on ^{27}Al and ^{28}Si. C. E. Moss, N. S. P. King, A. B. Comiter, and R. A. Ristinen, submitted to Nuclear Physics.

Reactions Induced by ^{3}He Ions on ^{64}Zn. D. F. Crisler, H. B. Eldridge, R. Kunselman, and C. S. Zaidins, submitted to Physical Review.

About the Half-Lives of ^{20}Na and ^{36}K. C. E. Moss, C. Détraz, C. S. Zaidins, and D. J. Frantsvog, submitted to Physical Review.

Linear Programming and Least Squares Techniques for Extracting Neutron Spectra from Bonner Sphere Data. J. B. Martin and C. S. Zaidins, submitted to Health Physics Journal.

A Low-Cost Stepping-Motor Controller for Goniometers. L. A. Erb, P. K. Govind, and C. D. Zafiratos, submitted to Journal of Physics.

Pion-Nucleus Charge-Exchange Scattering at Intermediate Energies, E. S. Rost and G. W. Edwards, submitted to Physics Letters.

C. Published Abstracts and Conference Presentations

Possibilités d'etude des noyaux loin de la zone de stabilité. C. Détraz, Jounées d'etude Tandem, Pout-ā-Mousson, France, April, 1971.

(^{3}He,^{7}Li) Reactions on ^{12}C and ^{19}F. C. Détraz, C. E. Moss, C. D. Zafiratos, and C. S. Zaidins, Bull. Amer. Phys. Soc. 15 (1970) 1597.

Beta-Decay of ^{26}Si, ^{30}S, and ^{34}Ar. C. Détraz, C. E. Moss, C. S. Zaidins, and K. W. Johnson, Bull. Amer. Phys. Soc. 16 (1971) 492.

Linear Programming Applied to Spectra Analysis. C. S. Zaidins and J. B. Martin, Colo.-Wyo. Acad. Sci.--AAPT Joint Meeting, April 1971.

Microscopic Form Factor for (p,α) Reactions. P. D. Kunz, Tucson Meeting of APS, Nov. 4-6, 1971.

Quantitative Trace Element Analysis by Charged Particle Induced Characteristic X-Rays. J. J. Kraushaar, R. A. Ristinen, H. Rudolph, and W. R. Smythe, Bull. Amer. Phys. Soc. 16 (1971) 545.

Investigation of the Excited States of ^{50}Mn at 21.5, 29.6, and 37.5 MeV, using the $^{50}Cr(^{3}He,t)^{50}Mn$ Reaction. W. L. Fadner, J. J. Kraushaar, and L. C. Farwell, Bull. Amer. Phys. Soc. 16 (1971) 575.

New 0^{+} States in ^{50}Cr. H. W. Baer, J. J. Kraushaar, J. Shepard, and B. W. Ridley, Bull. Amer. Phys. Soc. 16 (1971) 575.

A New Magnetic Spectrometer System. B. W. Ridley, R. J. Peterson, D. Prull, and J. J. Kraushaar, Bull. Amer. Phys. Soc. 16 (1971) 582.

Study of the (^{3}He,t) Reaction at 21.6, 30.0, and 37.7 MeV. S. I. Hayakawa, W. L. Fadner, and J. J. Kraushaar, Bull. Amer. Phys. Soc. 16 (1971) 600.

Structure of ^{62}Zn Studied via the (p,t) Reaction at 27.5 MeV. L. C. Farwell, J. J. Kraushaar, and H. W. Baer, Bull. Amer. Phys. Soc. 16 (1971) 626.

Elimination of Radiation Exposure by Substituting Stable for Radioactive Isotopes: The Stable ^{50}Cr RBC Survival Test. E. W. Stoub, J. J. Kraushaar, R. A. Ristinen, R. R. Quinto, and D. W. Brown, Presented at 18th Annual Meeting, Society of Nuclear Medicine, Los Angeles, June, 1971.

Inelastic Proton Scattering from ^{50}Cr. E. W. Stoub, R. J. Peterson, and R. A. Ristinen, Tucson Meeting of APS, Nov. 4-6, 1971.

Pion Induced Reactions from a Low Energy Point of View. E. Rost, Invited paper given at Tucson meeting of APS, Nov. 4-6, 1971.

Variations in Small-Angle Behavior of (p,n) Analog Transitions from ^{54}Fe, ^{58}Ni, and ^{90}Zr. J. D. Carlson, R. F. Bentley, D. A. Lind, and C. D. Zafiratos, Tucson meeting of APS, Nov. 4-6, 1971.

Microscopic Analysis of New (p,n) Analog Data at E_p=23 MeV. R. B. Perkins, R. F. Bentley, C. D. Zafiratos, Tucson meeting of APS, Nov. 4-6, 1971.

Systematics of (p,n) Reactions for Isobaric Sequences A=58, 64, and 96. D. A. Lind, H. Rudolph, and J. D. Carlson, Tucson meeting of APS, Nov. 4-6, 1971.

Energy Dependence in the ^{54}Fe(^{3}He,t)^{54}Co Reaction. W. L. Fadner, H. Rudolph, J. J. Kraushaar, Tucson meeting of APS, Nov. 4-6, 1971.

Macroscopic DWBA Analysis of (p,n) Analog Transitions at 23 MeV. J. D. Carlson, D. A. Lind, and C. D. Zafiratos, Tucson meeting of APS, Nov. 4-6, 1971.

Width of Analog States in ^{165}Er and ^{208}Bi. C. D. Zafiratos, D. A. Lind, and J. D. Carlson, Tucson meeting of APS, Nov. 4-6, 1971.

The (p,n) Reaction in the s-d Shell. R. F. Bentley, and H. Rudolph, Tucson meeting of APS, Nov. 4-6, 1971.

Excitation Energies of Low-Lying Levels in ^{24}Al. C. E. Moss, R. F. Bentley, J. D. Carlson, A. B. Comiter, D. A. Lind, H. Rudolph, and C. D. Zafiratos, Tucson meeting of APS, Nov. 4-6, 1971.

Experimental Study of the Tensor Component of the Effective Interaction in ^{54}Fe(p,n)^{54}Co. R. F. Bentley, J. D. Carlson, R. B. Perkins, and C. D. Zafiratos, Tucson meeting of APS, Nov. 4-6, 1971.

Investigation of ^{48}Cr via the (p,t) Reaction at 27.3 MeV. J. R. Shepard, J. J. Kraushaar, and R. H. Ware, Tucson meeting of APS, Nov. 4-6, 1971.

Two-Nucleon Pickup from ^{89}Y. H. Rudolph and R. J. Peterson, Tucson meeting of APS, Nov. 4-6, 1971.

The Structure of ^{57}Ni via the (^{3}He,α),(p,d), and (α,nγ) Reactions. F. M. Edwards, J. J. Kraushaar, B. W. Ridley, N. S. P. King, Tucson meeting of APS, Nov. 4-6, 1971.

Study of Isobaric Analogs of Excited States of Even Ti Isotopes Using the (^{3}He,t) Reaction. R. E. L. Green, R. R. Johnson, and H. Rudolph, Tucson meeting of APS, Nov. 4-6, 1971.

The (p,n) Reaction on Several 4n Nuclei. H. Rudolph, R. F. Bentley, and C. E. Moss, Tucson meeting of APS, Nov. 4-6, 1971.

Isospin Dependence of Mass-3 Optical Potential. B. W. Ridley, Conference on Optical Potentials for Complex Projectiles, Univ. of North Carolina, April, 1971.

Calculations of Pion Inelastic Scattering Reactions at Intermediate Energies. E. Rost, TRIUMF meeting, Vancouver, B. C., August, 1971.

D. Recent Publications of Nuclear Physics Laboratory Staff - Not Supported by Contract AT(11-1)-535

The Radial Variation of g in a Spherically Symmetric Mass with Non-Uniform Density. C. S. Zaidins, submitted to American Journal of Physics.

The Formation of the ^{6}Li g.s. and the ^{6}Li, 3.56 MeV, T=1 State in the ^{19}F(^{3}He,^{6}Li)^{16}O g.s. Reaction. W. J. Klages, H. H. Duhm, H. Yoshida, P. E. Schumacher, and C. Détraz, Nucl. Phys. A156 (1970) 65.

E. Theses

A (p,nγ) Reaction Study of Excited States in ^{58}Cu, ^{54}Co, ^{50}Mn, and ^{46}V. N. S. P. King, Ph.D., 1970.

A Study of Final State Proton-Proton Interactions and the ^{28}Si(^{3}He,2p) and ^{12}C(^{3}He,2p) Reactions at 40 MeV. D. M. Stupin, Ph.D., 1971.

A Study of ^{2}H + ^{3}He Elastic Scattering and the Reaction ^{2}H(^{3}He,^{4}He)^{1}H Between 17.5 and 44.1 MeV. T. R. King, Ph.D., 1971.

Nuclear Structure and Reaction Mechanism Studies Using the (^{3}He,t) Reaction. W. L. Fadner, Ph.D., 1971.

The Structure of ^{62}Zn Studied Through the (p,t) Reaction at 27.5 MeV. L. C. Farwell, M.S., 1971.

Excitation Functions of the Reactions Induced by ^{3}He Ions on ^{64}Zn. D. F. Crisler, Ph.D., 1971, University of Wyoming.

V. PERSONNEL

A. Academic and Scientific

H. W. Baer[1]	Research Associate
C. Détraz[2]	Research Associate
R. Graetzer[3]	Senior Research Associate
P. D. Ingalls[4]	Research Associate
J. K. Kliwer[5]	Visiting Associate Professor
J. J. Kraushaar	Professor
P. D. Kunz[6]	Professor
D. A. Lind	Professor
C. E. Moss[7]	Research Associate
R. J. Peterson	Research Associate
S. Pittel[8]	Visiting Assistant Professor
B. W. Ridley	Professor, Chairman of the Laboratory
R. A. Ristinen	Associate Professor, Chairman-Elect of the Laboratory
E. S. Rost	Professor
H. Rudolph	Research Associate
W. R. Smythe	Professor
C. D. Zafiratos	Associate Professor
C. S. Zaidins	Associate Professor

B. Technical and Support Staff

R. H. Akers	Electrician
R. C. Armstrong	Research Technician
E. C. DeGabain	Instrument Maker
B. A. Deobler	Design Engineer
R. A. Eidse[9]	Laboratory Mechanic
L. A. Erb	Electronic Engineer
J. L. Homan	Research Technician
W. G. Minor	Instrument Maker
A. B. Phillips	Cyclotron Engineer
J. N. Sonnenberg	Secretary
A. K. Wiles	Instrument Shop Foreman
D. H. Zurstadt	Systems Analyst

C. Research Assistants

V. J. Arora[9]
R. F. Bentley
J. D. Carlson
H. H. Chang
A. B. Comiter[9]
G. W. Edwards
F. M. Edwards
R. A. Emigh
W. L. Fadner[10]
K. W. Johnson[9]
N. S. P. King[11]
T. R. King[12]
D. R. Komonytsky
D. E. Prull
J. R. Shepard
S. D. Schery
E. W. Stoub
D. M. Stupin[13]
R. H. Ware

D. Other Students (Part-time)

D. A. Becker[9]
J. A. Boyd
B. L. Briggs
R. V. Brill
B. Buskirk
L. E. Cassin
D. L. Daum
L. C. Farwell[14]
J. B. Frankel[9]
D. J. Graham[9]
R. E. Hall[9]
D. S. Hamilton[9]
J. M. Hesse[9]
M. S. Iverson[9]
K. Leaver[9]
A. W. Mueller[9]
R. Rew[9]
B. G. Thompson[9]
S. L. Van Horn[9]
P. L. Williams[9]

NSF Summer Undergraduate Research Participants

R. V. Brill
L. E. Cassin
M. Lahana
R. T. Schlater
B. G. Thompson

---

[1] Appointment ended August, 1971. Now at Lawrence Radiation Laboratory, Berkeley, California.
[2] On leave from Institutet de Physique Nucléaire, Orsay, France.
[3] Appointed September, 1971. On leave from Pennsylvania State University.
[4] Appointed September, 1971.
[5] Appointed September, 1971. On leave from University of Nevada.
[6] Returned from leave at Niels Bohr Institutet, Copenhagen, Denmark, August, 1971.
[7] Appointment ended September, 1971. Now at Australian National University, Canberra, Australia.
[8] Appointment ended August, 1971.
[9] Appointment ended 1971.
[10] Ph.D. 1971. Now half-time at Department of Integrated Studies, University of Colorado, half-time Research Associate, Nuclear Physics Laboratory.
[11] Ph.D. 1970. Now at University of California, Davis.
[12] Ph.D. 1971. Now at University of Victoria, Victoria, B.C., Canada.
[13] Ph.D. 1971. Now at Laboratoire de Physique Nucléaire et d'Instrumentation Nucléaire, Strasbourg, France.
[14] M.S. 1971.